TIME-RESOLVED TWO-PHOTON ABSORPTION IN QUANTUM DOTS AND POLARITONS

by

Chitra Gautham

B.Sc., Madras Christian College, 2007

M.Sc., Indian Institute of Technology, Madras, 2009

M.S., University of Pittsburgh, 2010

Submitted to the Graduate Faculty of

the Kenneth P. Dietrich School of Arts and Sciences in partial fulfillment

of the requirements for the degree of

Doctor of Philosophy

University of Pittsburgh

2016

UNIVERSITY OF PITTSBURGH

DIETRICH SCHOOL OF ARTS AND SCIENCES

This dissertation was presented

by

Chitra Gautham

It was defended on

December 10th 2015

and approved by

David Snoke, Department of Physics and Astronomy

Brian D'Urso, Department of Physics and Astronomy

Andrew Zentner, Department of Physics and Astronomy

David Pekker, Department of Physics and Astronomy

David Waldeck, Department of Chemistry

Dissertation Director: David Snoke, Department of Physics and Astronomy

TIME-RESOLVED TWO-PHOTON ABSORPTION IN QUANTUM DOTS AND POLARITONS

Chitra Gautham, PhD

University of Pittsburgh, 2016

We used two-photon absorption to study semiconductor samples. The energy of the photons used to excite the particle is half the energy of the electronic transition. In one set of experiments we have performed time-resolved measurements of the time scale for conversion of excitons in dark states to bright (light-emitting) states in GaAs quantum dots. The dark states are pumped using two-photon absorption, while the bright state emission is observed in single-photon emission. This conversion time is connected to the spin flip time for carriers in the quantum dots. The time scale is found to be of the order of several hundred picoseconds.

In a second set of experiments, we performed time-resolved measurements of two-photon excitation directly into microcavity polariton states. Although this process is forbidden by symmetry for light at normal incidence, we observed that it is allowed at non-zero angle of incidence due to state mixing. Fermi's golden rule for bosons states that absorption into a final state is enhanced by the occupation of that state. This thesis reports experiments aimed at using a laser beam to create a condensate and modulate the two-photon absorption of a second beam.

TABLE OF CONTENTS

1.0 INTRODUCTION 1

1.1 Overview 1

1.2 Outline of thesis 4

2.0 THEORY 6

2.1 Excitons 6

2.2 Quantum Dots 9

2.3 Polaritons 11

2.3.1 Quantum wells 12

2.3.2 Distributed Bragg reflectors 12

2.3.3 Quantum superposition 16

2.3.3.1 Dispersion relationship of polaritons: 18

2.4 Bose-Einstein condensation 20

2.4.1 BEC in microcavity polaritons 21

2.5 Fermi's golden rule 23

2.6 Two-photon excitation 25

2.6.1 Two-photon absorption 25

2.6.2 Second harmonic generation 28

2.6.3 Selection rules 30

3.0 SAMPLES AND EXPERIMENTAL TECHNIQUES 33

3.1 Experimental apparatus 33

3.1.1 Laser system 33

3.1.2 Imaging devices 37

3.1.2.1 Spectrometer: . . . 37
3.1.2.2 CCD camera: . . . 37
3.1.2.3 Streak Camera: . . . 39
3.1.3 Cryostat . . . 39
3.2 Optical Imaging . . . 41
3.2.1 Real-space imaging . . . 41
3.2.2 Momentum space imaging . . . 42
3.3 Samples . . . 42
3.3.1 Quantum dots . . . 42
3.3.2 Polariton microcavities . . . 44
4.0 TWO-PHOTON ABSORPTION OF QUANTUM DOTS . . . 47
4.1 Introduction . . . 47
4.2 Experimental setup . . . 48
4.3 Data . . . 51
4.4 State model . . . 53
4.5 Calculation and discussion . . . 55
5.0 TWO-PHOTON EXCITATION OF POLARITONS . . . 56
5.1 Introduction . . . 56
5.2 Sample structure and properties . . . 57
5.3 Experimental setup . . . 59
5.4 Two time peaks . . . 59
5.5 Energy dependence . . . 62
5.6 Temperature and magnetic field dependence . . . 64
5.7 Theory and discussion . . . 64
5.8 Momentum dependence . . . 67
5.9 Conclusion . . . 69
6.0 CHARACTERIZATION OF TWO-PHOTON EXCITATION . . . 71
6.1 Magnetic field . . . 71
6.2 Lifetime of the polariton using two-photon excitation . . . 75
6.3 Polarization of the incident beam . . . 81

6.4 Polarization of the polaritons . . . 84
7.0 DETERMINISTIC ABSORPTION OF THE TWO-PHOTON BEAM 87
7.1 Polariton BEC . . . 87
7.2 Deterministic absorption of a Fock state . . . 88
7.3 Creating a polariton condensate . . . 90
7.3.1 Stress Trap . . . 90
7.3.2 Laser-generated trap . . . 91
7.3.3 Resonant excitation . . . 92
7.4 Stimulated absorption with non-resonant pumping . . . 93
7.4.1 Measurement of the beam going through the sample . . . 96
7.4.2 Measurement of the photoluminescence . . . 105
7.5 Stimulated absorption with resonant pumping . . . 105
7.5.1 Condensate creation with a CW beam . . . 106
7.5.2 Condensate creation with a pulsed beam . . . 109
8.0 CONCLUSIONS AND FUTURE DIRECTIONS . . . 112
8.1 Conclusion . . . 112
8.2 Future directions . . . 114
APPENDIX A. CONDENSATE CALCULATION . . . 115
APPENDIX B. GROUP THEORY CALCULATIONS . . . 117
APPENDIX C. EXPERIMENTAL DETAILS . . . 122
C.1 Quantum dot experiments . . . 122
C.2 Polariton experiment . . . 123
C.3 Deterministic absorption experiments . . . 126
BIBLIOGRAPHY . . . 132

LIST OF TABLES

1 Power of the two-photon beam in the presence and absence of the condensate. 97

LIST OF FIGURES

1 Schematic representation of an exciton. 7
2 Density of States in semiconductors. 10
3 Band Structure of GaAs. 13
4 Reflectivity spectrum of our DBR. 14
5 Schematic representation of a distributed Bragg reflector. 15
6 Energy vs. length of our polariton samples. 17
7 Dispersion curve of the polaritons. 19
8 Illustration of two photon absorption. 26
9 Schematic representation of the selection rules. 32
10 Schematic representation of a simplified experimental setup. 34
11 Illustration of our laser system. 38
12 Schematic representation of our Streak Camera. 40
13 Schematic representation of the quantum dot sample. 43
14 Schematic representation of our polariton sample. 45
15 Graph showing two-photon absorption. 48
16 Time resolved image of the high density QD sample. 50
17 Luminescence when J=1 and J=2 are pumped. 52
18 Representation of the energy levels. 54
19 Spectrum while exciting with half the energy of the LP. 58
20 Power dependence of the polariton emission intensity. 60
21 Intensity vs. time for different pump wavelengths. 61
22 Polariton emission intensity vs. pump photon energy. 63

23 Time vs intensity at various temperatures. 65
24 Intensity of two-photon absorption vs. the central in-plane momentum. . . . 70
25 Experimental setup to measure changes due to magnetic field. 72
26 Intensity vs Magnetic field. 76
27 Experimental setup used to measure the polariton lifetime. 77
28 Time-resolved measurement of the polariton photo-luminescence. 79
29 Polariton population showing exponential decay. 80
30 Representation of the in-plane momentum. 81
31 Intensity vs. rotated in-plane momentum. 83
32 Polarization of the polaritons. 85
33 A polariton condensate created by the power trap method. 89
34 Stimulated absorption by condensate created by non-resonantly. 94
35 Change in two-photon beam intensity due to condensate. 98
36 A schematic of the chopper experiment. 100
37 Position vs. change in power 101
38 Simulation of the change in absorption with intensity. 103
39 Change in absorption of two-photon beam due to intensity 104
40 Deterministic absorption by a condensate created resonantly(CW). 108
41 Deterministic absorption by a condensate created resonantly(pulsed). 110
42 A representation of the QDs experimental setup. 123
43 A representation of the initial polariton experimental setup. 124
44 Modifications to our experimental setup. 125
45 Experimental setup used to measure k dependence. 126
46 Experimental setup used to measure the lifetime of the polaritons 127
47 Setup for deterministic absorption by condensate created by a power trap. . . 128
48 Setup for deterministic absorption by condensate created by resonant excitation. 129
49 Setup for deterministic absorption by condensate created by a pulsed beam. . 130

ACKNOWLEDGMENTS

I would like to thank my PhD adviser, David Snoke, for the encouragement, support, and guidance he provided over the last six year. He guided me with a tremendous amount of kindness and patience, encouraged me to try new methods and experiments, and was always available to discuss my work. None of the work presented here would be possible if he hadn't given me the opportunity to work in his lab.

I would also like to thank my committee members, David Waldeck, Brian D'Urso, David Pekker, and Andrew Zentner, for making time for me every time I had a committee meeting, listening to me talk about my research, and giving valuable advice and feedback. They have helped mould my research and thesis into the shape it is in today and I would like to thank them from the bottom of my heart.

I am grateful to the staff of the Department of Physics and the University of Pittsburgh, who have been extremely helpful and supportive during my time here. I would especially like to thank Leyla for helping me out of tough situations numerous times. She made sure, every semester, that I met the deadlines, paid my fees and "magicked" up TA funding when it seemed unavailable. I would also like to thank Laura Provolt for making sure the helium orders went through even when I missed the department deadline.

Many teachers and professors have helped shaped my love for research and science over the years and I am terribly grateful to all of them for helping me get where I am today. I would especially like to thank Mrs. Lazarus, Dr. Lakshminarayan, Dr. Pattabiraman, Dr. Anantanarayan, Dr. Ghosh, and Dr. Sow Chaug Haur. I don't think I would be where I am today if it weren't for them. Thank you for being the inspiring teachers that you are.

To my labmates I owe a great debt of gratitude: To Bryan and Mark, for teaching me everything I know about running an experiment - from turning on the spectrometer to tweaking the laser; to Jeff and Nick, for being willing to let me bounce ideas off them and answer my questions patiently; to Johnny and David for helping my with my experiments and even staying late into the night to collect data; and most of all to Gangqiang for being a great friend and a source of motivation. Thank you, all.

My school friends (Samie, Anisha, Madhu, Rabia, Divvya, Sug, Deena and Rad), my

college friends (Pumpkin, Sai, Porge, Pipe and Danny), and my insti friends (Ranjini, Debo, Aarti, Shravani and Sarika) have taught me invaluable lessons - both in and out of the classroom. You guys are a constant source of joy, support, and love. Thank you for existing.

My classmates at Pitt (Gen, Mike, Rory, Kevin, Melanie, Stefanus, Sheng, Advait and Joe), there is something about spending 80 hours a week in a place with no windows solving Jackson problems that makes you bond in a way nothing else could. I'm incredibly happy to have met you and to know you.

My friends here in Pittsburgh (Anjana, Shravya, Sandeep, Vinay, Sudarshan, Ajit, Ji, Toups, Harini, Varun, Maddali, Kaushik, Swapna, Utsav, Aranya, Erle, Satya, BT, Uday, Ashwati, Lavanya, Keshav, Fester, and Samrat), you guys are awesome. Thank you for being there any time I needed you and making me not as homesick for Chennai as I could've been!

George Burns said, "Happiness is having a large, loving, caring, close-knit family in another city". My large, loving, caring, crazy, wonderful, super-smart set of grandparents, uncles, aunts, cousins, nieces, nephews, and in-laws have not stopped believing in me and loving me and I know they never will. To them I owe all my dreams and achievements. You people are incredible and a constant source of inspiration through the lives you lead. I am really lucky to be part of this family, to love you, and to be loved by you.

Most importantly, I'd like to thank the three people who made great personal sacrifices to help me achieve every dream of mine: My mother, Sethumathy, who showed me through example that social norms are meant to be broken and that there is nothing you cannot achieve if you really want to; my father, Gautham, who bought me my first book, taught me what science is and has never stopped encouraging me down this path; and my husband, Vinod, who has never let me stop believing in myself and has been my source of happiness these past eight(!) years. Thank you.

Finally, I'd like to dedicate this work to my beautiful city, Chennai, and its people, who in the face of an unprecedented natural disaster last month showed a tremendous amount of bravery, compassion, and solidarity.

1.0 INTRODUCTION

Two photon absorption was first proposed by Maria Goeppert-Mayer in 1931 in her doctoral dissertation where she considered the theoretical impact of a large concentration of photons at a particular point in space[1]. Using Dirac's dispersion theory and Kramer and Heisenberg's derivation of two-photon emission, she suggested that two photons of energy E_1 can combine in a medium to create a single photon with twice the energy, $E_2 = 2E_1$. However, the base assumption required a high concentration of photons since two photons needed to be incident at the same point at the same time. Since there was no means of producing the required concentration of photons at that time, the theory remained unproven for the next thirty years.

Although lasers were not invented until the 1960s[2], the first masers were invented by Bell labs in the mid 1950s[3, 4]. This maser was capable of producing short pulses of a high intensity beam, which enabled W. Kaiser and I.C. Garrett to run an experiment confirming two-photon excitation in 1961[5]. Since then two photon absorption has been used to study various materials and used in many applications such as florescence microscopy[6], data storage[7, 8], fabrication[9] and lithography[10, 11], etc. In this thesis I use two-photon excitation to study two systems in particular - microcavity polaritons and quantum dots.

1.1 OVERVIEW

Two-photon excitation is a process by which a particle is excited from one state to another (usually from the ground state to its lowest excitation state) by two photons which are incident simultaneously. The energy of the photons used to excite the particle is usually

half the energy of the electronic transition, but any two photons which have energies that adds up to be in resonance can give two-photon absorption. Apart from giving us a way to probe the allowed and disallowed transitions in a system, this process has an added advantage of making the obstruction of the signal by the pump photons unlikely since the signal is quite far away in energy from the pump beam. Since it requires two-photons to be incident simultaneously, the absorption goes as the square of the input intensity, making it a nonlinear process and a three-wave mixing process. Apart from the applications listed above, this property has been exploited in electronic gates[12], auto-correlators for pulse-characterization[13], and two-photon polymerization[10, 14]. "Bright" and "dark" states are defined as states accessible and inaccessible by single photon excitation. In this work, we use the fact that two photon excitation into a dark state can be used to study spin flip times in quantum dots, and dark state/bright state mixing in microcavity polaritons. The lowest electronic transition of both these systems are between 750-780 nm in wavelength (or 1.653-1.589 eV) in energy and we use a beam of wavelength 1500-1560 nm (0.827-0.795 eV) to study them. This is close to the optical communication range[15], and could potentially be used in biophotonic[16] and telecommunication applications.

Quantum dots (QDs) are structures in which the electrons are confined in all three directions, they are often referred to as 0-dimensional structures. They essentially behave like a particle in a box, which gives them discrete energy states, making them artificial controllable atoms. The theory of quantum dots is reviewed in Section 2.2. Semiconductor quantum dots - like the ones used in this dissertation - are sometimes embedded in bulk semiconductor structures. Since they interact with photons effectively, they have a variety of applications such as quantum logic gates[17], quantum dot lasers[18], and single photon emitters[19]. Spin states in quantum dots are studied for their applications in quantum computing[17] and in this respect there is a great need for a better understanding of spin flip times. Time-resolved spectroscopy gives us a means to study the spin flip times effectively. Although relaxation of the J=1 states have been studied[20, 21], the dark J=2 state had not been studied extensively before. In this thesis we aim to quantify the spin flip times of the dark state exciton by using time-resolved spectroscopy.

The exciton-polariton system is a quantum superposition of light and matter. A photon

is trapped between two mirrors which form a microcavity. Also placed inbetween the mirrors are quantum wells, which have discrete exciton energy levels. The electrons in quantum wells are bound along one direction as opposed to the electrons in quantum dots which are bound along three directions. The photon and the exciton undergo quantum superposition to form two new states called the upper and lower polaritons. The theory of exciton-polariton state is reviewed in Section 2.3. Polaritons have been studied in detail over the past 15 years - mostly for the bosonic properties[22, 23]. The mass of the polariton is $\approx 10^{-4} m_e$, and since the mobility of a particle depends on the mass, the exciton-polaritons have the ability to travel far and can be studied far from the point of excitation. While atomic Bose-Einstein condensates are created at nano-kelvin temperatures, it is possible to create polariton BEC at room temperatures[24, 25]. At low temperatures this system exhibits superfluidity[26], Bose-Einstein condensation[23, 27], and can act as a coherent light source. In this thesis, I look at the possibility of directly exciting the bright state of the exciton using two-photon excitation, and used time-resolved measurement to determine if this process is an allowed process or a forbidden process. This helped us study the dark/bright state mixing in the exciton-polariton.

Polaritons are metastable particles because they can leak through the mirrors and the energy escapes the cavity as photons. Although this feature may appear to be a drawback, in long-lifetime samples this gives us a way to look at the condensate continuously. Polariton condensates can be created by using harmonic traps in the plane of the polariton motion and varying the density. These harmonic traps can be made using stress traps[23] or by shaping an exciton cloud as explained in Section 7.3. Stimulated scattering into a state with an occupation N is enhanced by (N+1) for bosons[28]. In polariton condensates, this can be used to create polaritons using optical absorption. Thus, in principle, absorption into the final state can be controlled by the occupation of the final state. This process of deterministically absorbing the two-photon beam can be used as an optical switch. The laser beam used to excite our samples at half the energy is required to be around 1550 nm which lies in the optical communication band and can be propagated using a fiber. In this thesis, I explore the possibility of modulated absorption of the this beam.

1.2 OUTLINE OF THESIS

The main objective of this thesis is to study the two-photon excitation of quantum dots and microcavity polaritons, both experimentally and theoretically. In order to do so, I start by looking at the theory behind the two-photon process and determine whether it's an allowed process or a forbidden process.

Chapter 2 explains the theory and physics behind the various semiconductor structures I studied. There is a brief review of distributed Bragg reflectors, quantum wells, and excitons, following which the quantum superposition of a photon and exciton leading to the formation of two new states - the upper and the lower polaritons is explained. I also discuss quantum dots and look at how they differ from quantum wells. Finally, I study two-photon excitation and the selection rules that govern it.

In Chapter 3, I discuss the various experimental devices we used to study the sample, such as the laser system, the imaging devices, and the cryostat in detail. I also discuss the different techniques employed to image the sample. The sample structure and fabrication methods of both the quantum dots and polaritons we used in this thesis are explained.

In Chapter 4, I look at time-resolved two-photon excitation of quantum dots. In this experiment we studied high-density quantum dots and studied the rise and decay time of these quantum dots under femto-second excitation. Time-resolving the luminescence from the quantum dots told us the rise and decay time of the quantum dot excitation and we were able to measure a spin-flip time for the excited electrons.

In chapters 5 and 6, I discuss time-resolved two-photon excitation of polaritons. In this experiment we observed direct creation of polaritons using two-photon excitation. Time resolving the luminescence told us that there were two time peaks. I look at these time peaks and the theory behind them. We also looked at the polarization, magnetic field, and temperature dependence of these time peaks. I study the selection rules for polaritons and measured the k-dependence.

Finally, in Chapter 7, I study the possibility of deterministic absorption of a beam which is half the energy of the polariton. I create a condensate and send a beam at half the energy through the condensate. Fermi's golden rule tells us that the presence of the condensate

should give us an increased absorption of the beam. I study the modulation of this beam using various methods and set the limits to which we observe this beam.

Various detailed calculations, derivations and theory are reported in the appendices.

2.0 THEORY

Semiconductors can be broadly classified as elemental semiconductors and compound semiconductors. Elemental semiconductors are made up of a single element, while a compound semiconductor is made up of two or more elements. Different semiconductor materials have different optical and conduction properties. In our studies we use type I band alignment where if we place a piece of semiconductor with higher conductivity between pieces with higher band gap, the electrons in the middle semiconductor encounter a barrier as they move to the edge of the material. If we decrease the size of the middle semiconductor to quantum scale, the density of states is quantized. In this chapter we will study the theory behind two such semiconductor structures - semiconductor quantum dots and microcavity polaritons.

2.1 EXCITONS

For an undoped semiconductor in its ground state, the valence band of the semiconductor is fully occupied with electrons and the conduction band is "empty". An electron in the valence band cannot change its state by moving to another state since the other states are fully occupied. However, if we supply the system with sufficient energy, an electron can be excited from the valence band to the conduction band. This electron in the conduction band can move around freely since the states are empty. The excited electron is called a "free electron". At the same time, there is an empty state left behind in the conduction band which we call a "hole" (Figure 1).

The hole has a charge which is equal in magnitude to that of the free electron, but

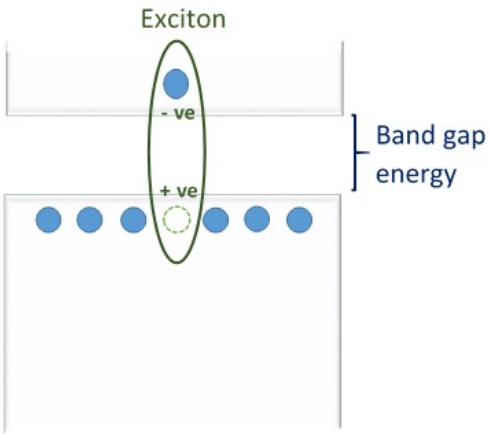

Figure 1: Schematic representation of an exciton. An valence band electron is excited to the conduction band to leave behind a "hole". The electron and the hole behave like a single particle called the exciton.

opposite in sign. The spin of the hole is also opposite to that of the electron. The free electron acts just like a electron in vacuum but has a different mass. Since the free electrons and holes are excitations of the system, they are called quasi-particles. The electrons and holes will feel a Coulomb force that will attract them to each other because they are oppositely charged. Thus, if one particle moves, it will cause the other to move along and they form a bound pair. This bound pair is called an "exciton". The effective mass of excitons in semiconductor GaAs is $\approx 0.1\ m_e$[29] making them much lighter than the hydrogen atom.

The kinetic energies of the free electron and hole are

$$\begin{aligned} E_e &= \frac{\hbar^2 k^2}{2m_e} \\ E_h &= \frac{\hbar^2 k^2}{2m_h} \end{aligned} \tag{2.1}$$

respectively[28]. Here, m_e is the effective mass of the free electron and m_h is the effective mass of the hole.

The total energy of the exciton is

$$E_b = E_g + E_k + E_C, \tag{2.2}$$

where E_g is the band gap energy, E_k is the kinetic energy of the exciton and $E_C = \frac{-R_y}{n^2}$ is the Colombic binding energy and R_y is the Rydberg constant given as

$$R_y = \frac{e^2}{8\pi\epsilon_{GaAs}a_{ex}}. \tag{2.3}$$

In a hydrogen atom an electron can be excited away by giving it energy corresponding to the binding energy. This leaves behind a proton. Similarly, we can say that the the electron and hole in an exciton are bound together similar to the electron and proton in a hydrogen atom. The binding energy of an exciton is similar to that of the Hydrogen atom and is given by

$$E = \frac{\mu_{ex}e^4}{8h^2\epsilon_{GaAs}^2}, \tag{2.4}$$

where μ_{ex} is the reduced mass of the electron and hole and ϵ is the permittivity. Similarly, the exciton radius can be shown to be:

$$a_{ex} = \frac{4\pi\hbar^2\epsilon_{GaAs}}{\mu_{ex}e^2}. \tag{2.5}$$

Excitons can generally be divided into Fresnel excitons and Wannier excitons depending on how strong the electron and hole are coupled. The Fresnel excitons are found in materials with a small dielectric constant where the electrons and holes are tightly bound. This causes the excitons to be small in size - of the order of a unit cell of the crystal. Alternatively, Wannier-Mott excitons are found in materials with a large dielectric constant. In these materials, there is less coupling between the electrons and the holes. This causes the electrons and holes to orbit around each other over several unit cells and, as a result, the radius of the exciton is larger than the unit cell.

Using Equation (2.5), we can calculate the size of the exciton and compare it to the lattice size to determine which limit we should use. For a bulk GaAs structure, the static dielectric constant near absolute zero is 12.7 and the reduced mass is $0.059m_e$, where m_e

is the electron mass[30]. Using this, we calculate the Bohr radius to be 11.4 nm while the lattice spacing for GaAs is 0.56 nm. This puts the excitons in the Warnier-Mott limit.

2.2 QUANTUM DOTS

Quantum dots (QDs) are nanocrystals which are a few nanometers wide in all three directions. Unlike a quantum well which offers confinement along only one axis, in a QD, the excitons are confined in all directions, effectively making them zero-dimensional (0D) particles. QDs display electronic and optical properties which are between that of a molecule and bulk semiconductor.

The de Broglie wavelength of the exciton is given by $\lambda = h/\sqrt{2\mu_{\text{ex}} k_B T}$ where μ_{ex} is the effective mass of the exciton. If the QD diameter is smaller than the exciton wavelength we find a dependence of their quantized energy level on the quantum dot size. The density of states of a QD is given as

$$\rho(E) = \sum_{n_x, n_y, n_z} 2\delta(E - E_{n_x, n_y, n_z}), \tag{2.6}$$

where E_{n_x, n_y, n_z} are the confined energies of the carrier characterized by the indices n_x, n_y and n_z (Figure 2). This is similar to that of an atom. Thus, although a QD is made up of many thousands of atoms, it can be treated like an artificial atom.

QDs are fabricated through many different processes - the more popular being colloidal synthesis and self assembly. Colloidal quantum dots[32] are created through a chemical process in which a precursor compound is dissolved in a solvent under heat. The precursor nucleates and generates a nanocrystal; the size control arises from quenching the reaction, e.g., by cooling.

A popular technique used in the self-assembled process is the Stranski-Krastanov growth technique[33]. In this technique, the sample is grown in layers. Islands are spontaneously formed due to strains in the monolayers and incomplete wetting of the surface - i.e., droplets are formed on the surface. The QD material nucleates around these islands and the unwanted material is dissolved in a suitable solvent by in-situ etching. In our studies, we used

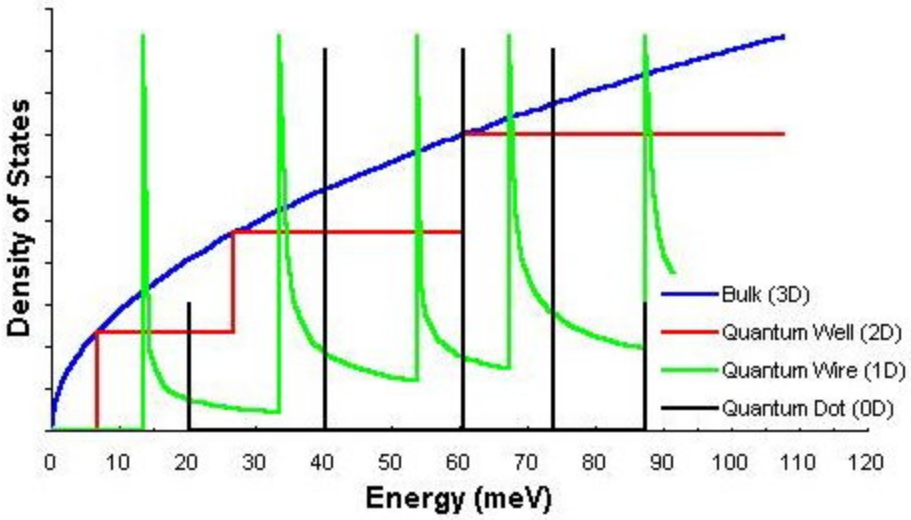

Figure 2: Density of States in semiconductors in 0D (quantum dots), 1D (quantum wires), 2D (quantum wells) and 3D (bulk) as a function of energy. We can see that as we reduce the number of degrees of freedom of the electron, the energy spectrum becomes more discrete[31].

hierarchically self-assembled GaAs/$Al_xGa_{1-x}As$ QDs grown by molecular beam expitaxy and in-situ etching of InAs. The fabrication process is elaborated in Section 2.4.

The lowest electronic transition in a QD is inversely proportional to the square of the length of a quantum dot. Thus, the energy of the photon emitted by the QD due to recombination can be tuned by changing the size of the QD. This property of the QD is used in various applications such as LEDs, photovoltaics, solid state lighting, etc[34, 35, 36]. QDs also have higher density of states due to which they are used in diode lasers and biological sensors.

The spin of the electrons in a QD can be controlled with the help of external magnetic fields. The flow of electrons can be controlled by applying voltages across the QD and the precise spin can be measured and controlled. These features make QDs interesting for applications in quantum computation and quantum information. In Chapter 4, we study the spin flip time of the electrons and holes in the QDs.

Quantum dots are studied for their applications in quantum information processing[37,

38] and quantum computing[39], both of which require a knowledge of the spin flip times of the excited electrons in these quantum dots[40, 41]. Spin flip also implies decoherence since the spin flip must involve a phonon which adds or carries away angular momentum[42, 43, 44]. A measure of this spin-flip time is of great interest to any quantum information scheme which requires coherence to be maintained in the excited states of quantum dots[45, 46, 47].

2.3 POLARITONS

Exciton-polariton condensates were first observed in the mid-2000s[48, 26] after which various aspects of Bose-Einstein condensation in polaritons such as quantized vortices[49, 50, 51], the Bogoliubov moving solitons of polariton condensates[52, 53, 54], Josephson junction oscillations[55, 56], etc.. were studied and the coherence properties of the condensate were measured[57]. In this thesis I investigate the possibility of increased absorption of a beam at half the energy of the condensate by the presence of the condensate.

An exciton-polariton is a quantum superposition of light and matter. In our studies photons are trapped inside a microcavity, and matter, in the form of excitons, is trapped in a quantum well. The semiconductor microcavity is formed by a Fabry-Perot cavity sandwiched between two sets of distributed Bragg reflectors. Our quantum wells are placed inside this cavity. While the study of light-matter interactions has been around for more than a century[58], we required the formulation of second quantization to fully understand and propose the existence of the microcavity polaritons[59]. The first microcavity polaritons were observed two decades ago[60] and since then we have used these polaritons to create condensates[26, 48], polariton lasers[61], etc..

In order to understand the theory behind exciton-polaritons, we start by studying the individual components which make up the polariton, namely, the quantum wells, and the distributed Bragg reflectors, followed by a study of the conditions under which they undergo quantum superposition with photons to form the polaritons.

2.3.1 Quantum wells

A quantum well (QW) is a structure in which the exciton is confined along one axis but is free to move along the other two axes. Hence, the QWs are referred to as two-dimensional (2D) structures. Modern growth techniques allow us to control the thickness of the layers grown on a surface. QWs are formed when a thin layer of semiconductor is sandwiched between two layers of a different semiconductor with wider band gap in a type I band alignment. If the energy level spacing is $\Delta E >> k_B T$, we have quantum confinement and the density of states become discrete as shown in Figure 2.

In our samples, we have GaAs layers between AlGaAs layers. These two materials are chosen because they have similar lattice constants - GaAs and AlAs have lattice constants of 5.660 Å and 5.653 Å respectively). This helps reduce lattice mismatch, which could lead to strain in the sample. Due to the difference in the band-gap energies of the two materials, they form a quantum well. Further, at non-zero in-plane momentum, we observe splitting of the highest valance band. This results in holes with different masses which we call the light hole and heavy hole. This leads to different confinement energies - the light hole having a higher confinement energy than the heavy hole. In our samples, the difference in confinement energies is ~ 30 meV and hence we ignore the occupation of the light hole states. A schematic of the GaAs band structure is given in Figure 3.

2.3.2 Distributed Bragg reflectors

Distributed Bragg reflectors (DBRs) are high quality reflectors which are formed by stacking alternate layers of two materials with different refractive indices. The thickness of these layers are constant and chosen to have a thickness of $\frac{\lambda}{4}$, where λ is the wavelength we wish to reflect. Because of their highly selective reflectivity, DBRs are used in optical fibers, VCSELs, and other laser diodes.

When light travels from a material with a lower refractive index to a higher refractive index, it undergoes a phase shift. However, this is not the case when light travels from a material of higher to lower refractive index. DBRs exploit this phenomena to reflect light to a high degree. A typical DBR schematic is given in Figure 5.

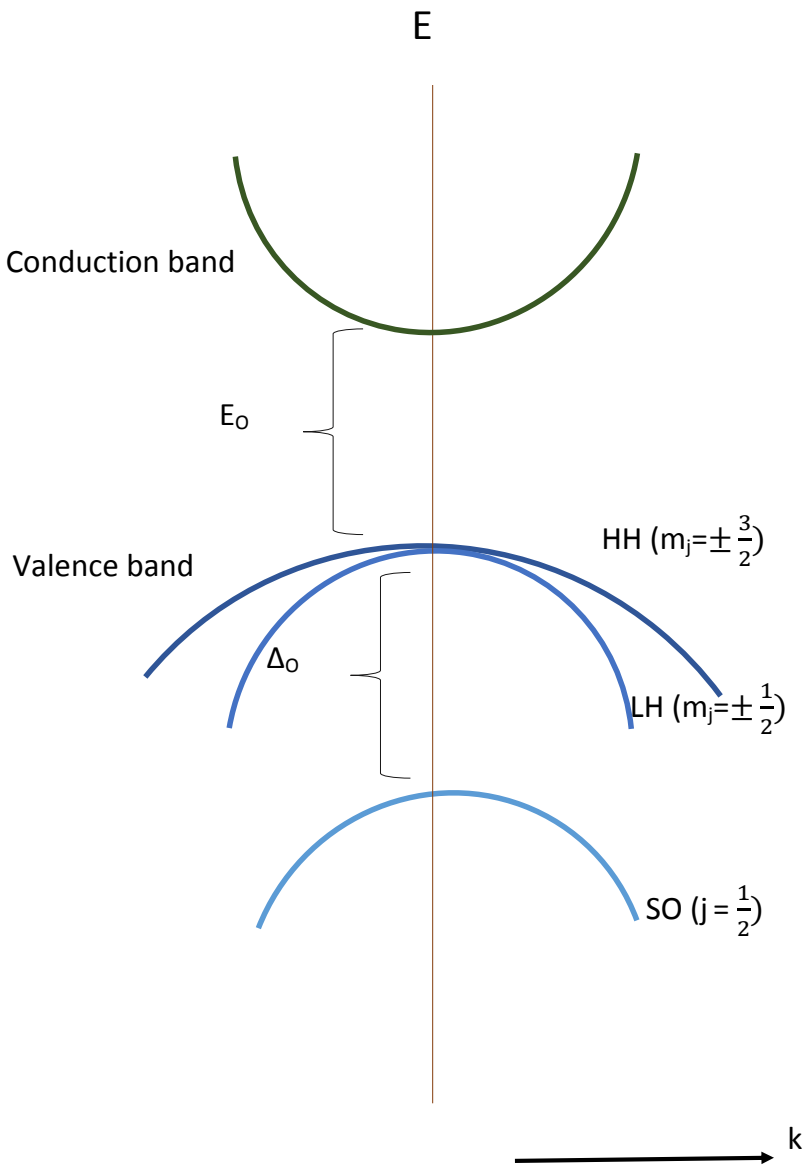

Figure 3: Sketch of the band structure of GaAs close to the fundamental gap.

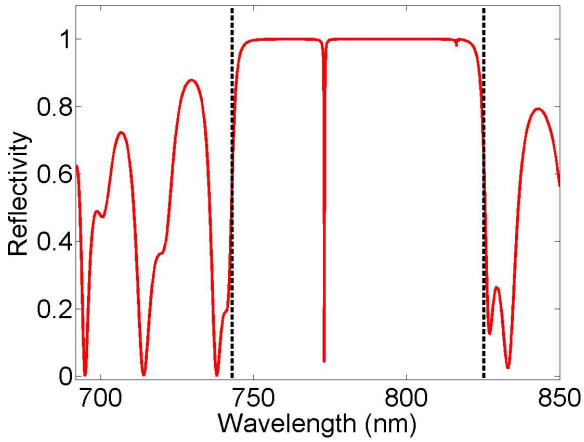

Figure 4: Calculated reflectivity spectrum of a microcavity sandwiched between two stacks of Bragg reflectors. The spectrum between the dashed lines is the stopband[62].

There are alternating layers of two materials with different refractive indices - n_1 and n_2, where $n_2 > n_1$. When light is incident on the first boundary and goes from n_1 to n_2, a fraction of the beam reflects back and undergoes a π phase shift. However, at the next boundary a fraction of the beam is reflected, but there is no phase shift since it is traveling from a material with higher refractive index to a material with lower refractive index. The beam reflected off the second surface travels an additional distance of $2\frac{\lambda}{4}$ before it meets up with the beam reflected off the first surface and the two beams are in phase with each other and add constructively. Similarly, the beams reflected off the third, fourth, etc. surfaces add constructively. Thus, even though only a part of the beam is reflected off each surface, we will have perfect reflection if we have an infinite system. The range of wavelengths reflected is called the stopband. A typical reflectivity spectrum of our samples is given in Figure 4.

Since it is impossible to have an infinite number of layers, the reflectivity of a stack of DBRs depends on the number of layers we use. In our design the reflectivity is greater than 99.99%. To form an optical cavity, we use two sets of DBRs and place them a certain distance apart. If the distance of separation between them is $n\lambda/2$, where $n = 1, 2$, etc.. , a photon which leaks through with a transmission probability of less than 0.01% bounces off

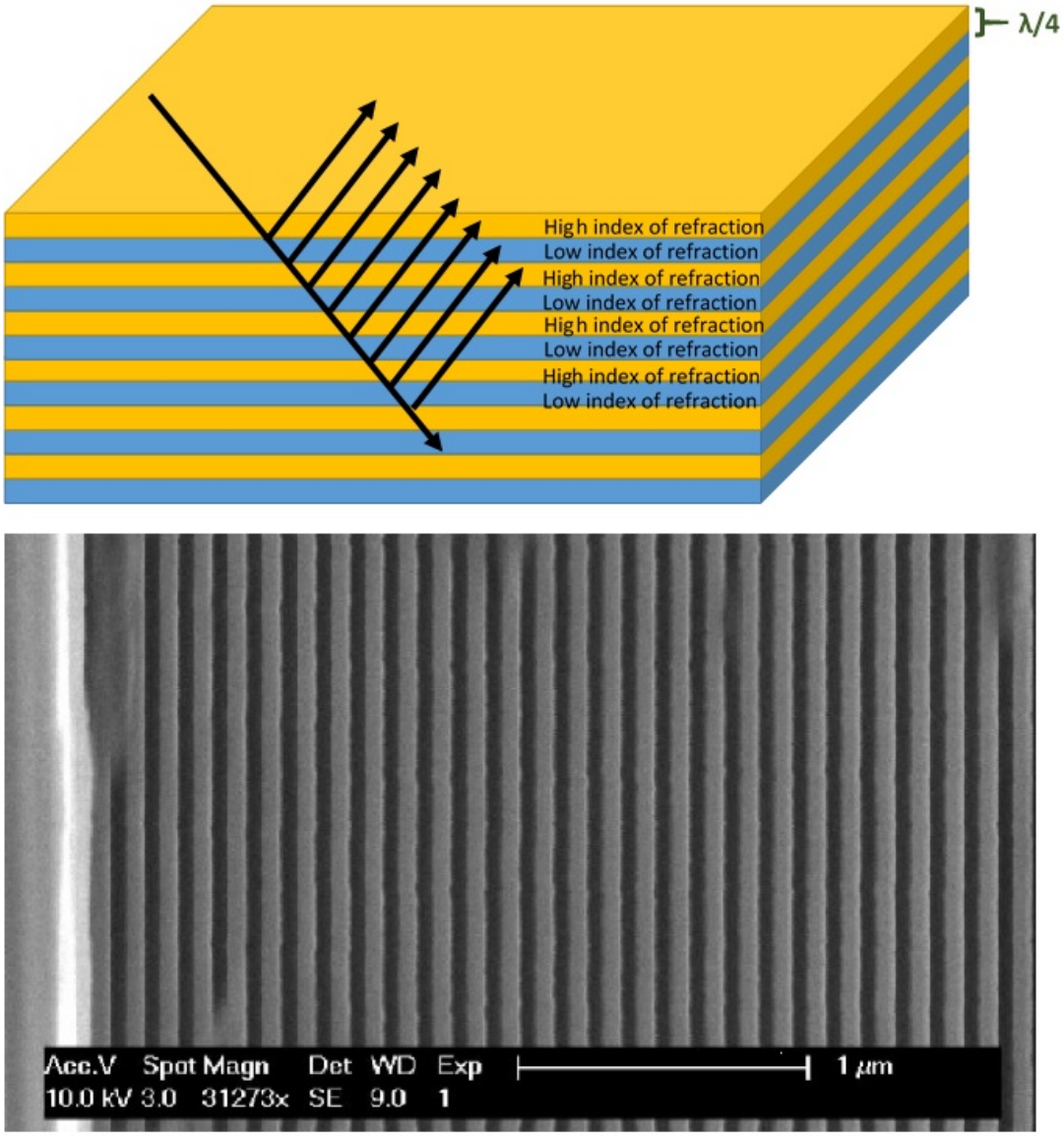

Figure 5: a) Schematic representation of a distributed Bragg reflector. There are two materials of different refractive indices each with a thickness $\lambda/4$. The phases of the reflected beam add up such that for an infinite number of layers, we get a perfect reflectivty. b) Scanning Electron Microscope image of our DBRs. We have layers of $Al_xGa_{1-x}As$ sandwiched between layers of AlAs[62].

the back mirror and creates a standing wave between the two sets of mirrors. This photon is referred to as the cavity photon.

Depending on the separation between the two mirrors and the wavelength of the photon trapped between the mirrors, we have n antinodes of the photon. By placing our quantum wells at these anti-nodes, we enhance the creation of the exciton. As further discussed in Chapter 2, the DBRs in our samples have a transmission $< 10^{-4}$ in the stop band.

2.3.3 Quantum superposition

The quantum wells trap the electron and hole which form the exciton, and the distributed Bragg reflectors confine the photons along the same axis as the exciton trap. If these quantum wells are placed at the antinodes of the cavity photons, the cavity photons couple to the dipole moment of the excitons in the quantum well and form a quantum superposition of the exciton and the photon. This leads to the formation of two new quasiparticles - the upper and lower polaritons.

The Hamiltonian of the cavity photon and the exciton are

$$H_{ph} = E_{ph} a_k^+ a_k, \tag{2.7}$$

and

$$H_{ex} = E_{ex} b_k^+ b_k, \tag{2.8}$$

respectively. Here, E_{ph} is the energy of the cavity photon and a_k^+ and a_k are the creation and destruction operators of the photon. Similarly, E_{ex} is the energy of the exciton and b_k^+ and b_k are the creation and destruction operators of the exciton.

In the rotating wave approximation, the Hamiltonian of this new state can be written as

$$H_{pol} = H_{ph} + H_{ex} + H_I \tag{2.9}$$

where H_I is the interaction Hamiltonian. If Ω is the coupling constant, the interaction Hamiltonian is given by

$$H_I = \Omega(a_k^+ b_k + b_k^+ a_k) \tag{2.10}$$

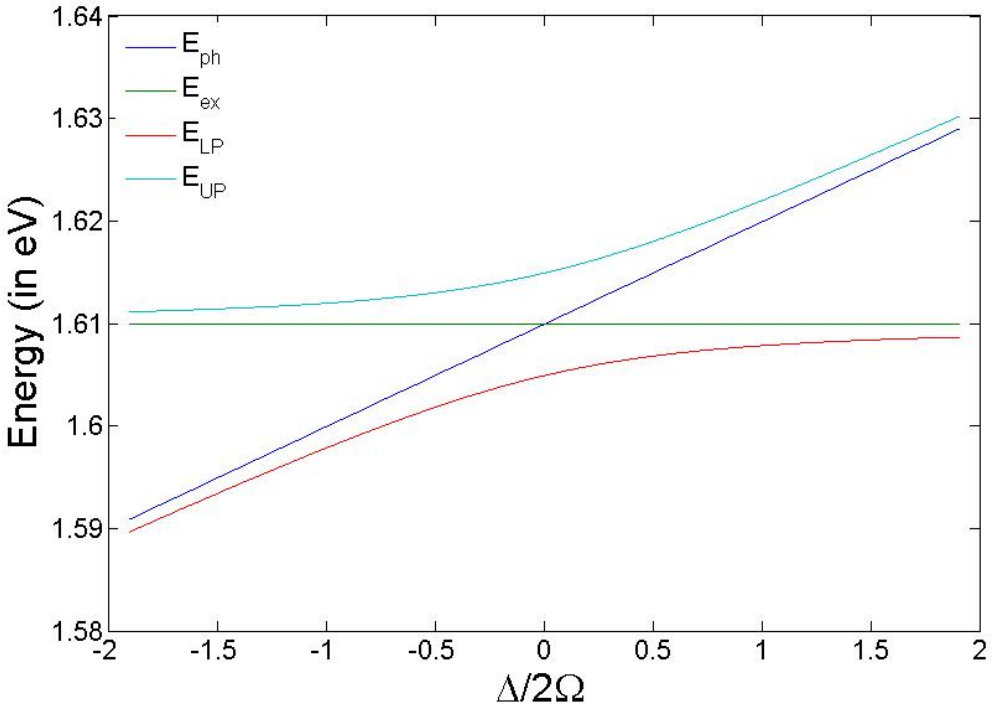

Figure 6: We use a wedge cavity for our experiments where as we change the position on the sample, the energy of the cavity photon changes which results in a change in energy of the upper and lower polariton.

Thus,

$$H_{pol} = E_{ph}a_k^+ a_k + E_{ex}b_k^+ b_k + \Omega(a_k^+ b_k + b_k^+ a_k). \tag{2.11}$$

Using the transformations

$$P_k = X_k b_k + C_k a_k \tag{2.12}$$

$$Q_k = -C_k b_k + X_k a_k, \tag{2.13}$$

we can write the Hamiltonian as:

$$H_{pol} = \sum E_{LP} P_k^+ P_k + \sum E_{UP} Q_k^+ Q_k. \tag{2.14}$$

Here, E_{LP} and E_{UP} are the energies of the lower and upper polaritons, respectively, and C_k and X_k are the Hopfield co-efficients, which satisfy the condition $\mid C_k \mid^2 + \mid X_k \mid^2 \ = 1$. Diagonalizing the Hamiltonian gives us the energies of the upper and lower polaritions to be:

$$E_{\substack{UP \\ LP}} = \frac{(E_{ex} + E_{ph})}{2} \pm \frac{\sqrt{(E_{ex} - E_{ph})^2 + 4\Omega^2}}{2}. \tag{2.15}$$

When $\Delta E = E_{ex} - E_{ph} = 0$, then $E_{UP} - E_{LP} = 2\Omega$ and the polaritons are exactly half photon and half exciton and it is said to be at resonance and there is a strong coupling between the photon and exciton. ΔE is the energy detuning between the exciton and photon. When $\mid \Delta E \mid >> \Omega$, the polaritons become nearly a pure photon or a pure exciton[22]. In our sample we use a wedge cavity which gives us a gradient in the energy of the photon across the sample. Thus, the energy of the polaritons varies across the sample and we can look at the region where the energy of the photon is near the energy of the exciton. One of the engineering challenges is to obtain strong coupling between the photon and the exciton. We discuss the sample we use in more detail in Section 3.3.2.

2.3.3.1 Dispersion relationship of polaritons: As shown in Figure 7, near resonance, the exciton and the photon dispersion curves turn into two new dispersion curves of the upper and lower polaritons. At low $k_{||}$, when $\hbar^2 k^2 / 2m_{ph} << \Omega$, the dispersion relationship is parabolic since

$$E_{LP,UP}(k_{||}) \simeq E_{UP,LP}(0) + \frac{\hbar^2 k^2}{2m_{LP,UP}}. \tag{2.16}$$

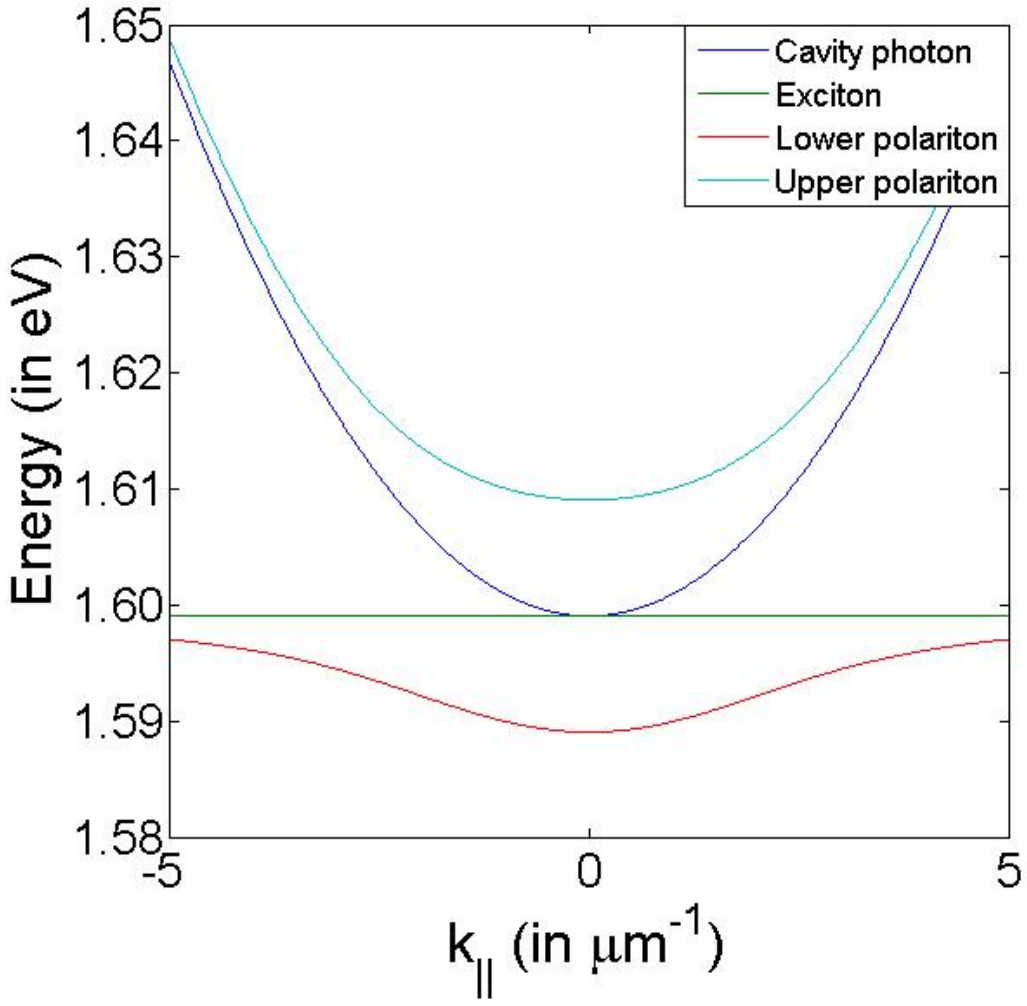

Figure 7: Dispersion relation of the photon, exciton and the polaritons. Near resonance, at $k_{||} \approx 0$, we see that the dispersion curve is parabolic and the effective mass of the LP is small. As $k_{||}$ increases, the LP becomes more like an exciton and its effective mass approaches that of an exciton.

The effective mass of the polaritons is given by the weighted effective mass of the exciton and photon and is[22]

$$\frac{1}{m_{LP}} = \frac{\mid X^2 \mid}{m_{ex}} + \frac{\mid C^2 \mid}{m_{ph}} \tag{2.17}$$

$$\frac{1}{m_{UP}} = \frac{\mid C^2 \mid}{m_{ex}} + \frac{\mid X^2 \mid}{m_{ph}} \tag{2.18}$$

Since $m_{ex} >> m_{ph}$,

$$m_{LP} \approx \frac{m_{ph}}{\mid X^2 \mid} \sim 10^{-4} m_{ex} \tag{2.19}$$

$$m_{UP} \approx \frac{m_{ph}}{\mid C^2 \mid}. \tag{2.20}$$

where the m_{ph} is typically of the order of 10^{-5} m_e.

As shown in Figure 7, at small $k_{||}$, the effective mass of the LP is $\sim 10^{-4}$ m_e. However, as we increase $k_{||}$, the LP becomes more like a exciton and the effective mass approaches that of the bare exciton[22]. This helps in phase transitions as discussed in Section 2.4. However, when $\Delta E >> \Omega$, the $m_{LP} \approx m_{ex}$ and the LP behaves like an exciton.

2.4 BOSE-EINSTEIN CONDENSATION

Particles with a integer spin, such as a polariton, are called "bosons". Unlike the fermions (particles of half-integer spin) which follow Pauli's exclusion principle which forbids two fermions from being in the same state, multiple bosons can occupy the same state. At low temperatures, a macroscopic number of bosons can enter a single energy state. Such a phenomenon is called the Bose-Einstein condensation (BEC). BEC occurs below a "critical temperature", denoted by T_c, or, when the density of particles is above a critical density, n_c. When the particles undergo condensation, coherence of the particle wavefunction is maintained at a distance much larger than the particle separation, and there is a highly

ordered phase. Since the particles are in phase with each other, the quantum nature of these particles is amplified, which results in a change in their theromodynamic properties as well.

BEC in ideal gases has been discussed in various books and review papers[28, 63, 64]. In the following section we will discuss BEC for microcavity polaritons.

2.4.1 BEC in microcavity polaritons

Since the spin of a photon is $\pm$ 1 and the spin of an exciton is $0, \pm$ 1, a polariton has an integer spin and is a boson. The behavior of a polariton is described with the help of Bose-Einstein statistics.

The critical density to achieve BEC in a 3D Bose gas is given as[28]

$$n_c = \frac{2.612}{\lambda_{dB}^3} \tag{2.21}$$

where λ_{dB} is the thermal de Broglie wavelength and is given by

$$\lambda_{dB} = \left(\frac{2\pi\hbar^2}{mk_BT}\right)^{\frac{1}{2}}. \tag{2.22}$$

Above the critical density, all the particles are forced into the ground state. This essentially tells us that as the temperature decreases, the de Broglie wavelength of a particle increases until the wavelengths are comparable to the spacing between the particles. At this point, the wavefunctions start to overlap and eventually merge into a single wavefunction with a macroscopic number of particles in it.

In our case, we are interested in microcavity polaritons which are two-dimensional. For a 2D system ($A = L^2$) the density of states is given as[65]

$$\rho_{2D}(\epsilon_k) = \frac{dN_k}{dk}\frac{dk}{d\epsilon_k} = \frac{Am}{2\pi\hbar^2} \tag{2.23}$$

where m, the mass of the polaritons, is $\approx 10^{-4} m_e$.

The energy distribution function is given as[66]

$$f_B(k, T, \mu) = \frac{1}{\exp\left(\frac{\epsilon(\mathrm{k})-\mu}{\mathrm{k_B T}}\right) - 1} \tag{2.24}$$

and the total number of particles in the excited states at a temperature T is given as

$$N_T = \int_0^\infty f_B(k, T, \mu)\rho_{2D}(\epsilon_k)d\epsilon \tag{2.25}$$

Substituting Equation (2.23) and Equation (2.24) in the above equation, we obtain

$$N_T = \frac{Am}{2\pi\hbar^2}\int_0^\infty \frac{1}{\exp\left(\frac{\epsilon(\mathrm{k})-\mu}{\mathrm{k_B T}}\right)-1}d\epsilon \tag{2.26}$$

which diverges except at $T = 0$. This tells us that at non-zero temperature, μ doesn't go to zero, which means that at $T > 0$, we can never achieve a true BEC since the low energy states are able to include all the particles and the occupation of the individual states is negligible compared to the total number[67].

However, at low temperatures we can see the appearance of "quasi-condensates" where the spatial coherence length is larger than the size of the system. As we increase the temperature, we see the system transition into an incoherent system as the coherence length decreases. However, if we decrease the temperature, we see a transition to a superfluid state given by the Berezinski-Kosterlitz-Thouless phase transition[68].

The situation changes drastically if we use a harmonic potential to trap the polaritons. We create a Harmonic trap using methods described in Chapter 7. This gives us a harmonic potential given by $V = \alpha r^2$ and the density of states is now given as

$$\rho_{2D}(\epsilon_k) = \frac{Am}{\alpha\hbar^2}\epsilon \tag{2.27}$$

where the total number of particles is

$$N_T = \frac{Am}{\alpha\hbar^2}\int_0^\infty \frac{\epsilon}{\exp\left(\frac{\epsilon(\mathrm{k})-\mu}{\mathrm{k_B T}}\right)-1}d\epsilon \tag{2.28}$$

where the integral can be solved as μ approaches 0.

Thus for a harmonic trap potential, the critical polariton number is given as

$$n_C = \frac{m\pi^2}{12\hbar^2\alpha}(k_B T_C)^2 \tag{2.29}$$

While it is true that a harmonic oscillator has discrete energy levels and is thus not strictly in the thermodynamic limit, in the 2-D harmonic oscillator case it is possible to achieve a density above the critical density. The 3-D case also has a finite number of atoms, since there is no true infinite 3-D system and can have only a finite occupation. Thus, we can say that the 2-D harmonic oscillator case is fundamentally the same as a finite 3-D system. In both cases, there is a macroscopic occupation, but neither case has a delta function occupation number at a given energy.

2.5 FERMI'S GOLDEN RULE

First order time-dependent perturbation theory tells us that for a Hamiltonian of the form $H = H_0 + V_{int}$, with an eigenstate of $|\psi_t\rangle$, the Schrodinger equation can be written as[28]

$$i\hbar\frac{\partial}{\partial t}|\psi(t)\rangle = V_{int}(t)|\psi(t)\rangle \tag{2.30}$$

Here, $|\psi(t)\rangle = e^{iH_0t/\hbar}|\psi_t\rangle$. Integrating the above equation on both sides and writing the first-order expansion in time where $|\psi(t')\rangle \approx |\psi(t_0)\rangle$, we obtain

$$|\psi(t)\rangle = \left(1 + \frac{1}{i\hbar}\int_{t_0}^{t} V_{int}(t')dt'\right)|\psi(t_0)\rangle \tag{2.31}$$

By substituting repeatedly back into Equation (2.30), we obtain

$$|\psi(t)\rangle = \left(1 + \frac{1}{i\hbar}\int_{t_0}^{t} V_{int}(t')dt' + \frac{1}{(i\hbar)^2}\int_{t_0}^{t} dt' \int_{t_0}^{t} dt'' V_{int}(t')V_{int}(t'') + ...\right)|\psi(t_0)\rangle \tag{2.32}$$

This can be written as

$$|\psi(t)\rangle = e^{-(i/\hbar)\int dt V_{int}(t)}|\psi(t_0)\rangle \tag{2.33}$$

Suppose the system is in a state i at time t_0, then the probability amplitude of being in a state n at time t is

$$\langle n|\psi(t)\rangle = e^{-(i/\hbar)E_n t}\langle n|\psi(t)\rangle \tag{2.34}$$

Substituting the form of $|\psi(t)\rangle$ from Equation (2.33), we obtain

$$\langle n|\psi(t)\rangle = e^{-(i/\hbar)E_n t}\frac{1}{i\hbar}\langle n|V_{int}|i\rangle \int_0^t e^{(1/\hbar)(E_n - Ei)t'}dt' \tag{2.35}$$

We obtain the total probability of being in the state n by squaring the probability amplitude and obtain

$$\begin{aligned} |\langle n|\psi(t)\rangle|^2 &= \frac{1}{\hbar^2}|\langle n|V_{int}|i\rangle|^2 \left| \int_0^t e^{(1/\hbar)(E_n - Ei)t'}dt' \right|^2 \\ &= \frac{1}{\hbar^2}|\langle n|V_{int}|i\rangle|^2 \left| \frac{e^{(1/\hbar)(E_n - E_i)t} - 1}{(i/\hbar)(E_n - E_i)} \right|^2. \end{aligned} \tag{2.36}$$

Thus the probability of being in a final state $|n\rangle$ at time t is

$$|\langle n|\psi(t)\rangle|^2 = |\langle n|V_{int}|i\rangle|^2 \frac{\sin^2[(\mathrm{E_n} - \mathrm{E_i})\mathrm{t}/2\hbar]}{[(E_n - E_i)/2]^2}. \tag{2.37}$$

If there are a number of final states we could transition into, the total probability is determined by summing over all the possible final states. If the density of states is given by $D(E)$, we get

$$\sum_n |\langle n|\psi(t)\rangle|^2 = \frac{2\pi t}{\hbar}|\langle n|V_{int}|i\rangle|^2 D(E_n)\Big|_{E_n = E_i}. \tag{2.38}$$

Writing the density of states in the form of a delta function, we obtain the rate of transition from the initial state to the final state as

$$\frac{\partial}{\partial t}|\langle n|\psi(t)\rangle|^2 = \frac{2\pi}{\hbar}|\langle n|V_{int}|i\rangle|^2 \delta(E_n - E_i). \tag{2.39}$$

The above equation is known as Fermi's golden rule. For a coherent system, the eigen states can be represented in terms of Fock states. In this case, V_{int} can be written in terms of the creation and destruction operators. We note that for a transition from the initial state to the final state, the N_i state is one photon less and N_f state has one photon more. In other words, $|i\rangle = |N_1, N_2, ...N_i, ...N_f, ...\rangle$ and $|f\rangle = |N_1, N_2, ...N_i - 1, ...N_f + 1, ...\rangle$. Inserting this into Fermi's golden rule we obtain

$$\frac{\partial}{\partial t}|\langle n|\psi(t)\rangle|^2 = \frac{2\pi}{\hbar}|A_{i,f}|^2(1 + N_f)(N_i)\delta(E_n - E_i). \tag{2.40}$$

Here $A_{i,f}$ tells us the strength of interaction between these two states. The term $(1+N_f)$ describes the stimulated scattering of bosons. If there are N_f particles in the final state, then the rate of transition into that state is proportional to $(1+N_f)$. As in the case of the BEC, if the number of particles in the final state is large, the rate of scattering into the final state increases tremendously.

In the derivation of Fermi's golden rule, we have made two assumptions about the time scales involved. On the one hand, in order to apply first order perturbation theory, we assumed that the time involved was short. However, in the derivation of Fermi's golden rule, we assumed that $t >> \hbar/\Delta E$. The time involved needs to be long compared to the energy scale under observation, but it shouldn't be so long that the final state gets completely depleted. While this seems contradictory, it is possible for both these conditions to be met for an intermediate time scale.

2.6 TWO-PHOTON EXCITATION

Generally, when two photons simultaneously interact with a material, various processes can occur. We are particularly interested in two processes. In the first process, the two photons can be simultaneously absorbed by the material they are incident on and an electronic transition equal to twice the energy of the photons could occur. The absorbed energy is later re-emitted. This process is called two-photon absorption. In the second process, the two-photons incident on the material could directly convert into a third photon with twice the energy. This process is called second harmonic generation.

2.6.1 Two-photon absorption

The simultaneous absorption of two photons to produce a transition is called two-photon excitation. This leads to an excitation of a particle to a higher energy state where the energy difference is twice the energy of the photon we are exciting with. Two-photon absorption is a nonlinear process where the absorption is proportional to the square of the input intensity

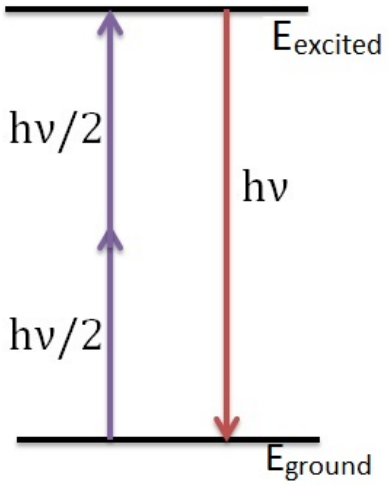

Figure 8: Illustration of two photon absorption. It two photons with energy equal to half the energy gap are used to excite the particle from the ground state to the excited state.

and hence is favored by a highly intense incident beam. Recently, two-photon excitation of quantum dots and exciton-polaritons has gained attention[66, 69, 70] for its possible application in polariton lasers[66, 71, 72].

Two-photon excitation is a nonlinear process (as opposed to single-photon excitation, which goes linearly with the intensity of the input beam). In our experiment, we use a pulsed femtosecond laser with 250 kHz repetition rate to achieve the required intensity.

Two-photon absorption can be explained by second-order perturbation theory[73, 74]. The Hamiltonian is

$$H = H_o + V(t) \tag{2.41}$$

where H_o is the unperturbed Hamiltonian for a free atom, $V(t) = -er\mathbf{E}(\mathbf{t})$ is the perturbation and $\overrightarrow{E}(\mathbf{t}) = \mathbf{E_0}(e^{i\omega t} + e^{-i\omega t})/2$ is the electric field. We assume that the solution to the Schrodinger equation for a free atom can be written in the form $\psi_n(\mathbf{r}, t) = u(\mathbf{r})e^{-iE_n t/\hbar}$. The time dependent Schrodinger equation is now

$$i\hbar\frac{d\psi(t)}{dt} = (H_0 + V(t))\psi(t) \tag{2.42}$$

The solution for this equation can be in the following form

$$\psi(\mathbf{r},t) = \sum_l a_l(t)u_l(\mathbf{r})e^{-iE_lt/\hbar} \tag{2.43}$$

Subsituting the above equation back into Equation (2.42), and using the orthonormality conditions, we get

$$i\hbar\frac{da_m(t)}{dt} = \sum_l a_l(t)V_{ml}(t)e^{-i(E_m-E_l)t/\hbar} \tag{2.44}$$

where $V_{ml} = \langle u_m|V|u_l\rangle$. The coefficients can be expanded perturbatively as

$$a_l(t) = a_l^{(0)}(t) + \lambda a_l^{(1)}(t) + \lambda^2 a_l^{(2)}(t) + .. \tag{2.45}$$

where we use λ as a tool to keep track of our coefficients.

In the above equation, the first and second approximations represent one-photon absorption and two-photon absorption respectively. Since we are interested in two-photon absorption, we will concentrate on that coefficient. We write V_{ml} as λV_{ml} in Equation (2.44) in order to solve it perturbatively and equate the powers of λ to get

$$i\hbar\frac{da_m^{(N)}(t)}{dt} = \sum_l a_l^{(N-1)}(t)V_{ml}(t)e^{-i(E_m-E_l)t/\hbar}. \tag{2.46}$$

Substituting for V_{ml} and integrating, we get

$$a_m^{(1)} = \frac{\langle m|er\mathbf{E}|g\rangle}{\hbar(\omega_{mg}-\omega)}(e^{i(\omega_{mg}-\omega)t}-1) + \frac{\langle m|er\mathbf{E}|g\rangle}{\hbar(\omega_{mg}+\omega)}(e^{i(\omega_{mg}-\omega)t}-1) \tag{2.47}$$

where g represents the ground state, m represents the excited state, and ω is the energy of the photon. Here, the first term represents single-photon absorption while the second term represents single-photon stimulated emission.

Solving again to calculate the two-photon case,

$$a_f^{(2)} = \sum_m \frac{\langle f|er\mathbf{E}|m\rangle\langle m|er\mathbf{E}|g\rangle}{4\hbar(\omega_{mg}-\omega)}\frac{e^{i(\omega_{fg}-2\omega)t}-1}{(\omega_{fg}-2\omega)} \tag{2.48}$$

where f is the final state and m is the intermediary state. The probability, $p_f^{(2)}(t)$ of finding the particle in state f is

$$p_f^{(2)}(t) = |a_f^{(2)}|^2 = \left|\sum_m \frac{\langle f|er|m\rangle\langle m|er|g\rangle}{4\hbar(\omega_{mg}-\omega)}\right|^2 2\pi t\delta(\omega_{fg}-2\omega)\mathbf{E^4} \tag{2.49}$$

We can see that the transition is possible only if two photons are resonant with the transition energy. We also notice that the transition is proportional to the square of the initial intensity. It is important to remember that two-photon absorption involves the absorption of two photons, unlike second harmonic generation discussed below. Thus luminescence from a system which has undergone two-photon absorption would have a lifetime associated with it.

2.6.2 Second harmonic generation

Second harmonic generation occurs when two photon are incident on a crystal and are converted to a third photon of twice the energy. This nonlinear process can be understood from the Maxwell-Bloch equations. If we assume that we can write the electric polarization as a series in powers of the electric field, it is given as[28]

$$P = \chi\epsilon_0 E + 2\chi^{(2)}E^2 + 4\chi^{(3)}E^3 + ..., \tag{2.50}$$

where P is the polarization, E is the electric field, χ is the susceptibility, ϵ_0 and μ_0 are the universal free space permittivity and permeability constants respectively.

The current density, J can be written in terms of the polarization vector as $J = \frac{\partial P}{\partial t}$. Substituting the polarization vector, as given by Equation (2.50), and expanding to second order, we obtain

$$J = \frac{\partial}{\partial t}(\chi\epsilon_0 E + 2\chi^{(2)}E^2). \tag{2.51}$$

From Maxwell's equations we have

$$\begin{aligned} \nabla \cdot \vec{E} &= \frac{\rho}{\epsilon_0} \\ \nabla \cdot \vec{B} &= 0 \\ \nabla \times \vec{E} &= -\frac{\partial \vec{B}}{\partial t} \\ \nabla \times \vec{B} &= \mu_0\epsilon_0\frac{\partial \vec{E}}{\partial t} + \mu_0\vec{J}. \end{aligned} \tag{2.52}$$

In a typical solid $\rho = 0$ since there is no net charge. Using Maxwell's equations and the vector identity $\nabla \times \nabla \times \vec{A} = \nabla \cdot (\nabla \cdot \vec{A}) - \nabla^2 \vec{A}$, we obtain

$$\nabla^2 E - \mu_0 \epsilon_0 \frac{\partial^2 E}{\partial t^2} = \mu_0 \frac{\partial J}{\partial t}. \tag{2.53}$$

Substituting current density as given by Equation (2.51) in Equation (2.53) and expanding to second order we get

$$\frac{\partial^2 E}{\partial x^2} = \frac{(1+\chi)}{c^2}\frac{\partial^2 E}{\partial t^2} + 4\mu_0 \chi^{(2)} \left(\left(\frac{\partial E}{\partial t} \right)^2 + E \frac{\partial^2 E}{\partial t^2} \right). \tag{2.54}$$

Next, we assume that the solution for E is of the form

$$E = E_0(x) e^{i(kx - \omega t)} + E_2(x) e^{i(k_2 x - \omega_2 t)}, \tag{2.55}$$

where $\omega_2 = 2\omega$ and $E_2 << E$.

Since $\chi^{(2)}$ is also small, we can neglect all terms that contain $E_2 \chi^{(2)}$. Substituting this form of the electric field into Equation (2.54), we obtain

$$\frac{\partial^2 E}{\partial x^2} = -\frac{n^2}{c^2}\omega^2 E_0(x) e^{i(kx-\omega t)} - \frac{n^2}{c^2}\omega_2^2 E_2(x) e^{i(k_2 x - \omega_2 t)} - 8\mu_0 \chi^{(2)} \omega^2 E_0^2(x) e^{2i(kx - \omega t)}. \tag{2.56}$$

The left hand side of the equation, i.e, the second order spatial derivative of the electric field is given by

$$\begin{aligned} \frac{\partial^2 E}{\partial x^2} = \frac{\partial^2 E_0}{\partial x^2} e^{i(kx-\omega t)} + 2ik\frac{\partial E_0}{\partial x} e^{i(kx-\omega t)} - k^2 E_0(x) e^{i(kx-\omega t)} \\ + \frac{\partial^2 E_2}{\partial x^2} e^{i(k_2 x - \omega_2 t)} + 2ik_2 \frac{\partial E_2}{\partial x} e^{i(k_2 x - \omega_2 t)} - k^2 E_2(x) e^{i(k_2 x - \omega_2 t)}. \end{aligned} \tag{2.57}$$

Combining the above equations and expanding to the first derivative of the electric field, we obtain

$$\begin{aligned} 2ik\frac{\partial E_0}{\partial x} e^{i(kx-\omega t)} + \left(\frac{n^2}{c^2}\omega^2 - k^2 \right) E_0(x) e^{i(kx-\omega t)} + 2ik_2 \frac{\partial E_2}{\partial x} e^{i(k_2 x - \omega_2 t)} \\ + \left(\frac{n^2}{c^2}\omega_2^2 - k_2^2 \right) E_2(x) e^{i(k_2 x - \omega_2 t)} = -8\mu_0 \chi^{(2)} \omega^2 E_0^2(x) e^{2i(kx-\omega t)}. \end{aligned} \tag{2.58}$$

From linear, first order optics we get $\omega = \frac{c}{n}k$, and $\omega_2 = \frac{c}{n}k_2$. Also, in the first order $\frac{\partial E_0}{\partial x} = 0$.

Substituting these in Equation (2.58), we obtain

$$2ik_2\frac{\partial E_2}{\partial x}e^{i(k_2x-\omega_2 t)} = -8\mu_0\chi^{(2)}\omega^2 E_0^2(x)e^{2i(kx-\omega t)}. \tag{2.59}$$

Substituting $\omega_2 = 2\omega$,

$$\frac{\partial E_2}{\partial x} = i\sqrt{\frac{\mu_0}{\epsilon}}\chi^{(2)}E_0^2(x)(2\omega)e^{i(2k-k_2)x}. \tag{2.60}$$

Integrating this for a crystal of length L, and squaring the amplitude, we obtain

$$|E_2(x)|^2 = \frac{\mu_o}{\epsilon}|\chi^{(2)}|^2(2\omega)^2E_o^4L^2\frac{\sin^2\delta kL/2}{\delta kL/2}, \tag{2.61}$$

where $\delta k = 2k - k_2$ and L is the length of the crystal through which the beam propagates. If $\delta k \neq 0$, a phase mismatch occurs. In certain anisotropic crystals, it is possible to obtain $\delta k = 0$ for certain angles. This is called phase matching.

The rate of frequency conversion in this process should be proportional to the probability of the two input photons colliding which will go as the square of the input intensity. Accordingly, we observe from Equation (2.61) that the intensity of the output beam goes as the square of the input intensity. It is important to note that in second harmonic generation, there is no absorption of the incident photons, and the process occurs instantaneously and thus there should be no lifetime associated with the emission.

2.6.3 Selection rules

When a photon is absorbed by a solid, an electron can be excited and go from the valence band to the conduction band. This leads to the creation of two new quasiparticles - an electron and a hole. Since these quasiparticles are made up of equal and opposite charge, they feel a Coulomb force attracting them to each other. If the energies of the particles are low enough, they form a bound state. This bound state is called an exciton.

The total angular momentum is given by $J = L + S$, where L is the orbital angular momentum and S is the spin angular momentum. The eigenvalues of J are given by j,

where $|l - s| \leq j \leq |l + s|$. Here l is the orbital angular momentum quantum number and s is the spin quantum number, respectively. For GaAs, the valence band corresponds to the **p**-orbital which is the $l = 1$ state. Since the spin quantum number is $s = 1/2$, the eigenvalues of the hole are $j = 3/2, 1/2$.

In this system the $j = 1/2$ states have a two-fold degeneracy which corresponds to the "split-off" holes with $m_{j(h)} = \pm 1/2$. The $j = 3/2$ state has a four-fold degeneracy corresponding to the light holes ($m_{j(h)} = \pm 1/2$) and the heavy holes ($m_h = \pm 3/2$). The spin of the electron is $m_{elec} = \pm 1/2$. Thus, the total spin of the exciton is given by $m_{j(ex)} = m_{j(elec)} \pm m_{j(h)} = \pm 2, \pm 1$ and the total angular momentum of the exciton, $J = 2, 1$

The angular momentum of photon is given by $J = \pm 1$. Therefore, while exciting with a single photon, only the $m_{j(ex)} = \pm 1$ states are accessible. These states can also relax to the ground state by emitting a single photon and hence are called the "bright" states. The optically inactive $m_{j(ex)} = \pm 2$ states, i.e., the states that cannot be accessed by exciting with a single photon are called the "dark" states. However, these "dark" states are accessible through a two-photon excitation since $\sigma + \sigma = \pm\ 2$ or 0.

Since the ± 2 excitons cannot relax by emitting a single photon, they primarily relax by turning into J=1 excitons, undergoing a spin flip through the Elliot-Yafet (EY) mechanism[75, 76] or the Dyakonov-Perel mechanism (DP)[77].

If the excition is in the "bright" ± 1 state, a spin flip of either the electron or the hole will result in a transition to the "dark" ± 2 state and vice versa. The coupling between the J=2 state and the J=1 state has been studied by Maialle et al[78].

In our experiments with quantum dots and polaritons, we excite the J=2 "dark" state and study the luminescence from the J=1 "bright" state. The luminescence is time-resolved using a streak camera, allows us to study. This allows us to study the spin flip time between the "dark" and "bright" states.

The Elliot-Yaret mechanism uses inversion symmetry to explain spin relaxation[75, 79, 80, 81]. It proposes that the spin orbit coupling does not split the spin up and spin down states and the two states are degenerate. However, under first-order time perturbation, nearby lying band states can weakly mix the two states. For example, the spin up state is given by $|\uparrow\rangle = a_k|\uparrow\rangle + b_k|\downarrow\rangle$ and $b_k = a_k L/\Delta$, where L is the spin orbit coupling and Δ is

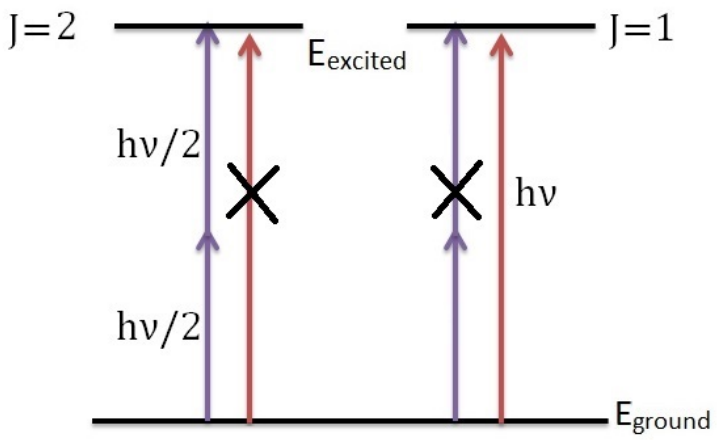

Figure 9: Schematic representation of the selection rules. A two-photon excitation can excite only to the "dark" ($J = 2$) state while a single-photon excitation can only excite to a "bright" ($J = 1$) state.

the splitting between the bands.

An electron can flip its spin with a probability of $(L/\Delta)^2$ when it undergoes scattering. The probability of spin flip increases as the number of scattering events increases and the spin relaxation time is directly proportional to the momentum scattering time.

The Dyankonov-Perel mechanism considers the case where the spin up and spin down states are not degenerate, but split in energy[77, 82]. This occurs in semiconductors without inversion symmetry. The spin orbit coupling causes an effective magnetic field. This magnetic field causes random variations to the direction and magnitude of the spin precession axis. The culmination of many small precessions causes spin relaxation.

3.0 SAMPLES AND EXPERIMENTAL TECHNIQUES

In this chapter we will look at the equipments and various techniques used in this research and the description of general experimental setup. We will also look at the fabrication process of samples used.

3.1 EXPERIMENTAL APPARATUS

The samples were mounted in a cryostat and our experiments were performed at temperatures of 4 to 7 K. A general and simplified experimental setup is as shown in Figure 10. Depending on the experiment performed and quantities measured, the path, shape and properties of the pump and signal beam was modified using components such as lenses, mirrors, filters etc.. However, the basic components such as laser system, cryostat, dichroic mirror, spectrometer, CCD camera and streak camera remained constant for all experiments. I used the beam from a tunable pulsed laser and reflected it off a dichroic mirror onto the sample. The dichroic mirror helped separate the pump beam hitting the sample from the signal emitted by the sample. After spectrally-resolving the signal with the help of a spectrometer, we studied the signal using a Princeton CCD camera as well as a Hamamastu streak camera, which was used to time-resolve the signal.

3.1.1 Laser system

As explained in Section 2.6, two-photon excitation is proportional to the square of the pump beam and typically requires an intense pump beam. Also, we wished to perform time-resolved

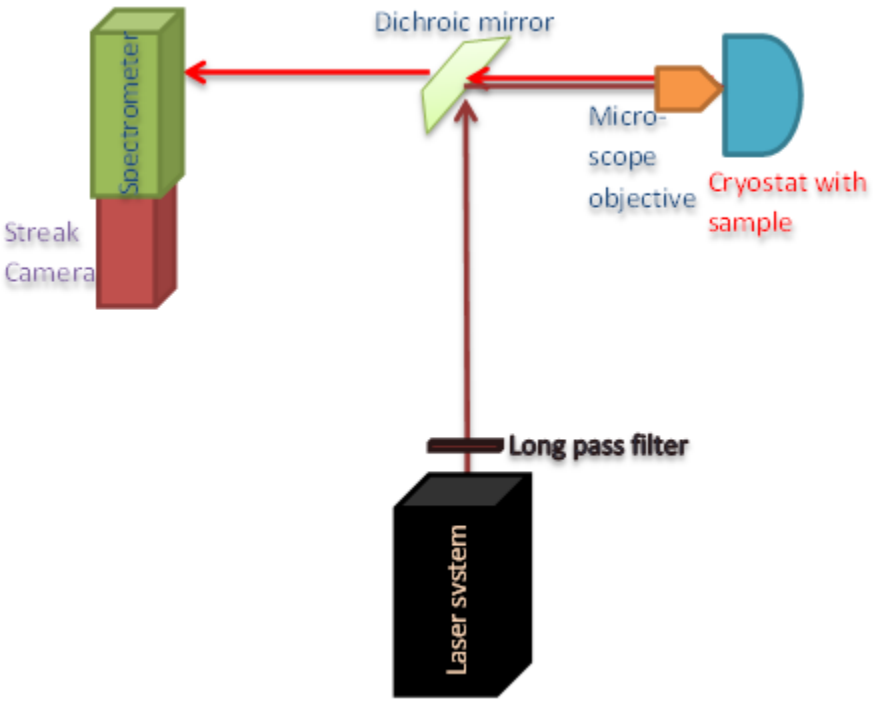

Figure 10: Schematic representation of a simplified experimental setup used for all the experiments in this thesis. While the smaller components such as lenses, mirrors, filters etc.. were changed and tweaked for each individual experiment, the basic components such as laser system, cryostat, dichroic mirror, spectrometer, CCD camera and streak camera remained constant for all experiments.

measurements on a microcavity whose energy varied with position. These measurements required a tunable pulsed laser, which was satisfied by the Coherent femtosecond pulsed laser system. A schematic of the laser system is given in Figure 11.

The laser system consists of four separate lasers, where the output from each laser feeds into the subsequent laser. The pump laser is a high-powered continuous wave (CW) laser - the Verdi V-18. The Verdi is a solid-state diode-pumped, frequency doubled Nd:Vanadate ($Nd:YVO_4$) laser, which produces a monochromatic beam with a wavelength of 532 nm (green). The Nd ion is the gain medium in the Verdi, and there is a lithium triborate (LBO) crystal which acts as a frequency doubler. The Verdi is capable of producing an output of 18 W which is split with a beam splitter and sent into a Titanium:sapphire, mode-locking laser and the regenerative amplifier (RegA).

The Mira is a modelocked, ultrafast laser which uses Titanium:sapphire (Ti:Sapph) as the gain medium. This laser is tunable between 700-1000 nm and can run in both CW as well as pulsed mode. A portion of the beam ($\sim$12 W) from the Verdi pumps the gain medium. The Ti:Sapph crystal has an emission range of 680-1100 nm, but can be restricted to the wavelength we want with the help of a prism and filters. The wavelength is further restricted due to resonance conditions imposed by the end mirrors. The Mira can be mode-locked spontaneously or with the help of an external stimulus. When it is mode-locked, the medium emits pulses of coherent laser light which travel to the output coupler(OC) (end mirror). A part of the beam goes through the OC and becomes the beam coming out of the laser, while the rest bounces off the output coupler. This beam returns back to the medium after a time period of 13.2 ns and causes stimulated emission for a few hundred femtoseconds. The beam then travels back to the output coupler again and the process is repeated. In the time taken by the beam to travel back and forth, a large number of atoms collect in the excited state of the medium. The Mira is also equipped with prisms which allow us to choose the wavelength that we desire and amplify that energy. The inverse of the time period gives us the repetition rate of the laser (76 MHz). The CW (non-modelocked) signal has an average power of 1.7 W while the modelocked beam has an average power of 1.1 W. A small portion of this beam is picked off and sent to the RegA. The rest of the beam was used as a pump beam directly, or is sent to the diode in the streak camera in order to

synchronize it with the laser. This is further explained in Section 3.1.2.3.

Ultrafast pulses from the Mira are amplified by the RegA laser. The gain medium of the RegA is a Ti:Sapph crystal as well and it is pumped with the remaining Verdi beam(∼6 W). There is a tellurium dioxide (TeO_2) Q-switch in the RegA, which is an acousto-optic modulator which cuts the RegA cavity and prevents it from lasing when there is no input beam from the Mira. An input beam from the Mira is sent through a Faraday isolater which separates the Mira beam from the output RegA beam. A single pulse of the Mira beam is sent into the RegA cavity by a TeO_2 cavity dumper. This beam undergoes 20-30 round-trips and passes through the Ti:Sapph gain medium each time and gets amplified. The cavity dumper then extracts a single pulse and dumps it out through the Faraday isolater. This beam is sent through a compressor which corrects for the beam expansion that happens in the RegA cavity. The compressor uses the traditional geometry of sending a beam through two gratings to compress the beam twice. The beam is sent through four passes off a gold-coated holographic grating and finally picked off by a mirror. The output beam is ∼1 W in intensity, has a full width half maximum(FWHM) width of 300 fs, a wavelength of ∼800 nm and a repetition rate of 250 kHz. This beam is sent to the optical parametric amplifier (OPA).

The OPA coverts the beam from the RegA into a tunable beam in the wavelength range of 400-1600 nm. The 800 nm RegA beam is sent through a beam splitter which sends 75% of the beam to a BBO crystal which acts as a second harmonic generator (SHG) and frequency doubles the beam. The rest of the RegA beam is focused onto a sapphire crystal. The intensity of the focused beam creates a strong whole beam self focusing effect which collapses the beam size and increases the intensity. The high intensity causes a self phase modulation which generates a frequency sweep from ultra-violet to infra-red and produces a white light continuum peaked around 800 nm. The white-light continuum is sent to the OPA crystal where it meets the frequency doubled beam. Since different wavelengths have different indices of refraction, we can select the wavelength of interest by rotating the crystal. At the crystal we have three-wave mixing and the frequency doubled beam is converted to the signal wavelength we select and an idler beam, where the corresponding frequencies are given by $2f_{RegA} = f_{idler} + f_{signal}$. The spectral FWHM of the resulting beam is about 5 nm. This output beam has a repetition rate of 250 kHz and an average output power in the range

5-20 mW (depending on wavelength). Each pulse is a few hundred femtoseconds long, which gives us a peak power between 200-1000 kW.

3.1.2 Imaging devices

The photoluminesence signal from our samples is collected with the help of a coupled device camera (CCD) attached to a spectrometer and a streak camera. These devices allow us to both spectrally resolve and time resolve our signal.

3.1.2.1 Spectrometer: The signal emitted by our sample is sent through a spectrometer which helps us spectrally resolve the light coming from our sample. Spectrally resolving helps us separate the luminescence from our quantum dots and polaritons from the luminescence from our substrate and any scattered laser light that might be present. The spectrometer used in these experiments is a Princeton instruments Acton SP2500. We can switch between three different gratings - 50 lines/mm, 300 lines/mm, and 1200 lines/mm. This gives us a spectral resolution of 0.1 nm to 2.4 nm. All the quantum dot experiments were performed using the 300 lines/mm grating while the polariton experiments were mostly performed using the 1200 lines/mm grating.

We sacrifice one of spatial axes to energy while the other axis continues to contain spatial information. If we wish to view our signal without spectrally resolving the signal, we have the option of moving the grating aside and sending the signal straight into the camera. We can send the signal to the streak camera or the CCD camera by flipping a mirror present inside the spectrometer.

The spectrometer is calibrated periodically with the help of halogen lamps, which have spectral lines in the visible and near infra-red region.

3.1.2.2 CCD camera: To collect the spectrally resolved data, we use a thermoelectrically cooled, 512x512 pixel Photometrics Cascade CCD camera. The camera can be operated at 10 MHz for high speed or the frame rate can be lowered significantly if we wish to capture data that requires long integration times. Our camera has a spectral range between

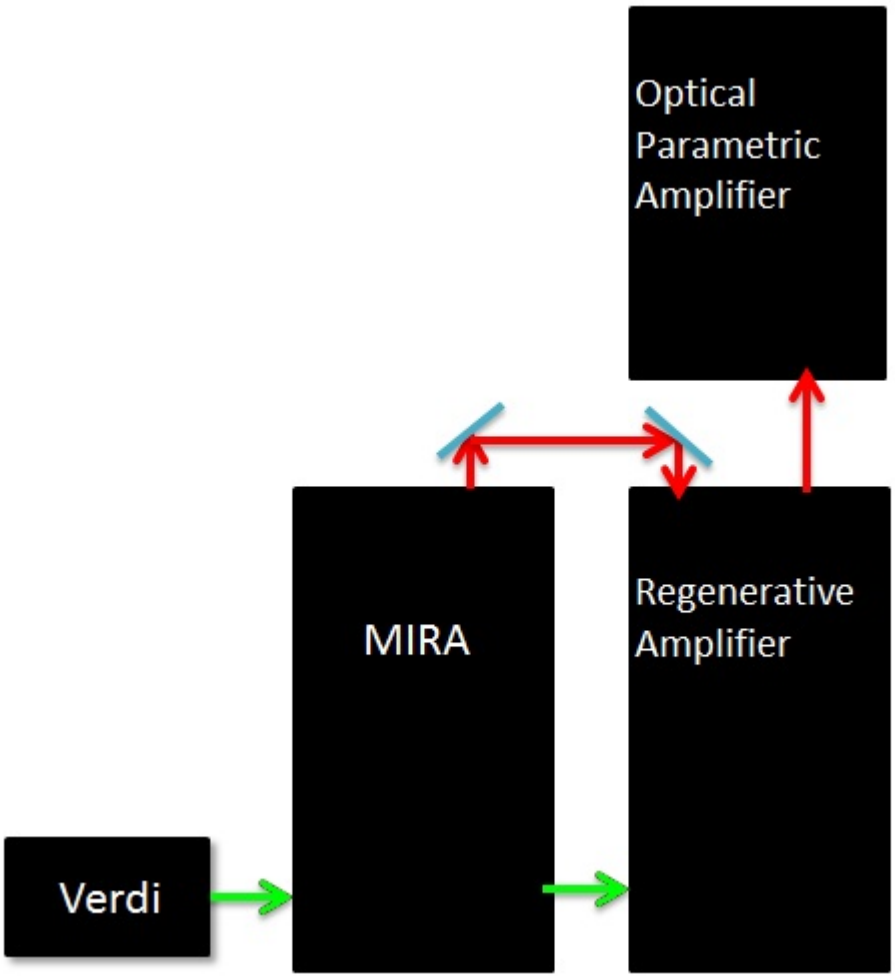

Figure 11: Illustration of our laser system. The Verdi emits a 18W CW beam which is sent into the MIRA. The MIRA modelocks the beam to the wavelength we choose (∼800 nm). This beam is amplified by the RegA laser which sends a pulse to the OPA. The OPA lets us tune the wavelegth.

400-1100 nm, which means that it does not pick up the incident pump beam in the case of two-photon pumping - which is ∼1500 nm for the quantum dot experiements and ∼1550 nm for the polariton experiments. This reduces noise and interference from scattered laser beam significantly.

3.1.2.3 Streak Camera: We use a Hamamastu streak camera (model: C5680) which allows us to time resolve the signal on the order of picoseconds. While CCDs are limited to nanoscale timescale or longer, our streak cameras has a resolution of two picoseconds. It allows us to sacrifice one spatial axis for time and synchronize the signal with the laser pulse by using an external photodiode and a delay circuit. The streak camera is connected to a spectrometer, which allows us to spectrally resolve the signal as well.

As discussed above, the photoluminesence from our sample is sent through a spectrometer which spectrally resolves the beam. A slice of this beam is sent into the streak camera, where it is incident on a photocathode which converts the light incident on it into a electron beam (Figure 12). The electron beam is then accelerated by an accelerating mesh and passed through a set of sweeping plates. A high-speed sweep voltage is applied to these plates, which causes the electron beam to be swept from top to bottom - along the y-axis, so that the y-axis reads time. The sweeping signal is synchronized with the electron beam coming through with the help of an external photodiode and a delay circuit which controls the timing. A small portion of the Mira signal is incident on this photodiode and serves as a trigger signal. After passing through the sweep plates, the electron beam is incident on a microchannel plate where it is magnified immensely and sent to a phosphor screen, which emits photons. These photons are captured by a CCD camera and presented as an image. It is possible to record a single sweep or perform multiple integrations. We have four different time ranges (160 ps - 2200 ps) and can trigger from a picosecond or femtosecond laser source.

3.1.3 Cryostat

In order to achieve the low temperatures between 4 K to 7 K, two different cryostats were used in the experiments described in this thesis. In order to achieve a high intensity for

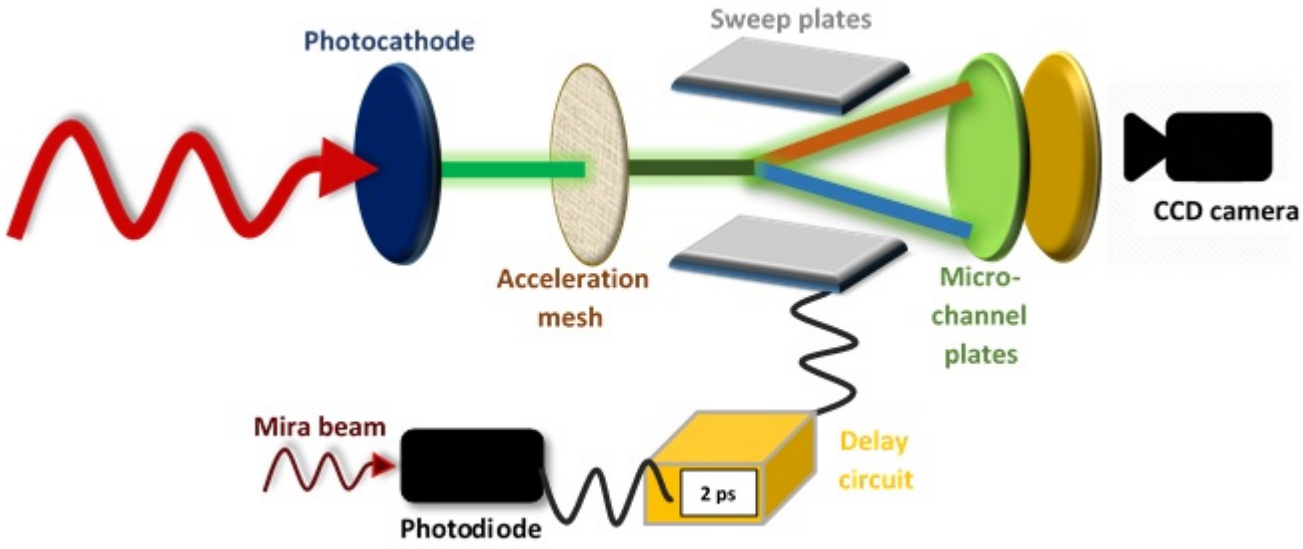

Figure 12: A schematic representation of our Streak Camera. The signal hits a photocathode and gets converted into electrons which pass through sweep plates before hitting a phosphor screen. The phosphor screen is viewed by a CCD camera. The sweep plates are controlled by a photodiode triggered by a laser pulse and an external delay circuit.

our two-photon experiments, we used a microscope objective to focus the beam onto the sample. In the Oxford instruments microscope cryostat, the sample can be brought right to the window such that the sample to be cooled to a temperature of $\sim$4 K and studied with a microscope objective. The sample is thermally insulated from the surroundings by a vacuum chamber and it is cooled down by a cold finger. For a few of our experiments, detailed in Chapter 7, we needed to cool down to temperatures of < 2 K. The Janis bath cryostat allows us to immerse the sample in liquid helium and by reducing the pressure, we can reach low temperatures.

3.2 OPTICAL IMAGING

Optical imaging is done with the help of a lens that sends the beam into the spectrometer through a slit present on the front of the spectrometer.

3.2.1 Real-space imaging

As discussed above, the grating in the spectrometer can be bypassed and the image can be sent directly to the camera. The spectrometer is provided with an entrance slit which can be opened to view the full image without spectrally resolving it. This gives us the real space image and helps us study the sample. By using the right lenses, we can achieve a highly magnified image and make sure that the sample is in focus. For the two-photon experiments, it is highly crucial that we obtain a tight focus of the pump beam on the sample.

We used two types of imaging to study the sample - white light reflectivity and photoluminesence. We use a high intensity white light beam to study the reflectivty of the sample, measure the magnification and look for defects or other scatter sites present on the sample. White light reflectivity also helps us focus the sample and put our lenses in the right position.

Photoluminesence is obtained when we pump the sample with a laser and observe the output. To characterize the sample, and study its effects with a single-photon excitation, the beam is pumped both resonantly as well as non-resonantly. If the beam is pumped

non-resonantly, the spectrometer is used to spectrally resolve the luminescence and only the signal corresponding to exciton/polariton recombination is viewed on the camera to avoid interference with the camera. We also insert long pass filters in the signal path to the spectrometer to cut out the pump beam. If the sample is pumped resonantly, we pump at a spot away from the spot we view on the camera in order to avoid interference from the pump beam. However, for two-photon excitation, we pump both resonantly and non-resonantly with a beam of energy half the lowest transition energy at the spot where we view the sample. Since the pump beam is far away spectrally and our cameras do not respond to the pump beam, we do not see any interference of the signal with the pump.

3.2.2 Momentum space imaging

In the polariton samples, the angular distribution of the signal in the far field tells us the momentum of the polaritons, since the in-plane momentum is conserved according to Snell's law. The higher the in-plane momentum decay, the higher is the angle of emission. By measuring the intensity distribution at various angles and energies, we obtain a dispersion spectrum.

This can also be used in an inverse mode to induce high momentum polaritons into the sample. By varying the angle of the incoming beam, we can control the in-plane momentum, which helps us study the momentum dependence detailed in Chapter 5.

3.3 SAMPLES

3.3.1 Quantum dots

The quantum dots (QDs) used in this thesis are self-assembled, unstrained, inverted semiconductor quantum dots with a large confinement energy, and good size homogeneity, which were grown by Armando Rastelli and Oliver G Schmidt from Institute for Integrative Nanosciences, IFW Dresden. They used in-situ etching to grow these samples. These QDs have transition energies which fall in the working range of Si photodetectors and Ti:sapphire lasers,

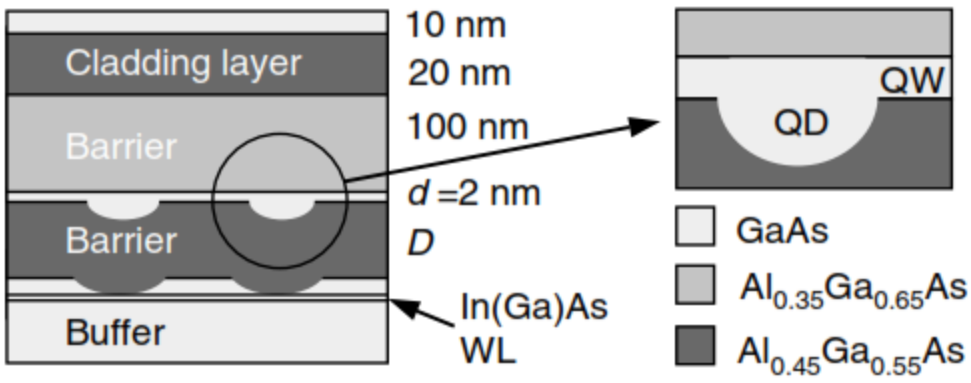

Figure 13: Schematic representation of the quantum dot sample[83].

making them ideal candidates to be studied for use in quantum information and quantum computation and make them preferable to InGaAs/GaAs QDs[84].

As shown in Figure 13, our quantum dot samples are grown on a (001) GaAs substrate by a solid-source molecular beam epitaxy system[85, 86]. A 340 nm thick GaAs layer was grown over the substrate at a rate of 0.6 monolayers/s, to act as a buffer layer. Large islands of InAs/GaAs were grown on the buffer layer by growing the InAs at 0.01 monolayers/s at 500^{o}C. A 10 nm layer of GaAs was grown over the top of these islands and the InAs were preferentially etched by $AsBr_3$. About 5 nm of InAs was etched by this process. Strain-enhanced etching causes the buried InAs to be removed causing nanoholes to be formed spontaneously in their place. A layer of $Al_{0.45}Ga_{0.55}As$ (thickness D) is deposited. The slow diffusivity of Al causes the nanoholes to be transferred from GaAs to the $Al_{0.45}Ga_{0.55}As$ surface. In order to form the quantum dots, the $Al_{0.45}Ga_{0.55}As$ nanoholes needed to be filled with GaAs and so, a 2 nm layer of GaAs was grown over this surface, which results in the recovery of a flat surface. A 100 nm layer of $Al_{0.45}Ga_{0.55}As$ was grown as a barrier on top of this surface, followed by a 20 nm cladding layer of $Al_{0.45}Ga_{0.55}As$. Finally, a 10 nm layer of GaAs was grown in order to cap the structure[83].

By varying the thickness of the $Al_{0.45}Ga_{0.55}As$ layer, the size of the QDs could be con-

trolled. As the thickness of the $Al_{0.45}Ga_{0.55}As$ increases, the nanohole depth of the QDs decreases. However, due to anisotropy of surface diffusion between Ga and Al, the dots shrink in size along $[1\bar{1}0]$ with increasing D while the size along [110] remains unchanged. For the quantum dots studied in this thesis, D=10nm and the holes have a depth of 3.2 nm[83] with high density of 40 dots per μm^2. The electronic transitions in the quantum dots fall in the energy range of $1659 \pm 10meV$. However, we study an ensemble of quantum dots whose sizes vary with increasing D due to relative hole-width distribution. Due to the dispersion in the size of the quantum dots, we observe a broad spectral band with a FWHM of about 10 meV.

3.3.2 Polariton microcavities

The theory of polaritons was given in Section 2.3. In this section we talk about the samples we used in our experiments. In our samples, the polaritons are present on a two-dinensional plane which is bound on both sides by mirrors. The $k_{||}$ and k_z of the polaritons depend on the incoming pump beam that creates the polaritons. The samples we use in our experiments were grown by Kenneth Pfeiffer and Loren West at Princeton University using molecular beam epitaxy (MBE), which gives us a single atomic layer precision. The MBE growth mechanism gives us a non-uniform growth rate across the sample, where the width varies along the length of the sample. Since the width is a function of the the distance from the center of the wafer, there is a variation in the cavity photon energy along the sample. Depending on the location of the sample, the cavity photon energy, E_{ph}, can be less than, equal to, or greater than the exciton energy, E_{ex}. If the cavity photon energy is below the energy of the exciton, the LP behaves more "photon-like" and we are at "negative detuning", while, if the cavity photon energy is above the energy of the exciton, the LP behaves more "exciton-like" and we are said to be at "positive detuning". When $E_{ph} = E_{ex}$, we are at resonance, where the polaritons are a superposition of exactly half photons and half excitons. The energy spliting between the polaritons is equal to the Rabi splitting, which in our samples is 13 meV. The Rabi splitting is large compared to the line width, and hence we are in the strong-coupling limit.

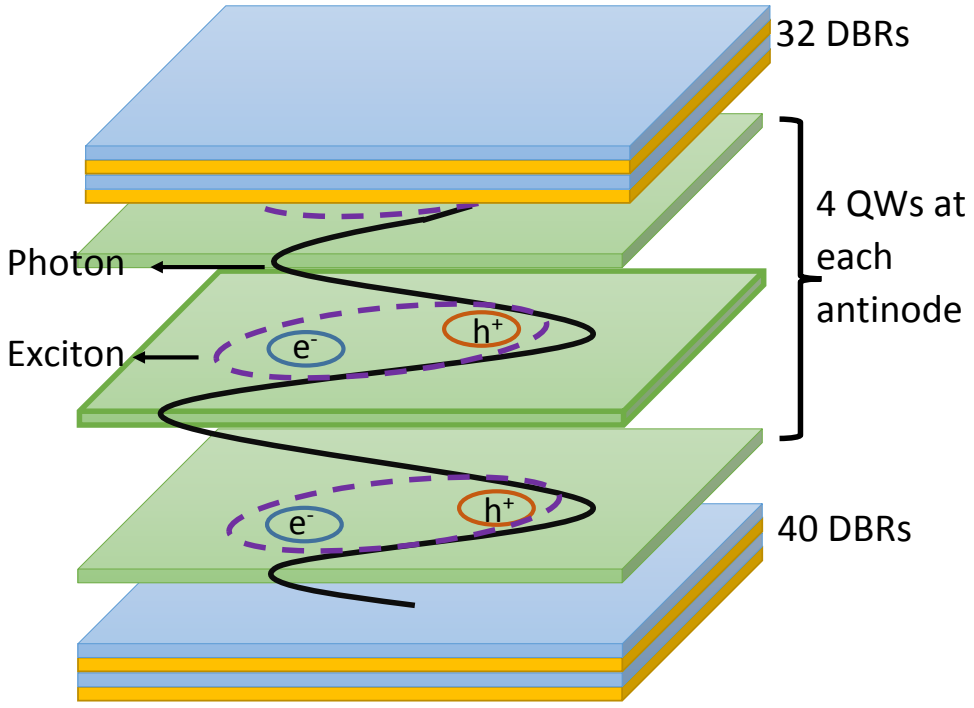

Figure 14: Schematic representation of our polariton sample. We have 3/2 λ cavity and 4 QWs are placed at each of the the antinodes. Excitons form at each antinode and couple with the photon to give us a polariton

The samples are made up of GaAs/AlAs alloys because of the lattice matching between these two materials. This helps us reduce the strain across the sample. The samples were grown on a GaAs substrate. Forty dielectric Bragg reflector (DBR) layers are grown over the substrate which act as our back mirror (Figure 14)[87]. The DBRs are made up of alternating layers of AlAs and $Al_xGa_{1-x}As$. The set of DBRs is made up of thirty-two alternating layers of AlAs and $Al_xGa_{1-x}As$. The two mirrors are separated by a distance equal to 1.5 times the wavelength reflected by the DBRs, to give us a n=3 cavity mode so it would match with the energy of the excitons formed in the quantum wells. This gives a 3/2 λ cavity with three anti-nodes where the energy field of the photon is strong. Four quantum wells are placed at each anti-node. The quantum wells are composed of a 7.5 nm layer of GaAs sandwiched between AlGaAs layers. The quantum wells confine the excitons along the same direction as the photon confinement. Cavity photons - trapped by the DBRs - couple to the dipole moment of the excitons to form a superposition, which leads to the formation of upper and lower polaritons.

The large number of DBR layers give our samples a high quality factor of 10^6 and a long cavity photon lifetime of 135 ± 10 ps. The high quality factor of the sample is confirmed by the intrinsic linewidth of the lower polaritons, which is smaller than the resolution of our instrument (0.05 nm), as reported in Ref. [87], while the lifetime is reported in Ref. [88].

4.0 TWO-PHOTON ABSORPTION OF QUANTUM DOTS

The material in this chapter was published in *Applied Physics Letters* in 2014[89]. The quantum dots sample was grown at Institute for Integrative Nanosciences, IFW Dresden, by A. Rastelli and O. G. Schmidt and the time-resolved measurement and analysis was performed at University of Pittsburgh by C. Gautham and D. Snoke.

4.1 INTRODUCTION

In quantum dots (QD's) made from III-V semiconductors, there are both "bright" excitonic states, which couple to photons, and "dark" states, which do not[90]. The lowest-energy dark exciton states arise from the two spin-1/2 conduction band electrons and two spin-3/2 heavy holes, which combine to make two doublets, the $J = 1$ (bright) and $J = 2$ (dark) excitons. The light hole states can typically be ignored because of the large energy separation between the heavy hole and the light hole states[91, 92, 93, 94]; in the self-assembled dots which we study here[83, 95], the difference between the light hole and the heavy hole is approximately 40 meV.

The two bright exciton states in the quantum dots can mix with each other to create states with linear polarization, and the dark excitons can similarly mix, but in the absence of a magnetic field, the $J = 1$ and $J = 2$ states do not mix with each other[96]. Since the dark states do not couple to light directly, they are hard to observe, but they are important since the bright states will equilibrate with dark states by undergoing a spin flip. A spin flip also implies decoherence since the spin flip must involve a phonon which adds or carries away angular momentum[42, 43, 44]. A measure of this spin-flip time is of great interest to any

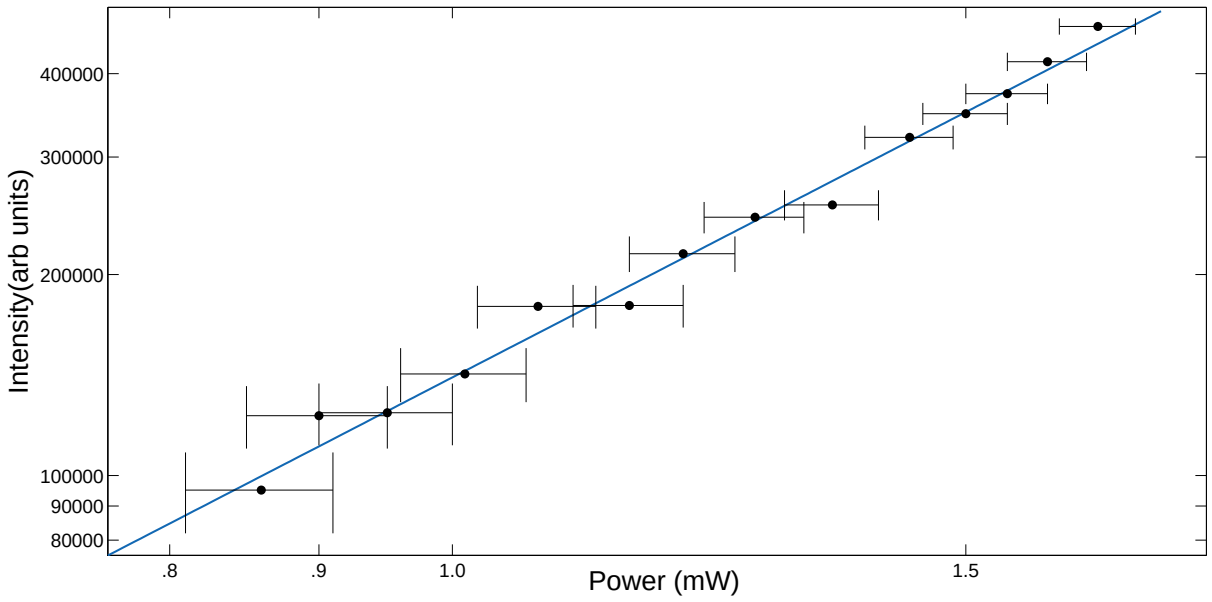

Figure 15: Solid dots: the observed total spectrally integrated intensity versus pump power. Solid line: P^2 power law, indicating two photon absorption.

quantum information scheme which requires coherence to be maintained in the excited states of quantum dots[45, 46, 47]. When looking at conversion between the two bright states, prior work[20, 97, 98] has shown very long decoherence times in certain types of quantum dots, but a previous study[99] showed a much shorter time scale for the bright-to-dark coupling. It could be argued that the latter result was an accident of the specific geometry of the dots used; therefore further study on QDs with different geometry is of value. The theory of dark-to-bright spin flip has been addressed by Maille et al[78].

4.2 EXPERIMENTAL SETUP

Our approach is to excite the dark states by two-photon absorption, which does not excite the bright states. We then record the emission from the bright states with picosecond time

resolution; the data then tells us of the spin flip time since the bright states cannot be created in any other way.

We used hierarchically self-assembled GaAs/$Al_xGa_{1-x}As$ QD's grown by molecular beam expitaxy and in-situ etching of InAs. A GaAs buffer is grown over a (001) GaAs substrate. InAs is grown on the GaAs buffer. A 10 nm layer of GaAs is grown over the InAs following which 5 nm of InAs is etched preferentially by $AsBr_3$. A layer of $Al_{0.45}Ga_{0.55}As$ (thickness D) is deposited followed by a a 2 nm layer of GaAs and a 100 nm layer of $Al_{0.45}Ga_{0.55}As$. This is followed by a final 20nm cladding layer of $Al_{0.45}Ga_{0.55}As$. The low diffusivity of $Al_{0.45}Ga_{0.55}As$ causes the holes to be transferred and we have GaAs QD's. By varying the thickness of the $Al_{0.45}Ga_{0.55}As$ layer, the size of the QDs can be controlled[83]. For the samples studied here, $D = 10$ nm and the holes have a depth of 3.2 nm with density of 40 dots per μm^2. The quantum dot photoluminescence appears in the photon energy range of $1.659 \pm .010$ eV.

The sample was mounted in a continuous flow microscope cryostat and our experiments were performed at a temperature of 7 K. Our laser system consists of a Coherent femtosecond Ti:Sapphire laser, the output of which was amplified by a regenerative amplifier (RegA). This beam has a repetition rate of 250 KHz and a spectral full width at half maximum (FWHM) of 4 nm. This beam was sent through a frequency doubler in an optical parametric amplifier (OPA), and the frequency-doubled pulse was converted to a pulse with photon energy of 0.8428 eV and FWHM of 10 nm. This was used to pump the sample, and corresponds to a two-photon transition of 1.685 eV, which is about 26 meV higher than the peak photoluminesence energy of our QD's, given above. We used a 1000 nm long-pass filter to ensure there was no leaked signal at higher photon energy; we also note that the RegA beam has lower photon energy than the excited states of the QD's. The signal was time-resolved using a Hamamatsu streak camera. Since the camera does not respond to the energy of the pump beam, the QD's can be pumped resonantly and observed at all times before, during, and after the laser pulse. Figure 16 shows a typical time-resolved spectrum. We simultaneously measured the time-averaged spectrum using a Princeton CCD camera.

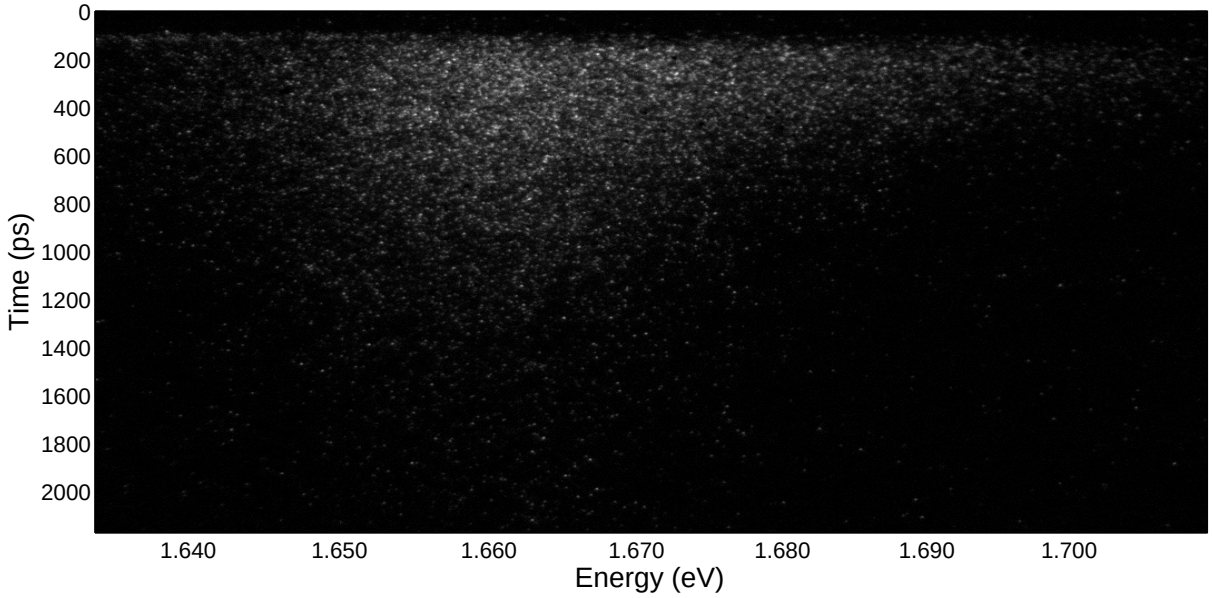

Figure 16: Time resolved image of the high density QD sample when pumped by a pulsed laser at 0.8428 eV at a temperature of 7 K.

4.3 DATA

The two-photon absorption is a nonlinear process in which the absorption is proportional to the square of the intensity of the excitation. At very high intensity, there is a probability of generating excited carriers by means of three-photon excitation. This was avoided by defocusing the objective lens of the pump laser. To ensure that we were observing luminescence from QD's excited by the two photon process and not by leaked photons of higher energy or by three-photon excitation, we did a power-dependent measurement and plotted the intensity of the photoluminescence as a function excitation power. As seen in Figure 15, we obtained a $I \propto P^2$ power law, confirming two photon excitation.

Figure 16 shows a typical streak camera image, and Figure 17 shows typical integrated PL traces taken from streak camera images. For the two-photon excitation, we observed a rise time of 97 ± 4 ps, with a decay time of 492 ± 4 ps. Since the generated excitation has higher energy than the photoluminescence, one might attribute the rise time entirely to a thermalization time, as hot carriers emit phonons and settle into lower states. We can eliminate this possibility by measuring the thermalization time directly when the dots are excited by single-photon absorption. Figure 17(a) shows data from this case. The rise time is obscured at early times by scattered laser light in this case, unlike the two-photon absorption case, but it is still clear that the rise time of the luminescence is much less in this case than in the case of two-photon emission, shown in Fig. 17(b).

We performed the experiment at different excitation energies (0.8705 eV to 0.8892 eV), but fail to see a significant change in the spin flip times based on the excitation energy. The lack of a significant dependence on the excitation energy shows that it is a phonon emission process and not a carrier relaxation process. Previous results report a rise time of 38±4 ps for a single photon excitation[100] while pumping at 1.699 eV for this sample. However the longitudinal optical (LO) phonon in GaAs quantum dot has an energy of 29.6 meV,[101, 102] and therefore the thermalization time in that case could have been enhanced by the optical phonon emission. To ensure that the fast thermalization time we see in the case of single-photon absorption is not due to the carriers coupling with the LO phonons, we pumped the sample at 1.681 eV, which is well below one LO phonon energy above the photon emission

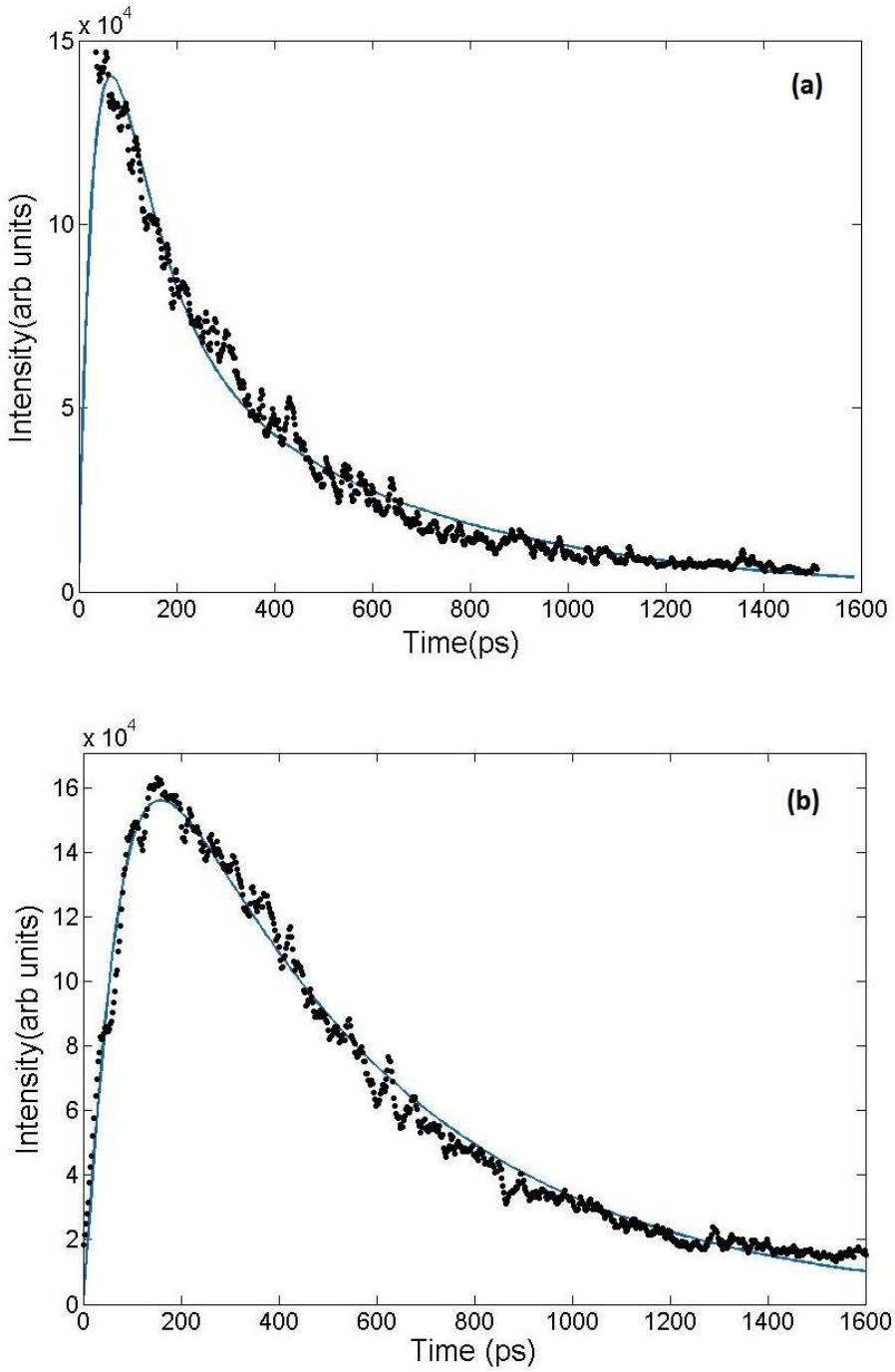

Figure 17: Luminescence from the J=1 state when (a) the J=1 "hot" state and (b) J=2 "hot" state is pumped. The black dots are the data points while the solid line is the fitted equation.

energy for the dots. In this case we obtained an upper bound for the rise time of 45 ps. Thus we conclude that the phonon involved is not the LO phonon but an acoustic phonon[103].

4.4 STATE MODEL

To model the system, we adopt a four-population model of "cold" and "hot", "dark" and "bright" excitons, and assume that at the low temperatures of the experiments, "hot" excitons convert down into "cold" excitons but there is no appreciable reverse conversion of "cold" into "hot". Figure 18 shows the relevant processes for these populations. The rate equations for the coupled system of "dark" and "bright" excitons can be written as

$$\frac{dn_{H1}}{dt} = -\frac{n_{H1}}{\tau_{12}} - \frac{n_{H1}}{\tau_{23}} - \frac{n_{H1}}{\tau_{24}} + \frac{n_{H2}}{\tau_{12}}, \tag{4.1}$$

$$\frac{dn_{H2}}{dt} = -\frac{n_{H2}}{\tau_{12}} - \frac{n_{H2}}{\tau_{23}} - \frac{n_{H2}}{\tau_{24}} + \frac{n_{H1}}{\tau_{12}}, \tag{4.2}$$

$$\frac{dn_{C1}}{dt} = -\frac{n_{C1}}{\tau_{12}} - \frac{n_{C1}}{\tau_{0}} + \frac{n_{C2}}{\tau_{12}} + \frac{n_{H1}}{\tau_{24}} + \frac{n_{H2}}{\tau_{23}}, \tag{4.3}$$

$$\frac{dn_{C2}}{dt} = -\frac{n_{C2}}{\tau_{12}} + \frac{n_{C1}}{\tau_{12}} + \frac{n_{H1}}{\tau_{23}} + \frac{n_{H2}}{\tau_{24}}, \tag{4.4}$$

where n_{H1} and n_{H2} are the populations of the "hot" $J = 1$ and $J = 2$ states, respectively, and n_{C1} and n_{C2} are the populations of the "cold" $J = 1$ and $J = 2$ states, respectively. The time constant τ_{12} is the spin flip conversion time between $J = 1$ and $J = 2$ states of equal energy, while τ_{23} is the spin flip time from the "hot" $J = 2$ and $J = 1$ states to "cold" $J = 1$ and $J = 2$ states of the other spin, τ_{24} is the phonon emission cooling time between the "hot" and "cold" states with the same spin, and τ_0 is the recombination lifetime to the ground state. Since the $J = 2$ states do not couple to the photon field, only $J = 1$ excitons are assumed to have radiative decay. Our experiments detect this emission from the "cold" $J = 1$ excitons. We thus have four rate constants for the coupled system.

Since two-photon excitation excites the $J = 2$ state, we have an initial condition of $n_{H2} = 1$ and $n_{H1} = n_{C1} = n_{C2} = 0$. Solving the above equations for this initial condition gives us the fit shown in Fig. 17(b).

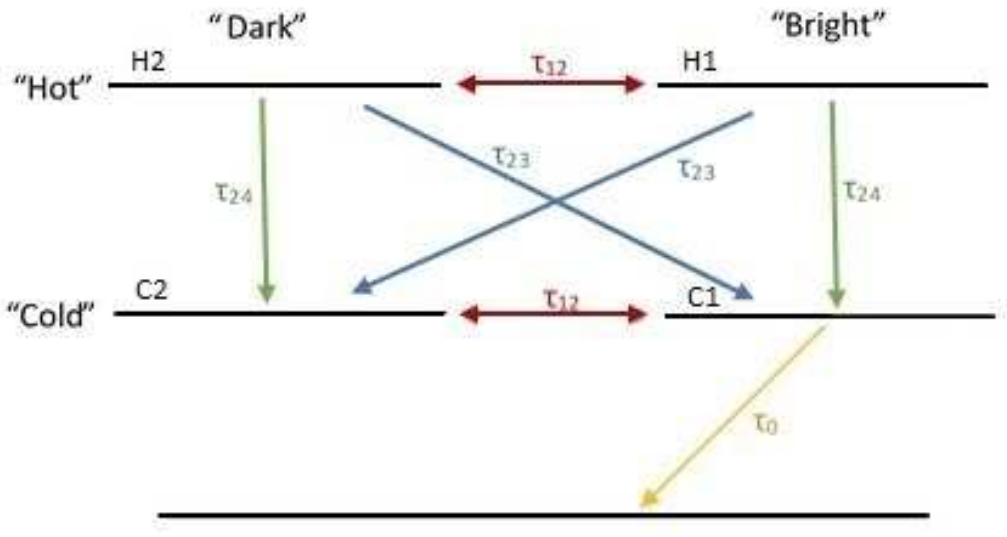

Figure 18: Representation of the energy levels we are studing and the transition and recombination times.

4.5 CALCULATION AND DISCUSSION

In order to get information about all four decay rates, we also solve for the single photon excitation where we excite the "hot" J=1 state and observe the "cold" J=1 state. By setting $n_{H1} = 1$ and $n_{H2} = n_{C1} = n_{C2} = 0$, and fitting the solution to our single-photon-excitation data (Fig. 17(a)), we obtain $\tau_0 = 170 \pm 30$ ps and $\tau_{24} = 50 \pm 10$ ps. Using these values in our two-photon-excitation fit (Fig. 17(b)), we obtain $\tau_{12} = 245 \pm 50$ ps and $\tau_{23} = 315 \pm 60$ ps, getting reasonably good fits for both the single-photon excitation as well as the two-photon excitation data.

We note that τ_{23} is greater than τ_{21} and τ_{24}, which is to be expected, since the excitons in the "hot-dark" state needs to undergo a spin flip as well as cool down in order to reach the "cold-bright" state, while τ_{21} undergoes only a spin flip and τ_{24} only cools down to a lower energy state.

Electron spins in quantum dots are studied for their possible application in quantum information and quantum computing. However, spin flip leads to dephasing and hence spin-flip times of excitons in quantum dots are important. Here we have probed the spin flip times of excitons in self-assembled GaAS quantum dots by exciting the dark state and time-resolving the luminescence from the bright state. While quantum dots in many systems have very long dephasing times, we see here, as in Ref. [99], that excitons can have very short spin flip time in quantum dots. The spin-flip time of the excitons in the dots examined here is of the order of a few hundred picoseconds, while the "cool-down" time is of the order of a few tens of picoseconds. In both cases the mechanism should be phonon emission, since phonons can carry both energy and angular momentum[104].

5.0 TWO-PHOTON EXCITATION OF POLARITONS

The material in this chapter was submitted to *Optica* in April 2015 and is currently under peer review. The sample was grown in Princeton university by L. Pfeiffer and K. West. The experimental setup was designed by C. Gautham and data-collection was performed by C. Gautham and M. Steger. Analysis of the data was done by C. Gautham and D. Snoke.

5.1 INTRODUCTION

The exciton-polariton is a quantum superposition of light and matter which has been studied extensively for its bosonic properties. The common experimental system consists of quantum well (QW) excitons embedded in a two-dimensional microcavity (for reviews see, e.g., Refs. [22, 105, 106, 107]). At low temperatures, this system exhibits Bose-Einstein condensation[26, 23, 108], superfluidity[52, 109, 110], and quantized vortices[51, 111, 112, 113, 114] and may have applications as a low-threshold coherent light source and highly nonlinear optical system. Polaritons are metastable particles, as they can leak through the mirrors into external photons. Although this may appear to be a drawback, it provides a way to look at the condensate continuously, and in long-lifetime samples, the polaritons can still thermalize to nearly equilibrium behavior.

Recently, two-photon excitation of exciton-polaritons has gained attention[66, 69, 70] for its possible application in polariton lasers[66, 71, 72]. In general, two-photon excitation of polaritons provides another way of using the super-nonlinearities of the polaritons for optical modulation schemes. Refs. [66, 70] proposed a mechanism via absorption into the 2p state while Ref. [69] investigated this claim using a narrowband source and cast doubt

on that mechanism because they saw no strong two-photon absorption at the energy of the 2p state. Since there exist other mechanisms that could permit the conversion of dark excitons into the lower polaritons, in this paper we perform time-resolved measurements to investigate this issue and show successful direct excitation of exciton-polaritons by two-photon absorption[115]. We show that this is possible with a beam incident with a finite in-plane momentum due to "bright" state/"dark" state mixing and study the polarization dependence of this absorption both theoretically as well as experimentally.

5.2 SAMPLE STRUCTURE AND PROPERTIES

In the GaAs-based structures we use, the lowest quantum well exciton states consist of the two $J = 1$ "bright" states and two $J = 2$ "dark" states. These states are made of the conduction electrons with spin $=\pm 1/2$ and the heavy holes with angular momentum $\pm 3/2$. In our samples with narrow (7 nm) quantum wells, the light hole exciton states are about 30 meV higher than the heavy hole states, which is greater than the upper polariton-lower polariton splitting and greater than the spectral width of the lasers we use, so the light hole states are unlikely to be excited in resonant excitation of the heavy hole states. The polaritons are formed by a coupling of the cavity photon to the $J = 1$ "bright" heavy hole exciton state. The coupling of the photon and exciton states leads to two new sets of states, the upper polaritons' and lower polaritons,' split by about 12 meV. The $J = 2$ "dark" exciton states do not couple to photons to make polaritons.

Our exciton-polariton samples are made up of GaAs quantum wells with AlAs barriers, in three sets of four placed at the antinodes of the microcavity made of two Bragg mirrors, which are made of AlAs and $Al_xGa_{1-x}As$ repeating layers. The details of these long lifetime samples is given is Ref. [87] and the measurement of the lifetime (180 ± 10 ps) is given in Ref. [88]. This lifetime corresponds to a quality factor of over 300,000, compared to a quality factor less than 10,000 for the samples used in Refs. [69, 70]. The long lifetime of the samples allowed us to study ballistic propagation of the population injected by two-photon excitation. The ballistic propagation was good evidence that the injection was directly into

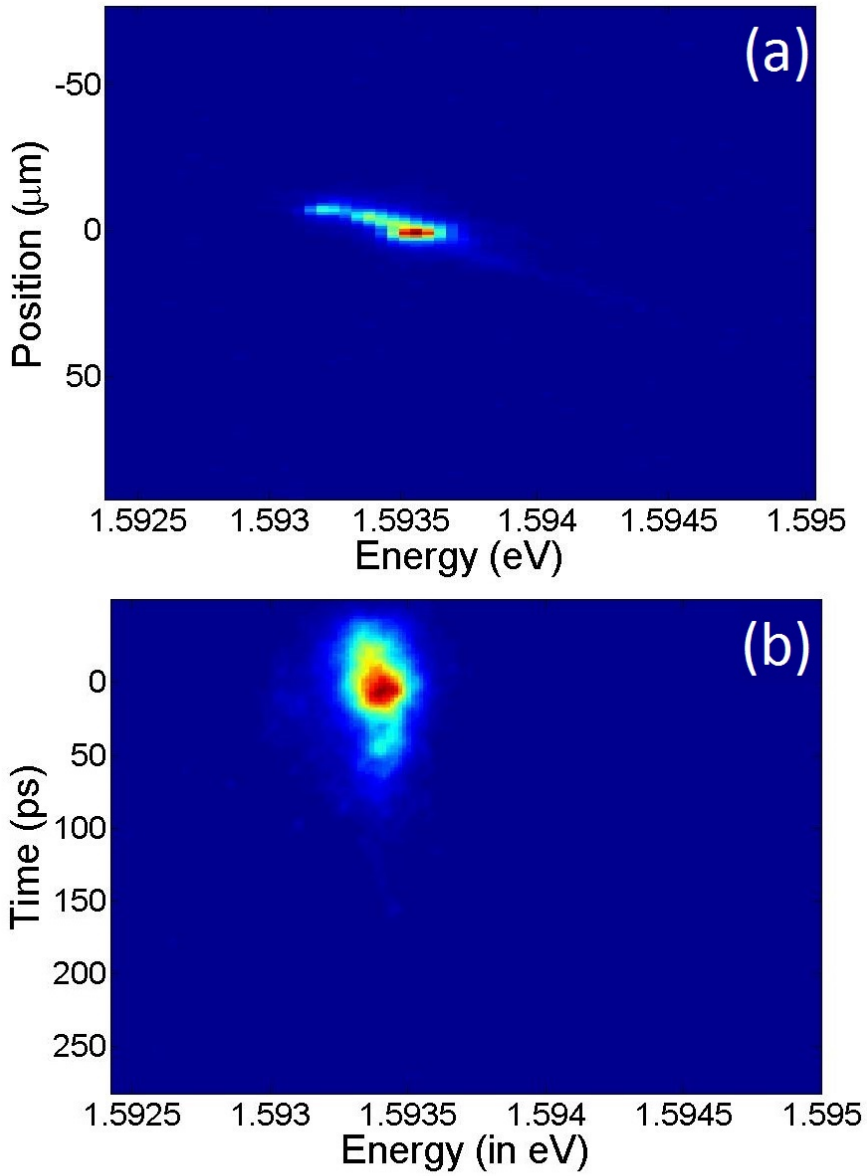

Figure 19: (a) Time-averaged spectrum while exciting with half the energy of the LP with a laser focused at $x = 0\mu m$. There is a spatial gradient to the polariton energy because there is a wedge in the cavity thickness across the sample. (b) Time-resolved spectrum at the generation spot while exciting with half the energy of the LP. There is a fast rise time of the emission comparable to our time resolution which indicates there is direct excitation of the the LP.

polariton states rather than higher energy states that would have to thermalize/scatter into the LP states.

5.3 EXPERIMENTAL SETUP

These samples were mounted in a cryostat and held at a fixed temperature in the range of 4-8 K. Two-photon excitation of the samples was done using a Coherent optical parametric amplifier (OPA) system consisting of a femtosecond pulsed Ti-Sapphire laser, a regenerative amplifier with a repetition rate of 250 kHz, and an OPA pumped with tunable output wavelength. Since the energy of the lower polariton in our samples was about 1.593 eV, we tuned the OPA to give a beam with half that energy (0.7965 eV). This output beam had a spectral full width at half maximum (FWHM) of 15 meV.

We used a dichroic mirror and a 1000 nm long pass filter in the path of our pump beam in order to remove leaked signal coming from the regenerative amplifier. Also, since the photon energy of the regenerative amplifier beam is much lower than the energy of the polariton emission, it was not detected by our spectrally-resolved detection system. The emission signal from the polaritons was spectrally resolved using a 0.25-m spectrometer and time-resolved using a Hamamatsu streak camera. The time-averaged signal was simultaneously viewed on a Princeton CCD camera.

5.4 TWO TIME PEAKS

Figure 19(a) shows a typical spatially resolved, time-averaged spectrum. The energy of the emission from the polaritons varies across the sample because there is a wedge in the cavity thickness, giving a spatial gradient to the photon energy. Figure 19(b) shows a typical time-resolved spectrum. As seen in this Figure (as well as Figure 21(b)), there is a fast rise time of the emission, comparable to our time resolution. The fast fall time of the emission is actually an artifact due to the motion of the polaritons in the cavity gradient. Instead of

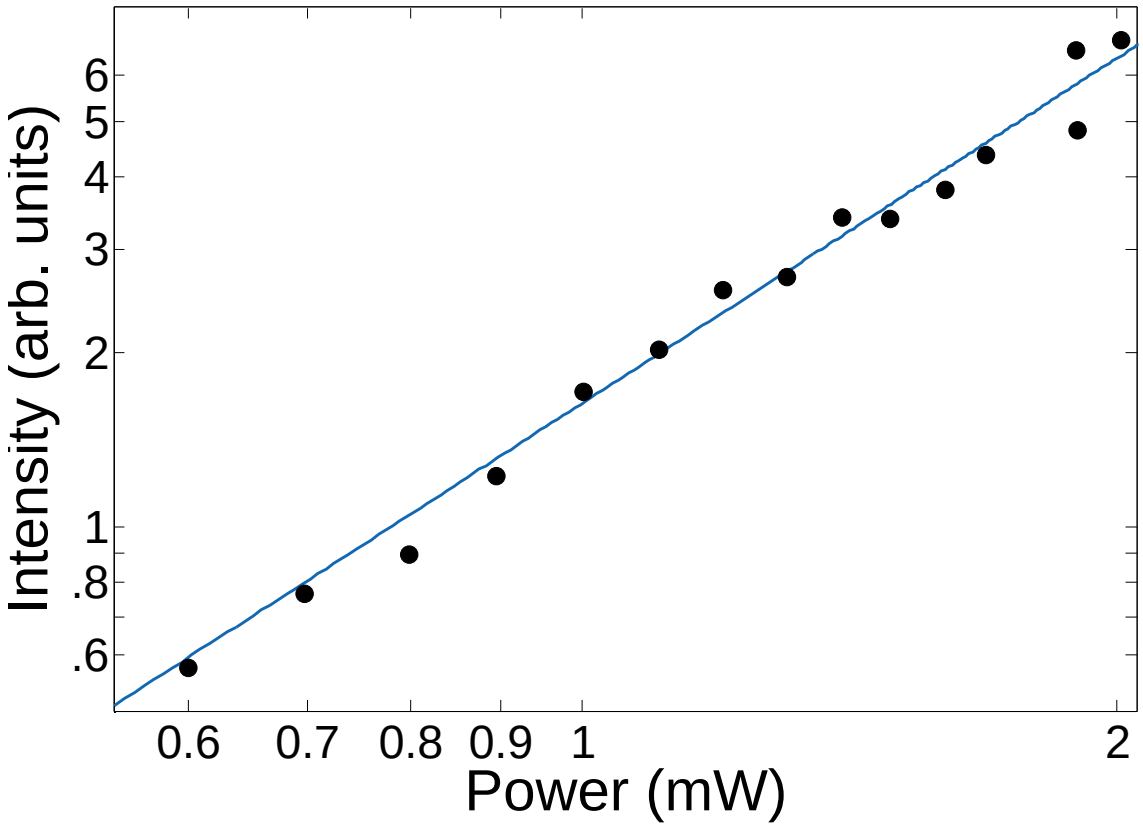

Figure 20: Power dependence of the polariton emission intensity at the creation spot. Solid line: fit to the square of the pump power, indicating two-photon absorption.

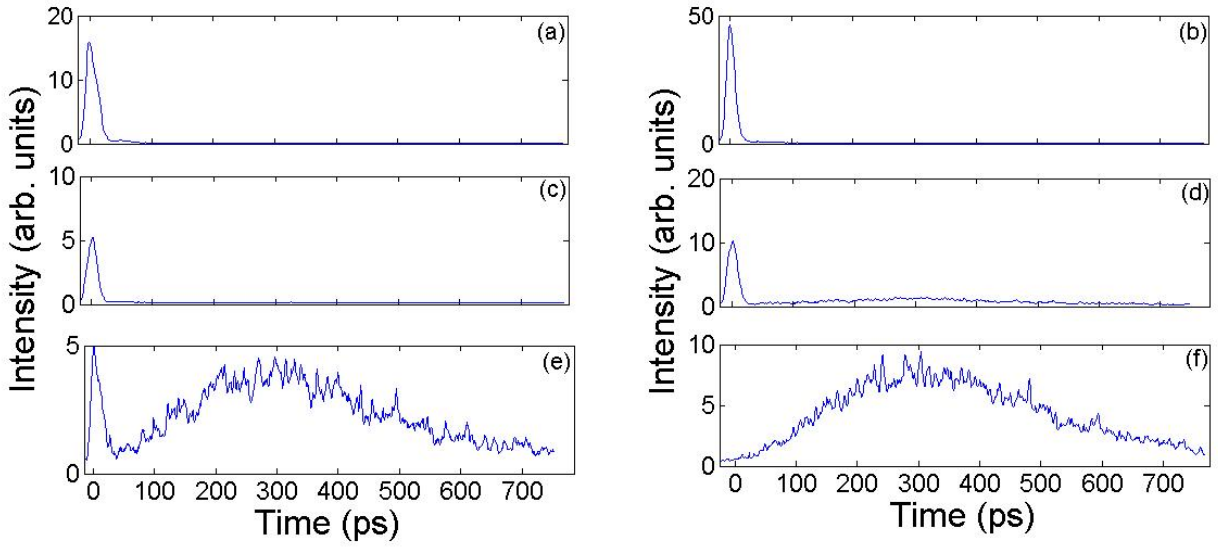

Figure 21: Intensity vs. time for different pump wavelengths of (a)0.7922 eV (b)0.7973 eV (c)0.8050 eV (d)0.8103 eV (e)0.8130 eV and (f)0.8183 nm. A fast initial peak appears when the median pump photon energy is at half the lower polariton energy ($\lambda = 0.7973$ eV). A later population dominates for higher pump energies.

remaining at the spot where they were generated, the polaritons experience the force due to the cavity gradient and accelerate in the direction toward lower cavity photon energy. This is further explained in Section 27. This leads to two effects that suppress their collection by our detection system. First, as they move, they can move out of the spatial field of view of the lens collecting the emission. Second, as they accelerate to higher momentum in the plane (corresponding to higher in-plane wave number $k_{\parallel}$), their photon emission occurs at higher angle, and therefore will not be collected by a low numerical-aperture system.

In order to ensure that we were observing two-photon excitation and not a higher-order excitation or single-photon excitation due to leaked photons in the pump beam, we did a power series measurement by varying the pump power and measured the time-averaged intensity. As seen in Figure 20, the good fit to $I \propto P^2$ power law confirms that we have observed two-photon excitation.

5.5 ENERGY DEPENDENCE

Figure 21 shows the results of the time-resolved measurements for various pump wavelengths. The wavelength of 1555 nm corresponds to the resonant condition of the pump photon energy exactly half the lower polariton energy.

When exciting with exactly half the resonant energy (Figure 21(b)), we see a short (16 ps) peak. However, as we increased the pump photon energy, we see the initial peak disappear and a signal with a long rise time take its place.

Figure 22 shows the polariton intensity at constant pump power as the pump wavelength is varied. When we plot only the intensity of the initial peak, as shown in Figure 22(a), we see that the intensity is maximum when the pump photon energy is half the LP energy and disappears at a higher pump photon energy. The FWHM of this peak is 15 meV, which is the same as the pump laser spectral FWHM. If we plot the total intensity, as shown in Figure 22(b), we see that the intensity increases with increasing pump photon energy. We also observe a small peak while pumping at an energy corresponding to half the energy of the upper polariton energy (0.807 eV) in both cases. The apparent dip in one of the data

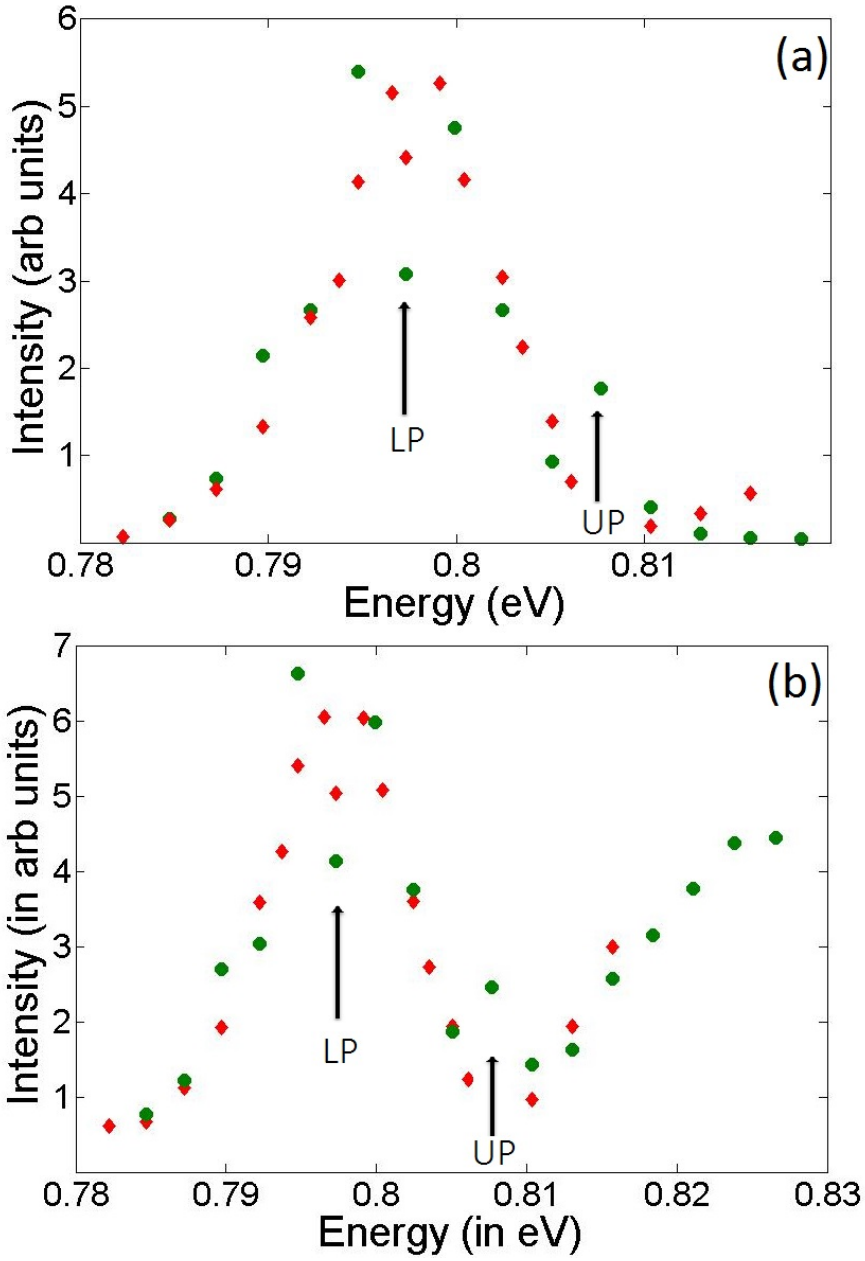

Figure 22: Polariton emission intensity vs. pump photon energy from the time-resolved data. (a) Initial peak intensity showing maximum absorption at the LP energy with a slight peak at the UP energy. (b) Total integrated intensity showing an increase in intensity as the energy is increased. The circles and diamonds represent two data sets obtained on two different days.

sets in Figure 22 falls within our uncertainty.

For each wavelength, we measured the power dependence for the initial fast-risetime peak and the slow-risetime signal separately. Both signals had intensity proportional to the square of the pump power, indicating that both cases correspond to two-photon absorption.

5.6 TEMPERATURE AND MAGNETIC FIELD DEPENDENCE

In order to understand the slow-risetime signal, we measured the signal as a function of temperature. As seen in Figure 23, when the temperature is lower, the slow-risetime signal has greater relative weight. This is consistent with higher energy states cooling down into the ground state of the lower polariton. At a higher temperature, these states will be scattered to higher k-states, while at a lower temperature, they can cool down to states near $k_{\|} = 0$. Since $k = 0$ corresponds to emission normal to the cavity, and our detection system has low numerical aperture, we observe only states with $k_{\|} \simeq 0$ in our experiment. The short initial peak shows no change in intensity in the temperature range we studied (2.5 K to 10 K).

5.7 THEORY AND DISCUSSION

The picture thus arises that polaritons are created by two different mechanisms. One mechanism is direct two-photon creation of polaritons, which occurs most efficiently when the pump laser photon energy is at exactly half the lower polariton energy. The second process is two-photon absorption into excitons in higher energy states, which then relax down into the lower polariton states with a time constant of several hundred picoseconds. These higher-energy states may be either "dark" ($J = 2$) exciton states or $2p$ states of the $J = 1$ excitons.

In order to explain the luminescence from two-photon absorption, other works[66, 70] considered a mechanism based on absoprtion into the 2p-state of the exciton, which then relaxes into the lower polariton by emitting a terahertz photon, while ref. [69] has found no

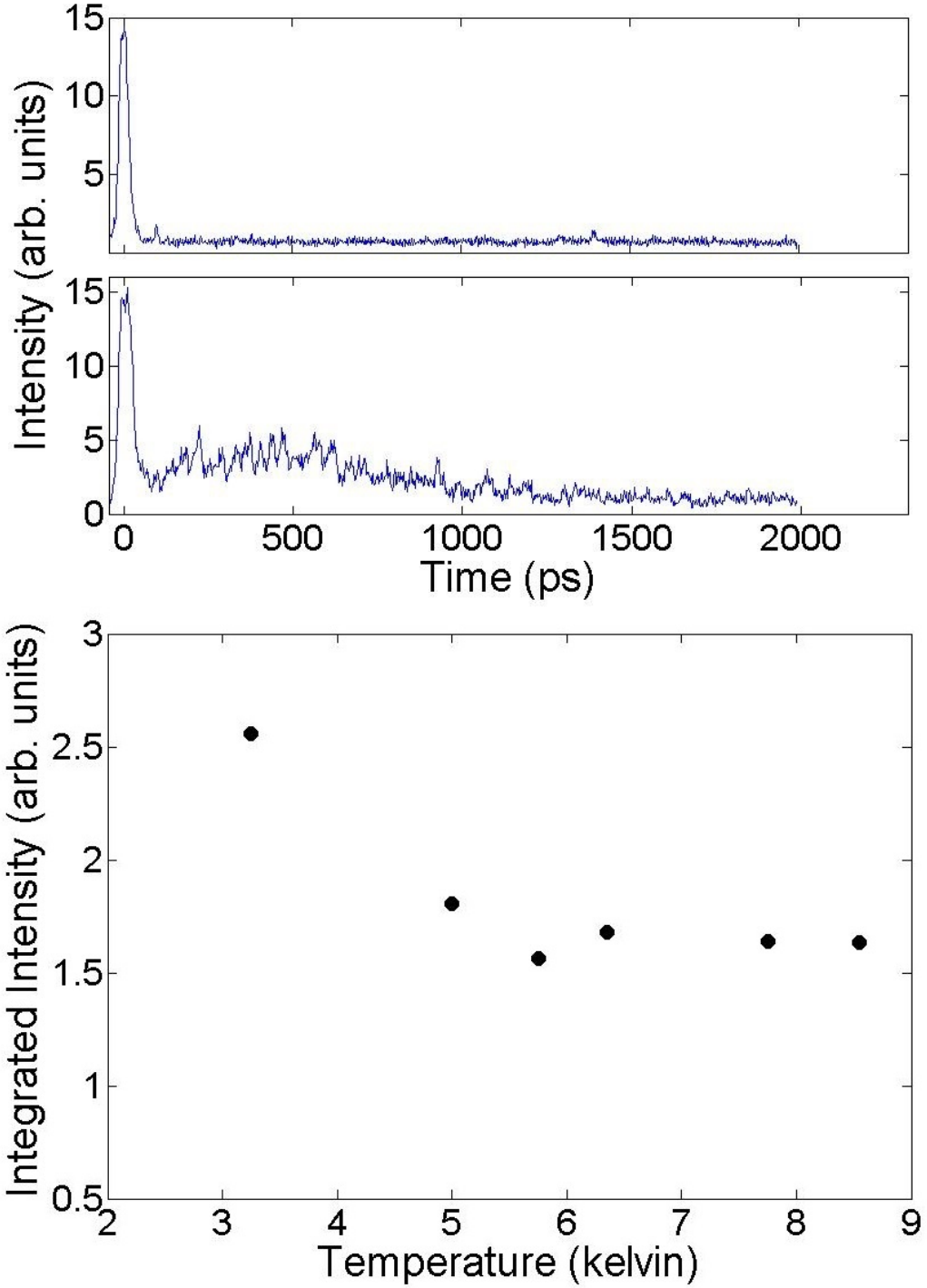

Figure 23: Time vs intensity at (a) 8.3K and (b) 2.5K. As the temperature is increased, the intensity of the later peak decreases. (c) Summary of the integrated late-time intensity data as a function of T.

evidence of direct two-photon pumping into the 2-p state. Time resolving the luminescence (Figure 21 and 22) leads us to believe that we are directly exciting the polariton states. Although two-photon excitation of the $J = 1$ states is forbidden by symmetry at $k_{\|} = 0$ (normal incidence), away from $k_{\|} = 0$, mixing of the $J = 1$ and $J = 2$ states occurs.

The coupling between the "dark" and "bright" exciton states can be understood from the Luttinger-Kohn (L-K) Hamiltonian[116, 117]:

$$H^{LK}|u_k\rangle = \begin{pmatrix} P+Q & -S & R & 0 & -S/\sqrt{2} & \sqrt{2}R \\ -S^* & P-Q & 0 & R & -\sqrt{2}Q & \sqrt{3/2}S \\ R & 0 & P-Q & S & \sqrt{3/2}S & \sqrt{2}Q \\ 0 & R^* & S^* & P+Q & -\sqrt{2}R & -S^*/\sqrt{2} \\ -S^*/\sqrt{2} & -\sqrt{2}Q^* & \sqrt{3/2}S & -\sqrt{2}R & P+\delta & 0 \\ \sqrt{2}R^* & \sqrt{3/2}S^* & \sqrt{2}Q^* & -S/\sqrt{2} & 0 & P+\delta \end{pmatrix} \begin{matrix} J, m_j \\ \begin{pmatrix} |\frac{3}{2},\frac{3}{2}\rangle \\ |\frac{3}{2},\frac{1}{2}\rangle \\ |\frac{3}{2},-\frac{1}{2}\rangle \\ |\frac{3}{2},-\frac{3}{2}\rangle \\ |\frac{1}{2},\frac{1}{2}\rangle \\ |\frac{1}{2},-\frac{1}{2}\rangle \end{pmatrix} \end{matrix}$$

where

$$\begin{aligned} P &= \frac{\hbar\gamma_1}{2m_0}(k_x^2 + k_y^2 + k_z^2) \\ Q &= \frac{\hbar\gamma_2}{2m_0}(k_x^2 + k_y^2 - 2k_z^2) \\ R &= \frac{\hbar}{2m_0}(-\sqrt{3}\gamma_2(k_x^2 - k_y^2) + i2\sqrt{3}\gamma_3 k_x k_y) \\ S &= \frac{\hbar\gamma_3}{2m_0}\sqrt{3}(k_x - ik_y)k_z. \end{aligned} \tag{5.1}$$

where γ_1, γ_2 and γ_3 are the band structure parameters.

Because δ is about 100 meV, we can ignore the split-off holes. We therefore restrict our attention to the 4×4 submatrix the light-hole heavy-hole states. The $J = 0$ light hole states couple to the $J = 1$ heavy hole states through the L-K Hamiltonian when $S \neq 0$. The S term increases linearly with k_x and k_y and is zero for $k_x = k_y = 0$. The value of k_z is determined by the quantum well confinement. The "bright" ($J = 1$) excitons for the heavy holes have conduction-band electrons with spin in the direction opposite to the hole angular momentum, i.e. $|\frac{3}{2}, \pm\frac{3}{2}; \mp\frac{1}{2}\rangle$, where the first label gives the value of J for the hole, the second label gives the value of m_j of the hole, and the third, the spin of the electron.

"Dark" heavy-hole ($J = 2$) excitons correspond to electron spin in the same direction as the hole angular momentum, i.e., $|\frac{3}{2}, \pm\frac{3}{2}; \pm\frac{1}{2}\rangle$.

Our pump photons are linearly polarized. Since linear polarization can be viewed as the superposition of two opposite circular polarizations, two photons from the pump beam will couple to a net $J = 0$ state of the excitons. Such a state exists for the light holes, corresponding to the two states $|\frac{3}{2}, \frac{1}{2}; -\frac{1}{2}\rangle$ and $|\frac{3}{2}, -\frac{1}{2}; \frac{1}{2}\rangle$. The "bright" state polaritons are nominally defined as $\alpha|\frac{3}{2}, -\frac{1}{2}\rangle + \beta|1\rangle$ and $\alpha'|-\frac{3}{2}, \frac{1}{2}\rangle + \beta'|-1\rangle$, where $|\pm 1\rangle$ are the cavity photon states with $J = 1$. The $J = 0$ light hole states couple to the $J = 1$ heavy hole states through the L-K Hamiltonian when $S \neq 0$. The S term increases linearly with k_x and k_y and is zero for $k_x = k_y = 0$. The value of k_z is determined by the quantum well confinement.

We thus see that the lower polaritons are not purely made from heavy hole excitons for finite in-plane $k_\parallel$; the excitonic part of the polariton includes a "dark" exciton fraction. The "dark" exciton fraction will slightly reduce the polaritonic coupling to the cavity photons but will not lead to drastic changes of the polariton behavior. Diagonalizing the L-K Hamiltonian, setting $R = 0$ and $P + Q = E_{hh}$ and $P - Q = E_{lh}$, and $\Delta = E_{lh} - E_{hh}$, which as mentioned above is about 30 meV, and $S \ll \Delta$, the hole eigenstates are

$$\begin{aligned} &|\tfrac{3}{2}, \tfrac{3}{2}\rangle + \frac{S}{\Delta}|\tfrac{3}{2}, \tfrac{1}{2}\rangle \\ &-\frac{S}{\Delta}|\tfrac{3}{2}, \tfrac{3}{2}\rangle + |\tfrac{3}{2}, \tfrac{1}{2}\rangle \\ &|\tfrac{3}{2}, -\tfrac{3}{2}\rangle + \frac{S}{\Delta}|\tfrac{3}{2}, -\tfrac{1}{2}\rangle \\ &-\frac{S}{\Delta}|\tfrac{3}{2}, -\tfrac{3}{2}\rangle + |\tfrac{3}{2}, -\tfrac{1}{2}\rangle. \end{aligned} \tag{5.2}$$

5.8 MOMENTUM DEPENDENCE

Although in these experiments we excited the sample at normal incidence, we used a focusing lens which introduced a finite range of angles of incidence, and therefore finite k_x and k_y, which caused direct excitation of the LP through coupling with the "dark" state excitons. The above interpretation implies that an increase in k_x and k_y should increase the absorption of the two photon absorption.

We further note that the eigenstates of the light holes are given by[116]

$$\begin{aligned}|\tfrac{3}{2},\tfrac{1}{2}\rangle = \tfrac{-1}{\sqrt{6}}|(\cos\theta\cos\phi - i\sin\phi)\hat{x} + (\cos\theta\sin\phi + i\cos\phi)\hat{y} - \sin\theta\hat{z}\rangle|\downarrow\rangle \\ +\sqrt{\tfrac{2}{3}}|\sin\theta\cos\phi\hat{x} + \sin\theta\sin\phi\hat{y} + \cos\theta\hat{z}\rangle|\uparrow\rangle\end{aligned} \tag{5.3}$$

$$\begin{aligned}|\tfrac{3}{2},-\tfrac{1}{2}\rangle = \tfrac{-1}{\sqrt{6}}|(\cos\theta\cos\phi + i\sin\phi)\hat{x} + (\cos\theta\sin\phi - i\cos\phi)\hat{y} - \sin\theta\hat{z}\rangle|\downarrow\rangle \\ +\sqrt{\tfrac{2}{3}}|\sin\theta\cos\phi\hat{x} + \sin\theta\sin\phi\hat{y} + \cos\theta\hat{z}\rangle|\uparrow\rangle,\end{aligned} \tag{5.4}$$

where θ is the angle between the normal to the sample and the polarization vector of the incoming light, ϕ is the angle of rotation about the normal, and $|\uparrow\rangle$ and $|\downarrow\rangle$ indicate the spin states.

Calculating the optical momentum matrix element between these states and the conduction band states for the "dark" exciton, we obtain

$$\langle iS\uparrow|\mathbf{p}|\tfrac{3}{2},\tfrac{1}{2}\rangle = \sqrt{\tfrac{2}{3}}(\sin\theta\cos\phi\hat{x} + \sin\theta\sin\phi\hat{y} + \cos\theta\hat{z})P \tag{5.5}$$

$$\langle iS\downarrow|\mathbf{p}|\tfrac{3}{2},-\tfrac{1}{2}\rangle = \sqrt{\tfrac{2}{3}}(\sin\theta\cos\phi\hat{x} + \sin\theta\sin\phi\hat{y} + \cos\theta\hat{z})P, \tag{5.6}$$

where $\mathbf{p}$ is the dipole operator, $|S\uparrow\rangle$ and $|S\downarrow\rangle$ are the conduction band eigenstates, and P is the dipole element.

If the plane of incidence is the $x-z$ plane, then $\phi = 0$ and the TE polarization is along the y-axis. We obtain the relevant matrix elements by looking at the $\hat{y}$ component which gives us $\sin\theta\sin\phi = 0$ since $\phi = 0$. To obtain the matrix element corresponding to the TM polarization, we look at the $\hat{z}$ component which gives us $\cos\theta$. In our experiment, we measure the angle θ' where θ' is the angle between the normal to the sample and the incident beam and $\theta' = \frac{\pi}{2} - \theta$, giving us a matrix element $\sim \sin\theta' \sim k_x$.

The dependence of the S term on k_x and the dependence of the polarization selection rule on k_x gives us a factor of k_x^2 for the matrix element. The rate of two-photon absorption is proportional to the square of the matrix element, which means that we should see the intensity increase as $k_{||}^4$ for TM polarized light, and we should not see any luminescence from

a purely TE polarized light. To check this, we varied the k for incident TM and TE polarized light, and observed the intensity consistent with a $k_{||}^4$ dependence in the TM polarized case (Figure 24), and no luminescence in the TE polarized case. The spread of angles in the incoming beam gives a non-zero contribution even at $k_{||} = 0$, i.e., normal incidence. When the signal was sent through a polarizer, the polaritons formed are seen to be TM polarized as well. A change of the polarization of the pump beam from linear to circular polarization causes a decrease in absorption.

Further support of this conclusion comes from experiments in which we placed the sample in a magnetic field. No change in the intensity of the polariton emission generated by two-photon excitation was seen. Since the "dark" state/"bright" state mixing is already allowed at finite in-plane $k_{||}$, a change in the magnetic field up to ~ 1 T did not give a substantial increase in the mixing.

5.9 CONCLUSION

In conclusion, direct two-photon excitation of the lower polariton branch of exciton-polaritons in a microcavity is possible at non-zero angle of incidence, without involving higher-lying $J = 2$ or $2p$ exciton states. When the pump photon energy is tuned to be resonant with those higher-lying states, we do see evidence for those states being excited, which then lead to polaritons appearing at lower energy with a long rise time. Direct two-photon excitation of polaritons leads us to expect novel nonlinear effects with interaction of macroscopically occupied polariton states and light waves at half their frequency. Future work will address this.

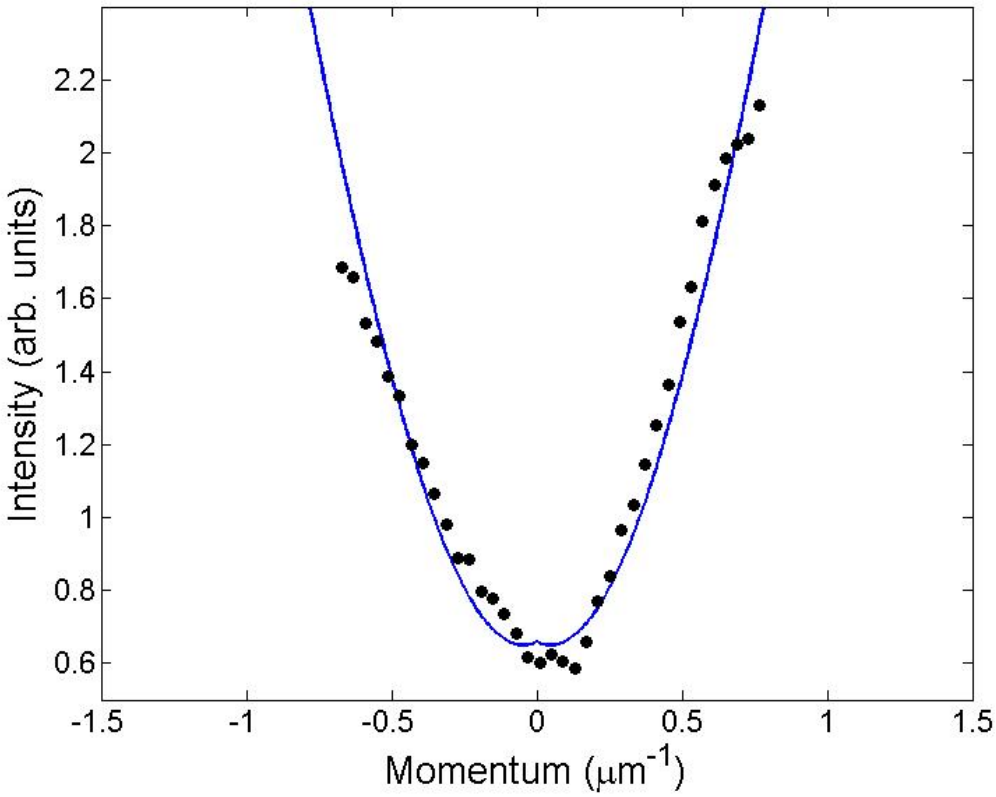

Figure 24: Intensity of the light from two-photon absorption vs. the central in-plane momentum of the incoming light beam. The dots represent our data and the solid line is a convolution fit $A(f * g) + B$, where $f = k^4$ and $g = e^{-\frac{k^2}{\sigma^2}}$ with $\sigma^2 = 0.07$, which takes into account the finite width of our laser spot. $A = 0.95$ and $B = 0.14$ are scaling parameters which take into account background light. This indicates that the absorption is $\propto k^4$.

6.0 CHARACTERIZATION OF TWO-PHOTON EXCITATION

In order to fully understand the two-photon absorption process in polaritons, we excited the sample under varying conditions of magnetic field, and polarization. We used the bath cryostat to measure changes due to varying magnetic fields, and the microscope cryostat to measure polarization dependence and perform polarization measurements of the photoluminescence from the sample. We also used two-photon excitation to measure the lifetime of the polariton and compare it with the measurement made using resonant excitation. The details of the lifetime measurements were reported in *Optica*[88]. In this chapter I will talk about the various measurements made and discuss how they can be exploited to achieve deterministic absorption of the two-photon beam to a greater degree. Single-photon measurements were also done and are reported in the thesis of Mark Steger.

6.1 MAGNETIC FIELD

The two-photon absorption process excites the exciton to a J = 2 or J = 0 "dark" exciton state. As explained in Chapter 5, this state can couple to photons to make a polariton at a non-zero in-plane momentum. However, the coupling is extremely weak only allowed at non-zero in-plane momentum. In order to achieve two-photon absorption at $k_{||} = 0$, we used an in-plane magnetic field to mix the bright and dark states.

In D_{2d} symmetry, at zero in-plane momentum, there is no mixing of the bright and dark states in the absence of a magnetic field. The interaction of the electron and the hole with

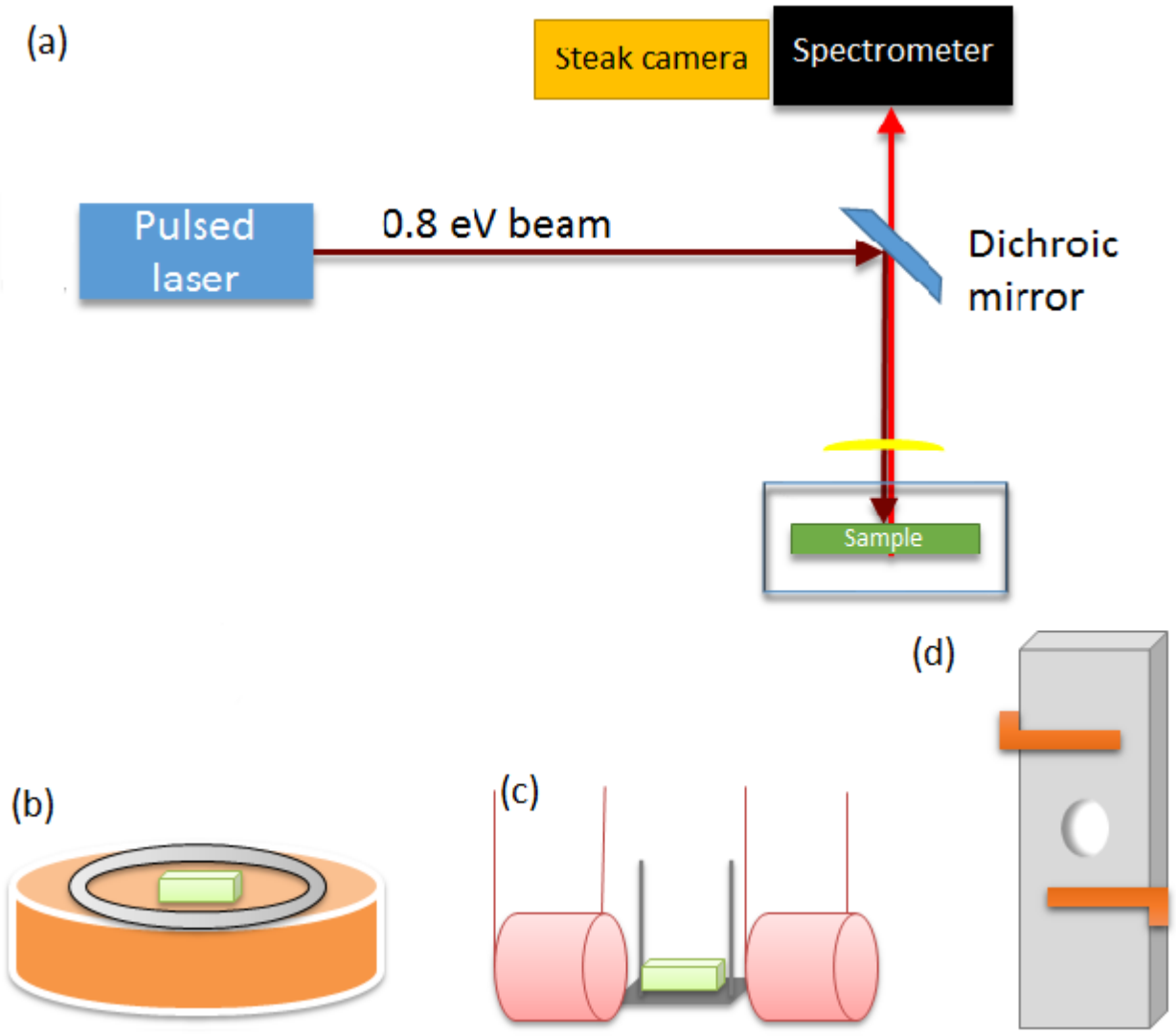

Figure 25: (a) A schematic of the experimental setup to measure change in luminescence in the presence of a magnetic field. (b) Sample placed at the center of a standard store bought ring-shaped magnet where it experienced a magnetic field of ∼0.1 T. (c) Two coils of the superconducting wire formed a solenoid and the sample was placed between them where the magnetic field was 2 T. (d) Our specially prepared sample holder with a hole in the center which allowed the beam to pass through.

an external magnetic field is given by[118, 119]

$$H_{\text{zeeman}}(B) = -\mu_B \sum_i (+g_{e,i} S_{e,i} - 2\kappa_i J_{h,i} - 2q_i J_{h,i}^3) B_i \tag{6.1}$$

where μ_B is the Bohr magneton, q_i and κ_i are the valance band parameters,J_h denotes the spin of the hole, S_e is the spin of the electron, and g is the g-factor of the particle. For the heavy hole $J_h = 3/2$, and $J_{h,z} = \pm 3/2$, and for the electron $S_e = 1/2$ and $S_{e,z} = \pm 1/2$.

If we use the exciton states $|+1\rangle$, $|-1\rangle$, $|+2\rangle$,$|-2\rangle$ as our basis states, along the growth direction (i.e., the z direction), we see that the Hamiltonian is given as

$$H_{\text{zeeman}}(B) = -\frac{\mu_B B_z}{2} \begin{pmatrix} +(g_{e,z} + g_{h,z}) & 0 & 0 & 0 \\ 0 & -(g_{e,z} + g_{h,z}) & 0 & 0 \\ 0 & 0 & -(g_{e,z} - g_{h,z}) & 0 \\ 0 & 0 & 0 & +(g_{e,z} - g_{h,z}) \end{pmatrix}$$

and we have no off-diagonal terms. Thus for a magnetic field along the z direction, there is no bright state/dark state mixing.

However, for a magnetic field perpendicular to the growth direction (i.e., in the $x - y$ plane), the matrix representation of the Hamiltonian for the same basis states is given as

$$H_{\text{zeeman}}(B) = -\frac{\mu_B B_z}{2} \begin{pmatrix} 0 & 0 & g_{e,x)} & g_{h_2,x} \\ 0 & 0 & g_{h_2,x} & g_{e,x} \\ g_{e,x} & g_{h_2,x} & 0 & 0 \\ g_{h_2,x} & g_{e,x} & 0 & 0 \end{pmatrix}$$

Thus, it is possible to mix the bright and dark states of the heavy-hole exciton with an in-plane magnetic field. Theoretically we could directly excite into the polariton state with two-photon excitation even at $k_{||} = 0$ if we apply an in-plane magnetic field.

For this experiment, we used the setup shown in Figure 25, which is similar to the basic set-up used in Chapters 4 and 5. A detailed description of the experimental setup is given in Appendix C. Two different magnets were used to create a magnetic field. In the first instance (Figure 25(b)) a standard neodymium ring-shaped magnet was used. The sample was placed

at the center of the ring where it experienced a magnetic field of ∼0.1 T. This magnet was chosen so that the sample could be placed in the microscope cryostat. A microscope cryostat allowed us to use a microscope objective to focus the beam onto the sample, which gave us a tightly focused beam, which is essential in two-photon excitation. However, our microscope cryostat only gave us a low temperature of $\sim 4\ K$. Furthermore, since the sample was right up against the window in a microscope cryostat, the size of the magnet was also limited and could not be much thicker than the sample itself. Luminescence from the sample was analyzed with and without the magnetic field, but no real change in two-photon absorption was noticed.

To give us greater control over the magnetic field, as well as, a much larger magnetic field, we placed the sample in a specially made sample holder between two solenoids which creates a constant magnetic field at the sample. We could control the strength of the magnetic field and changed it from 0 T to 2 T, which allowed us to study the system both with and without the magnetic field. A superconducting wire (a copper-clad Niobium-titanium wire with a clad-diameter of 0.114 mm and an insulated diameter of 0.14 mm) was used to construct the solenoid[120]. Two rolls of the super conducting wire was prepared (Figure 25(c))and the sample was placed between them. A current of up to 6 A was sent through the superconducting wires at a temperature of 1.9 K. When the current was 6 A, the magnetic field produced by each coil at the center of the sample was calculated to be 1 T, which gave us a total of 2 T at the point of interest[120]. However, as stated earlier, the microscope cryostat had a low temperature limit of ∼ 4 K, while we required a lower temperature to run the magnets. In order to reach such a low temperature, the setup was placed in the inner chamber of a bath cryostat and immersed in liquid helium while being pumped on by an external pump to reduce the pressure.

Using a bath cryostat meant we could no longer use a microscope objective to focus the beam onto our sample since the sample is receded from the front window of the cryostat by 7 cm. This forced us to use a longer focal length lens, which resulted in a bigger focusing spot and lower luminescence. However, our CCD camera and streak camera allowed us to perform time integrations which helped us collect the photoluminescence. By placing the sample at the center of the cryostat and the focusing lens against the front cryostat window

we were able to look at the luminescence from the sample on both the streak camera as well as the CCD camera.

The measured values are showed in Figure 26 where we see no real change in the two-photon absorption at different magnetic fields. This can be explained by the fact that dark/bright state mixing is already allowed at non-zero in-plane momentum and our optical pumping had a wide range of momentum. A magnetic field of 2 T might not be enough to sufficiently increase the change at $k = 0$ sufficiently for it to be observed. The apparent small decrease in intensity with increasing magnetic field can be explained by slight shifts of the pump beam path due to currents caused in the helium superfluid when we increase the magnetic field. Since two-photon absorption is proportional to the square of the input intensity, a slight shift in the beam path could cause large changes in absorption of the beam.

6.2 LIFETIME OF THE POLARITON USING TWO-PHOTON EXCITATION

As reported in Chapter 5, we generated polaritons via a 200 fs pump pulse tuned to one-half the energy of the polaritons which we call the "two-photon beam". Although we argued that there should indeed be an allowed two-photon process at non-zero in-plane momentum due to bright/dark state mixing, the lack of a lifetime in Figure 21 seemed to suggest that what we are seeing is second harmonic generation (Section 2.6.2) and not two-photon absorption (Section 2.6.1). In order to completely prove that we are seeing two-photon excitation, we measured to the lifetime of these polaritons.

We looked at the propagation of these long-lived polaritons created by the two-photon beam to study this lifetime. We performed two separate experiments to measure the lifetime in which we cooled down the sample to a temperature of $\sim$4 K in the microscope cryostat. We use a wide field objective to look at the polaritons and track their movement.

In the first experiment we injected at a large angle, far from our field of view (Figure 27). The polaritons were injected "uphill" - towards higher energy in the cavity gradient. A detailed description of the experimental setup is given in Appendix C. Since there is a

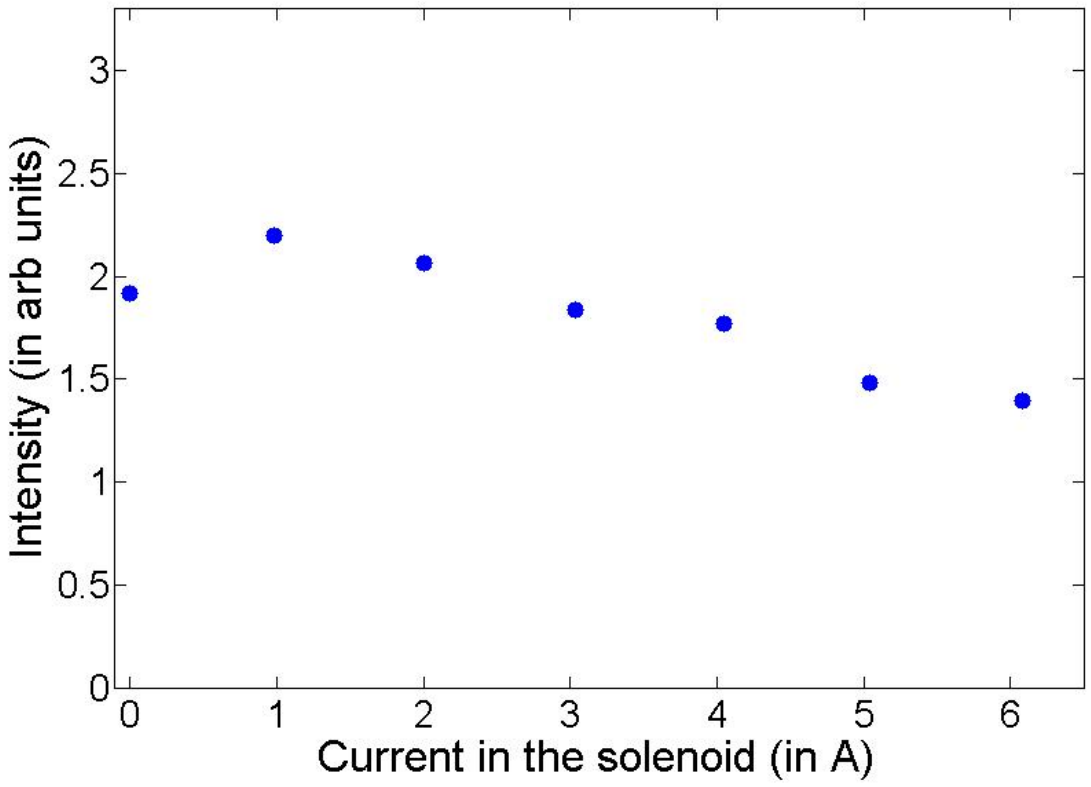

Figure 26: A measurement of the intensity of the signal at different magnetic fields.

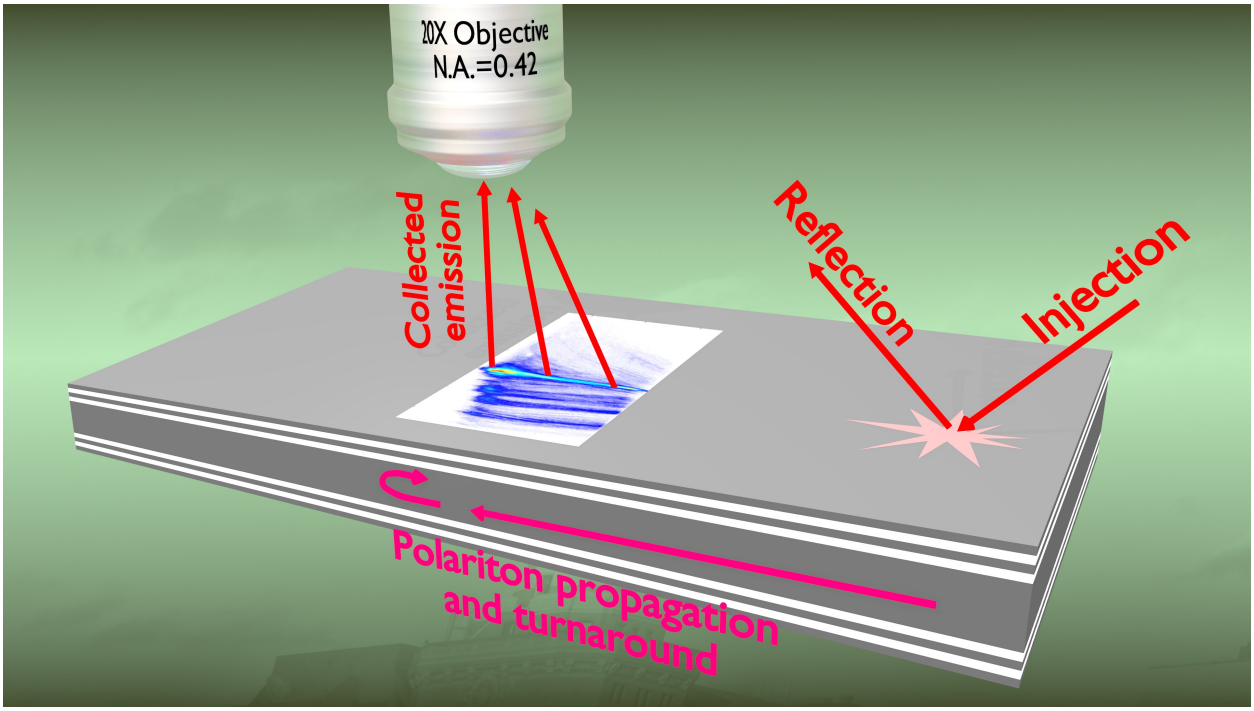

Figure 27: A representation of the experimental setup used to measure the polariton lifetime. The polaritons were injected at a point far away from our point of observation "uphill" into our cavity gradient. The polaritons were measured as they traveled into our field of view, turned around and moved back[88].

gradient in the sample, the polaritons feel a force due to the gradient which is akin to rolling a ball uphill, where there is energy conservation which is given as

$$H = \frac{\hbar^2 k^2}{2m_{\text{eff}}} - Fx \tag{6.2}$$

where m_{eff} is the effective mass of the lower polaritons which is approximately $10^{-5}\ m_e$. The effective mass does change with the position and wave vector, but can be approximated to be constant. The force F is given by the gradient in the region of the cavity studied here, and is approximately equal to 10.5 meV/mm for this section of the microcavity.

The polaritons initially had a large in-plane momentum due to the large angle of injection (Figure 30). The polaritons were viewed far from the point of injection in an effort to replicate the effects of resonant excitation[88]. They lost their momentum as they proceed up the gradient until they reached $k_{||} = 0$, at which point they turned around. We observed this turn-around spot and measured the change in luminescence over time which told us the lifetime of the polaritons. The polaritons entered our field of view ∼200 ps after the laser injected them, and were tracked as they entered our field of view, turned around and moved away. The results are shown in Figure 28(a) and are seen to be roughly parabolic and similar to the one-photon injection. However, the trajectory for the two-photon excitation case is extremely broad in comparison to the single-photon excitation case. This could be attributed to the large spectral width of the laser used for two-photon excitation. This created a large range of polaritons with varying energy and momentum which follow energy conservation laws and resulted in a broadening of the trajectory.

The lifetime of the polaritons were measured to be 178±28 ps which is similar to the lifetime measured through one-photon excitation which was 180±10 ps. The fit is shown in Figure 29. The black dots represent the data and the blue curve is an exponential fit to the data. The data is noisy due to broadening of the trajectory, which is a result of the broad spectral width of our laser. This also gives us a larger uncertainty in our fit.

In the second experiment, we excited the sample at the point of observation. It is rather hard to do this with one-photon excitation since the pump beam would interfere with the signal from the sample, but for two-photon excitation, since the pump beam is spectrally far from the signal, there is no interference or scattered light from the pump beam. We pumped

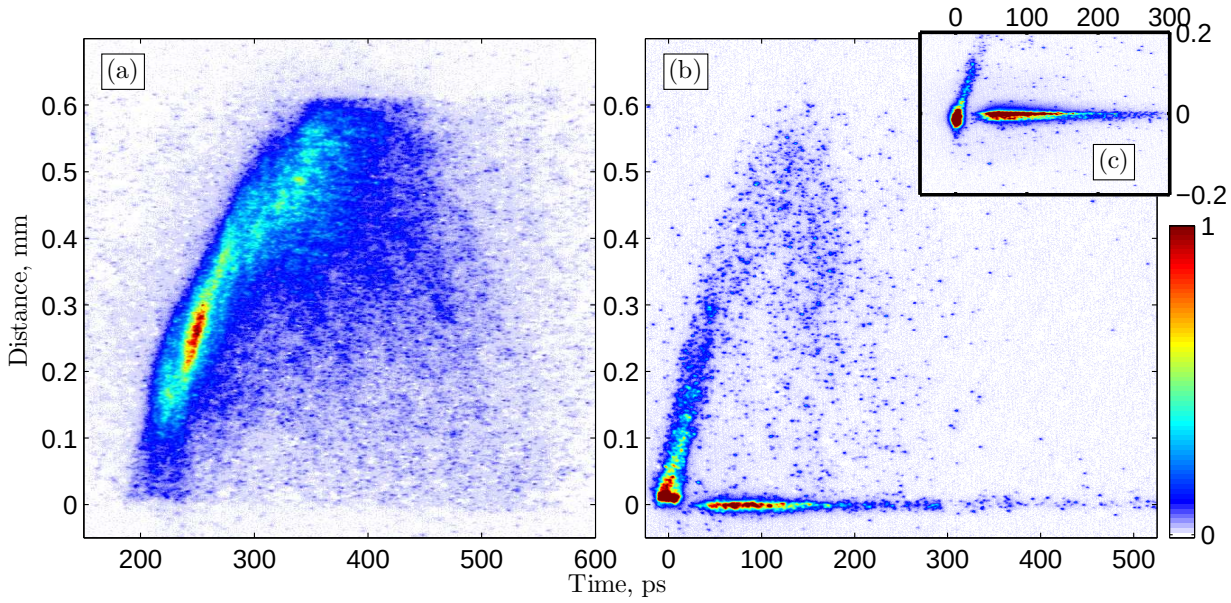

Figure 28: Time-resolved measurement of the polariton photo-luminescence while exciting with a femtosecond beam at half the energy. (a) The polaritons were created at a large angle far away from our point of observation. Due to the spectral width of our laser, we see a broad trajectory. (b) The polaritons were injected normal to our sample at the point of observation. We create a range of momentum states, but do not see the polaritons corresponding to k=0. The long-lived luminescence at the point of creation is from the substrate. The inset (c) is the same data as (b) except with the pump spot centered and unclipped[88].

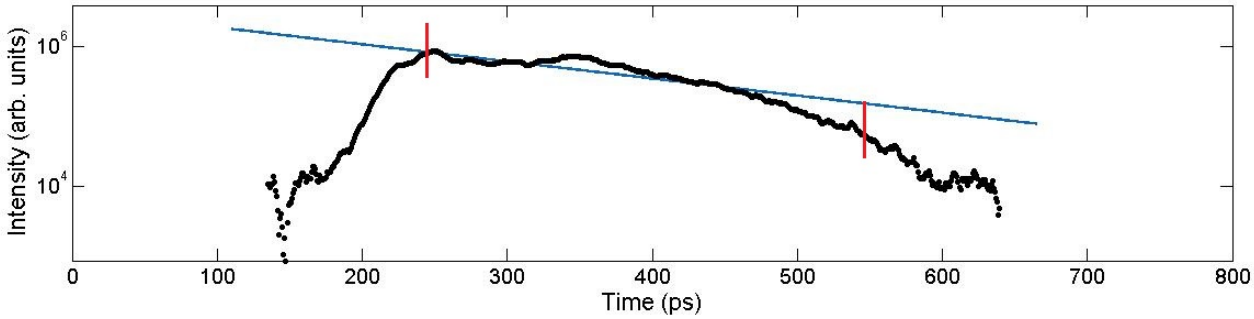

Figure 29: The polariton intensity of Figure 28 summed over space plotted against time to show the exponential decay of the population. The black dots represent the data and the blue curve is an exponential fit to the data which gives us lifetime of 178±28 ps. The red lines indicate the range of data considered for the lifetime fit - the photoluminescence outside these bounds are outside the range of collection of the CCD camera.

the sample through the microscope objective through which we were viewing the sample. In order to get a tight focus, we expanded the beam and made use of the full numerical aperture of the microscope objective. Thus, even though the maximum intensity of the beam was at the center, our angle of incidence was in a range between 0^o to 20^o. This gave us a range of k-states. The results are shown in Figure 28(b). The results showed no luminescence at $k_{||} = 0$ initially and the polaritons created with a non-zero k propagating out. However, since the in-plane momentum given to these polaritons is much less than those created in the first experiment, we see propagation to a shorter distance. The long-lived stationary luminescence we see is from the bulk GaAs substrate which can be excited with two-photon excitation. Substrate luminescence is present at a much lower energy and can usually be eliminated by spectrally resolving the signal. However, in this case, since we wish to measure propagation, we cannot spectrally resolve out the substrate luminescence.

As seen from Figure 28(b), although we injected such that we had the highest intensity at $k = 0$, the polaritons we see have a finite in-plane momentum. Figure 28(c) are the same data as Figure 28(b), except that the luminescence is centered while in 28(b), the beam

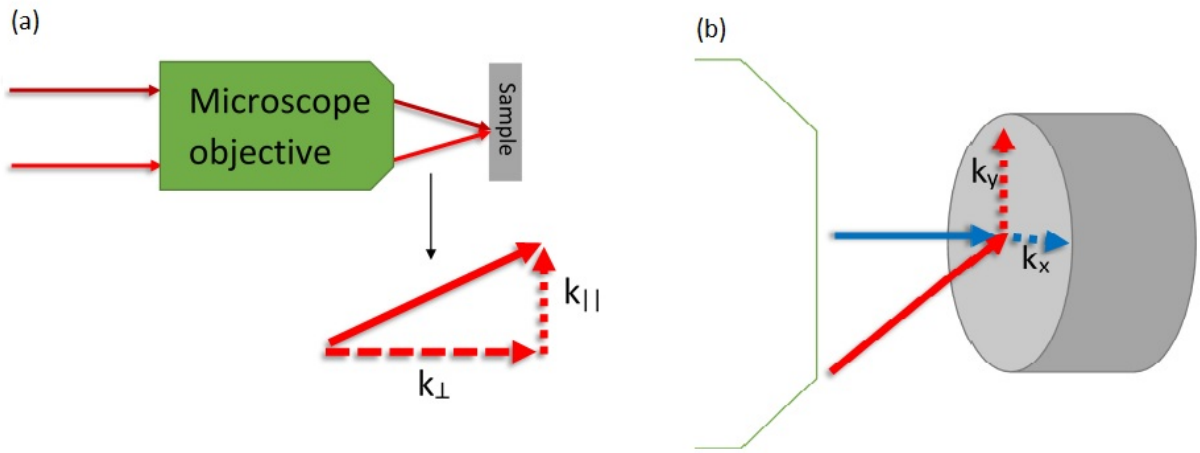

Figure 30: A representation of the in-plane momentum while going through the microscope objective. a) The point of incidence on the microscope objective determines the angle of the incoming beam, which in turn gives us an in-plane momentum. b) Control of magnitude and direction of the in-plane momentum by changing the angle of incidence on the sample.

traveling to x<0 is clipped. This further solidifies the arguments in Chapter 5, which claim that direct creation of polaritons with two-photon excitation is possible only with a beam which has finite in-plane momentum due to light hole/heavy hole mixing, while two-photon excitation is forbidden at $k = 0$ due to selection rules. These results further show, very clearly, that two-photon resonant generation of polaritons is possible.

6.3 POLARIZATION OF THE INCIDENT BEAM

As stated in Section 5.8, the two-photon pump beam needs to be transverse magnetic (TM) polarized in order to create polaritons directly. To confirm this, polarizers were placed on the pump beam path just before it was incident on the sample and the beam was polarized vertical to the optical table. We placed these polarizers just before the microscope objective in order to avoid any circular polarization components that could creep in if the beam was

not incident on the mirrors on the path at 45^o. The beam diameter was reduced by using a telescope to 0.5 mm and it was sent through a periscope before it hit the microscope objective. The periscope allowed us to control the position of the beam on the microscope objective. As shown in Figure 30 (a), the position that the beam was incident on the microscope objective was directly related to the angle of incidence on the sample. By using a telescope to control the size of the beam as it is incident on the microscope objective to have a spot size of 1 mm, which gave us $\Delta\theta = 3^o$. By changing the point of incidence on the back of the microscope objective, we were able to control the angle of incidence on the sample, and were able to span $\theta = 30^o$.

The sample was placed normal to the microscope objective and the beam was scanned across the microscope. As shown in Figure 30 (b), if we scanned along y-direction, increasing the angle θ_y while at $x = 0$ (which is the same as $\theta_x = 0$), we increased $k_{||y}$, but there would be no $k_{||x}$ component. For vertically polarized light, this would increase the amount of TM polarization in the pump beam. Similarly, for vertically polarized light, if we kept $k_y = 0$ and varied k_x, we increased the transverse electric (TE) polarized light. If the laser beam was initially polarized horizontal to the optical table, this effect would be reversed.

Although we shouldn't have observed any photoluminescence when the beam was TE polarized, it was impossible to make the spot size on the microscope objective small. Thus the beam always had a Δk component such that, even when the beam was fully TE polarized, it had a small TM polarization component which gave us luminescence.

As we scanned the sample along the $k_{||y}$ direction with TM polarized light coming from our laser, we observed a $k_{||y}^4$ intensity dependence of the polariton photoluminescence as shown in Figure 24, while scanning along $k_{||x}$ did not produce any luminescence. However, we might have a strain along one dimension of the sample which could cause asymmetry in absorption. We wanted to make sure this preference for absorption along one direction is indeed due to TM-polarization dependent bright/dark state mixing and not an artifact of the sample itself. To check this, we used two half-wave plates to rotate the incoming pump beam so it was horizontally polarized. This should give us TM polarization along $k_{||x}$ and TE polarization along $k_{||y}$. We scanned along both directions. As seen from Figure 31, we observe $k_{||x}^4$ intensity dependence. While we scanned along $k_{||y}$, we did not observe any

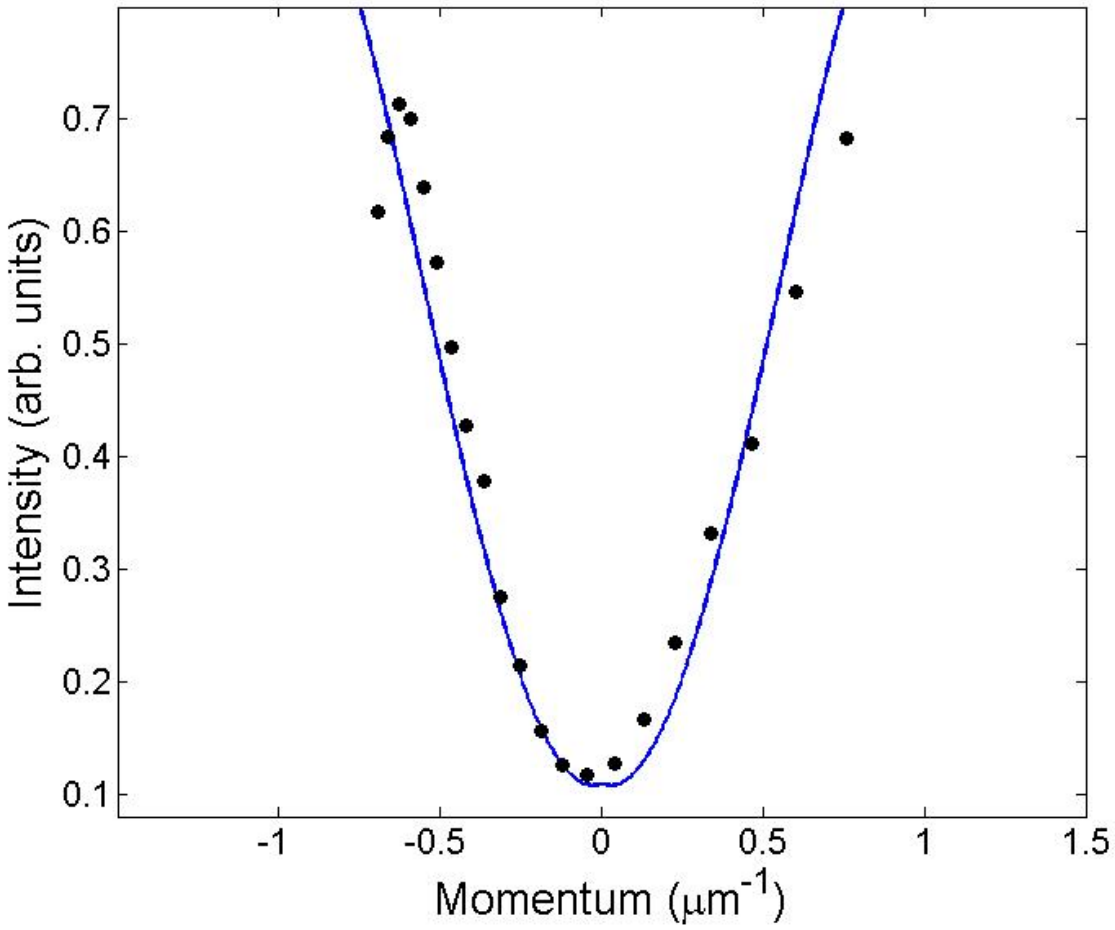

Figure 31: Intensity of the light from two-photon absorption vs. the central in-plane momentum of the incoming light beam. We used a waveplate to rotate the incoming two-photon beam to check that the preferential absorption along one direction was due to TM-polarization dependent bright/dark state mixing and not an artifact of sample. The dots represent our data and the solid line is a convolution fit $A(f * g)+B$, where $f = k^4$ and $g = e^{-\frac{k^2}{\sigma^2}}$ with $\sigma^2 = 0.44$, which takes into account the finite width of our laser spot. $A = 0.96$ and $B = 0.25$ are scaling parameters which take into account background light. This indicates that the absorption is $\propto k^4$.

luminescence , as expected.

As further elaborated upon in Chapter 7, the TM polarization dependence was important to keep in mind while performing deterministic absorption of the two-photon beam. If we are pumping at an angle we needed to make sure that we rotate the polarization of the pump beam such that we have a TM component.

6.4 POLARIZATION OF THE POLARITONS

If we use a non-resonant pump beam, polaritons are created when higher-energy excitons cool down by emitting phonons. The cool-down happens over a few hundred picoseconds and in the process the excitons lose the polarization of the pump beam, so that the photoluminescence from the polaritons is generally un-polarized. While this aspect can be exploited to separate the pump beam from the signal, if we polarize the pump beam along one direction and view only the signal polarized along the perpendicular direction, we cut down the signal along with the pump beam and we lose half of our signal.

However, in the experiments in which we directly create the lower polariton resonantly state with a two-photon beam, the polarization of the laser should be preserved in the polariton population. We also do not expect any cool-down period where the polarization of the exciton is dispersed to photons. Thus, we were interested in the polarization state of the polaritons we create using resonant excitation. In order to study this, we pumped resonantly with the two-photon beam and analyzed the luminescence from the sample using a polarizer. A detailed description of the experimental setup is given in Appendix C. The data is shown in Figure 32. In this Figure, the angle of the fast axis of the polarizer is along the x-axis and the intensity of the photoluminescence is along the y-axis. At 0^o, the fast axis of the polarizer is aligned with the polarization of the laser beam. We can see that the intensity is maximum at 0^o and 180^o and minimum along the perpendicular directions. This tells us that the polaritons were polarized along the same direction as our pump beam, which indicates that they retained the polarization of our pump beam.

This data is of special interest to us for our deterministic absorption experiments. If the

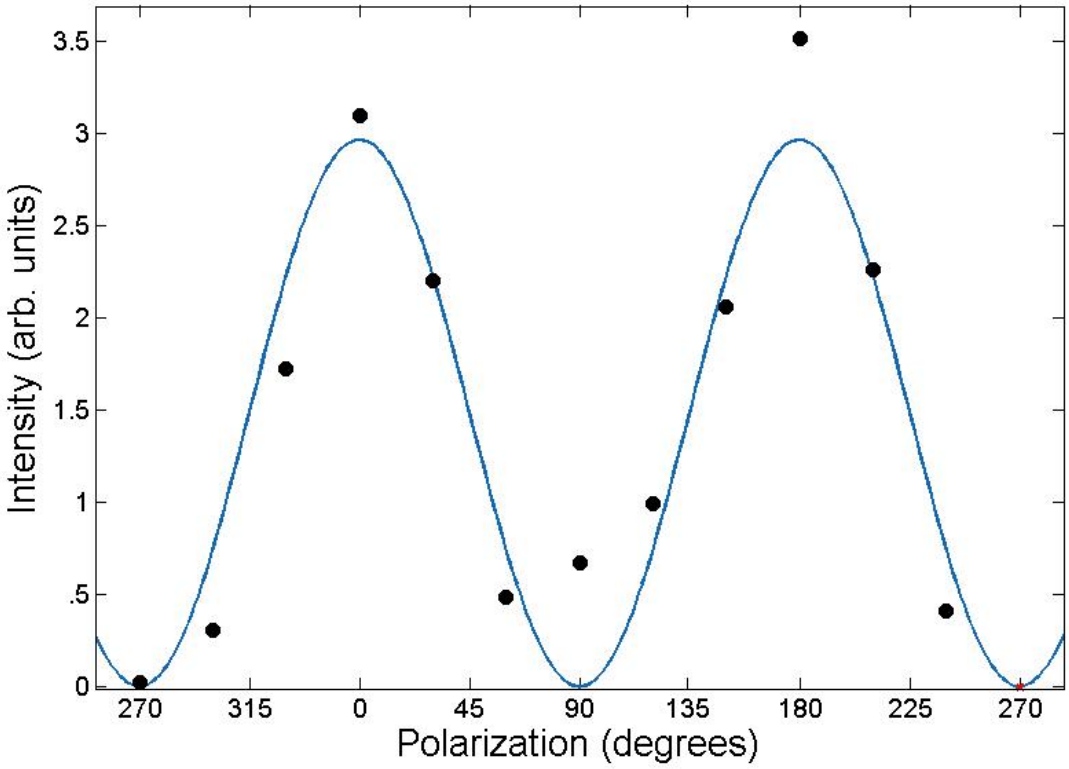

Figure 32: Polarization of the polaritons. At 0^o, the fast axis of the polarizer is aligned with the polarization of the laser beam. The intensity is maximum at 0^o and 180^o and minimum along the perpendicular directions, indicating that the polaritons were polarized along the same direction as our pump beam. The dots represent the data while the solid line is a fit to the data.

polaritons tend to hold the polarization of the pump beam state when pumped resonantly, we would maximize the chances of deterministic absorption if the condensate is polarized along the same direction. As elaborated upon in Chapter 7, we exploited this to create a condensate using a beam polarized along the same direction as the two-photon beam.

7.0 DETERMINISTIC ABSORPTION OF THE TWO-PHOTON BEAM

Polaritons, by virtue of being a particle with a integer spin, are bosons obeying Bose-Einstein statistics. Thus, they can form a Bose-Einstein condensate. The microcavity polaritons in our samples are metastable particles with long lifetimes, which gives us the opportunity to image and study the polariton condensates continuously. In this chapter, I discuss experiments in which a polariton BEC was created by using a laser-generated trap or by resonantly pumping the ground state. In both cases a beam with half the energy of the polariton is incident on the condensate. We will refer to this beam as the "two-photon" beam. Our aim was to see modulation of the two photon absorption due to the presence of the condensate.

7.1 POLARITON BEC

The mass of the polariton is $10^{-4}m_e$ (where m_e is the free electron mass), giving them a much higher critical temperature than a cold atom gas. In a cold atom gas, a Bose-Einstein condensate requires temperatures in the order of a few tens of nanokelvin, while polariton BECs are reported at room temperatures[24, 25]. Our experiments are generally conducted at temperatures between $5 - 10$ K. In that regime, with a polariton mass of $\approx 10^{-4}m_e$, we obtain a critical density of $10^7 cm^{-2}$ particles. Polariton BEC is recognized by spontaneous real-space and momentum-space narrowing while decreasing the temperature or increasing the density[23, 87].

In our samples, we can create polariton samples by creating a "trap" as shown in Figure 33. The exciton cloud is static compared to the polariton. Therefore a polariton created on the excitonic cloud moves down in energy on either side of the cloud. The polaritons

moving right flow "downhill" (towards lower energy in the sample energy gradient - right in the Figure), gain momentum and are lost, but the ones moving "uphill" (towards higher energy in the sample energy gradient - left in the Figure) are trapped in the energy minimum to the left of the cloud.

7.2 DETERMINISTIC ABSORPTION OF A FOCK STATE

Fermi's rule tells us that stimulated scattering into a state is enhanced by (N+1) if the occupation state is occupied by N as stated in Section 2.5[28]. In polariton condensates, this can be used to increase the number of polaritons using optical absorption. Thus absorption into the final state can be controlled by the occupation of the final state. This process of deterministically absorbing the two-photon beam can be used as an optical switch. The laser beam used to directly excite our samples are required to be around 1550 nm which is also in the optical communication band. The beam can be propagated using a fiber and can be used to modulate the absorption of the single photon excitation beam.

A coherent beam of light can be written as

$$|\text{coh}\rangle = \alpha_0|0\rangle + \alpha_1|1\rangle + \alpha_2|2\rangle + ... \tag{7.1}$$

where $|0\rangle$, $|1\rangle$ etc.. are the Fock states and α_n is the corresponding amplitude of the Fock states. If the light is attenuated to very low intensity such that α_3 and higher are very small, we can use two-photon absorption to absorb the two-photon $|2\rangle$ states, leaving behind a stream of single-photon $|1\rangle$ states. This can be tested by doing a standard Brown-Twiss photon-photon correlation experiment.

Photon-photon interaction between single photons is of great interest in the field of quantum information[121, 122]. The two-photon process could provide a logic gate acting on single photons by which single-photon states are unaffected but two-photon states are destroyed on demand.

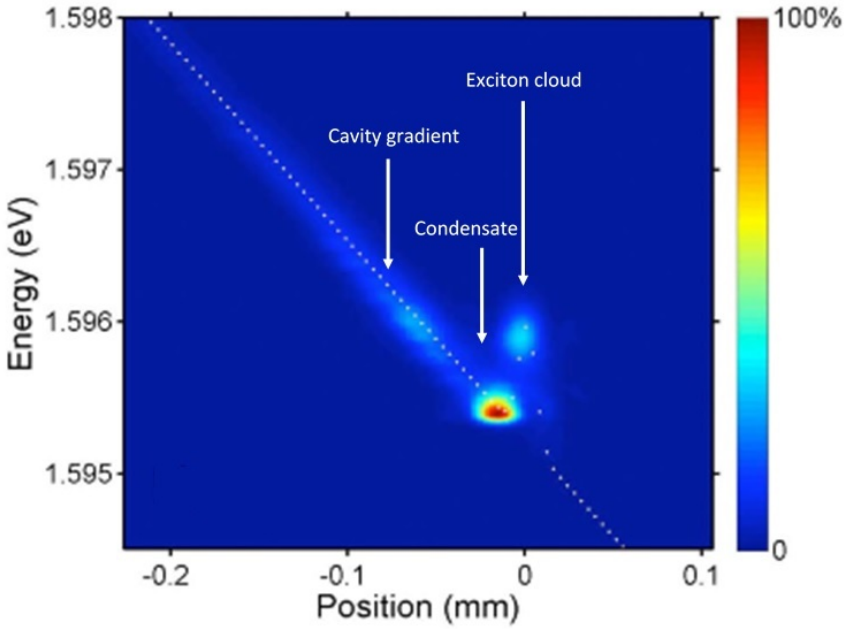

Figure 33: Real-space image of a polariton condensate created by the power trap method. The polaritons are created by a powerful laser which creates an exciton barrier at the point of incidence on the sample. They are trapped by the exciton barrier to form a condensate. The dashed white lines show the calculated potential-energy profile felt by the polaritons[87].

7.3 CREATING A POLARITON CONDENSATE

Polariton condensates can be created by using harmonic traps in the plane of the polariton motion and varying the density of the polaritons. These harmonic traps can be made using stress traps[48], changing the electric field[123], varying the cavity length during growth, or by shaping the exciton cloud. However, an electric field causes interference with the polariton since it could cause a change in the oscillator strength of the exciton while controlling the width of the cavity during growth can be really hard. Thus, our preferred approaches to create a harmonic trap are stress traps[23], shaping the excitonic cloud, and resonance excitation.

7.3.1 Stress Trap

A change in the width of the polariton cavity causes a change in exciton energy. This results in a change in the detuning and causes a drop in the polariton energy. The change in energy of the polariton is given by the Pikus-Bir Hamiltonian[124]. One way to change the cavity width would be to stress the back of the sample and make a depression into the sample and cause a localized change in the cavity width. In this method the sample is held between two plates and stressed from the back with a small pin. This causes a distortion in the cavity which causes an increase in the unit cell volume and results in a local energy minimum. The pump beam is incident on the front of the sample and luminescence from the same surface is observed as the cavity width is changed.

It must be noted that since the cavity width of our samples change along the length of the sample, this causes an asymmetric trap. This method further lets us stress any part of the sample and gives us the freedom to pick the strongest coupled region. If we excite the sample non-resonantly, the polaritons move to the local minima created in the sample and form a condensate. In my work I did not use a stress-trap. However, this method is available in our lab.

7.3.2 Laser-generated trap

For short lifetime polaritons, the interaction time between particles in the condensate is of the same order as the lifetime of the polaritons, i.e., 1-2 ps. This causes a discontinuity in the transition to a BEC and it becomes harder to reach an equilibrium state, which earns them the name of "non-equilibrium condensate"[125, 126]. However, our polariton samples have a high Q factor of $\geq 3 \cdot 10^5$ as a result of the high number of DBRs on the front and back which gives us a lifetime of 180 ps. As long as the polariton lifetime is longer than the interaction time between the particles, it is possible to achieve an equilibrium state quite easily.

As mentioned in Section 3.3.2, the width of the cavity varies across the sample and causes a change in the polariton energy across the sample. This acts as a potential gradient which produces a force of $-\partial U/\partial x$. When the sample is pumped non-resonantly with a high density beam, we create a large density of polaritons which experience a force due to the cavity gradient. Thus, the polaritons are accelerated along the cavity gradient and move towards a lower energy. However, if we create an exciton barrier, the moving polaritons will be stopped before the barrier and we can obtain a high intensity of polaritons in a single spot. By increasing the density of the polaritons above the critical density for condensation, we can create a polariton condensate.

As we increase the intensity of the pump beam, we create a large density of excitons at the pump spot, which we call the "exciton cloud" (Figure 33). Since the excitons, with a mass of $0.3m_e$, are much heavier than the polaritons, they cannot move more than a few microns in their lifetime and remain stationary compared to the polaritons. The excitons repel the polaritons due to Coulomb interactions, forming a positive potential. This causes a blue shift of the polaritons compared to their energy when created with a a low intensity pump beam.

The polaritons created at the pump spot are repelled by the excitonic cloud and move away in both directions. In one direction, the polaritons move towards lower energy in the sample. In Figure 33, this is to the right of the exciton cloud. In this case, they gain momentum as they move away and continue to move out of our field of view. In the other

direction (left of the exciton cloud in Figure 33), they encounter the cavity gradient which forms one wall of the harmonic potential. The exciton cloud forms the second wall. As we increase the intensity of pump beam we increase the density of the polaritons. At a particular density we see a sudden jump into a single-energy state at the bottom of the harmonic trap. This is the condensate state. Luminescence from this state is now brighter than the luminescence from the pump spot which is about 10μm away to the right of the condensate. Measurement of the spectral width of this luminescence is limited by our detection system.

One of the drawbacks of this method is the high intensity of the pump beam required to create the polaritons. The high intensity, coupled with the excitonic cloud, causes a localized hot region with an increased temperature. If we increase the intensity of the pump beam too much, we could push it above the critical temperature and the condensate could disperse or be unstable. Since we are viewing the time-averaged image of the condensate, this could be hard to pick out. Thus, while it is essential to use a high intensity laser beam, we should also take care to not increase the pump power too high. A solution to this problem is to use a chopper to chop the beam with a given intensity in order to reduce heating of the sample. Since more of the pump beam goes through the mirrors at this energy, a lesser pump power is required.

While using a power trap to create polariton BEC in the experiments described in this thesis, we used a picosecond Ti:Sapphire laser to create the condensate. This laser was used in the continuous wave mode, since we needed to synchronize it with a femtosecond laser at half the polariton energy. The sample was placed in a bath cryostat and the experiment was performed at liquid helium temperatures. Under these conditions it requires $\sim$ 200 mW to create the condensate.

7.3.3 Resonant excitation

Polaritons can also be created by pumping the sample resonantly at the polariton energy. We tweaked the laser beam to the exact polariton detuning we are looking at. Since this is resonant pumping, the pump beam is at the same wavelength as the signal and the reflection of the pump beam off the sample surface could interfere with the photoluminescence from

the condensate. In order to avoid that, we pumped at a spot far away from our point of observation and injected the polaritons with an in-plane momentum so they move into our field of observation.

We can check the energy of the polaritons at our point of observation by pumping the spot normally with non-resonant beam produced by a diode laser. This beam is at a much higher energy (~ 1.76 eV), so we can spectrally resolve the photoluminescence to eliminate the pump beam and look for the polariton. Once we determine the energy of the lower polariton at the detuning we're interested in, we tweak the Ti:Sapphire laser to produce a beam with the same energy. The FWHM of the laser is $<$ 0.2 nm.

Since we are pumping at a point away from our field of view, it is necessary to give the polaritons an in-plane momentum ($k_{||}$) for it to travel to our field of view. This is done by pumping "up-slope", i.e., towards a higher energy gradient in the cavity. As discussed in Chapter 6, the polaritons, which are created far away lose momentum as they exchange kinetic energy for potential energy until they reach $k_{||} = 0$, at which point they turn around. By controlling the angle of pumping, we can control the initial in-plane momentum and ensure that they turn around when they come into our field of view. This is done by adjusting the focusing lens.

This method gives us a way to directly pump into the ground state of the polaritons. If we increase the power of the laser such that occupation number is greater than 1, we can create a non-equilibrium condensate. Since we can adjust the angle of incidence and pump energy, we have the freedom to create a condensate at any energy detuning on the sample. Since we need to come in at a wide-angle for these experiments, we used the microscope cryostat to cool down the sample.

7.4 STIMULATED ABSORPTION WITH NON-RESONANT PUMPING

In order to study the stimulated absorption of the two-photon beam, we need to be able to measure the beam coming through back of the sample. However, we couldn't measure the absolute power and compare it with the pump beam since the DBRs at the back of

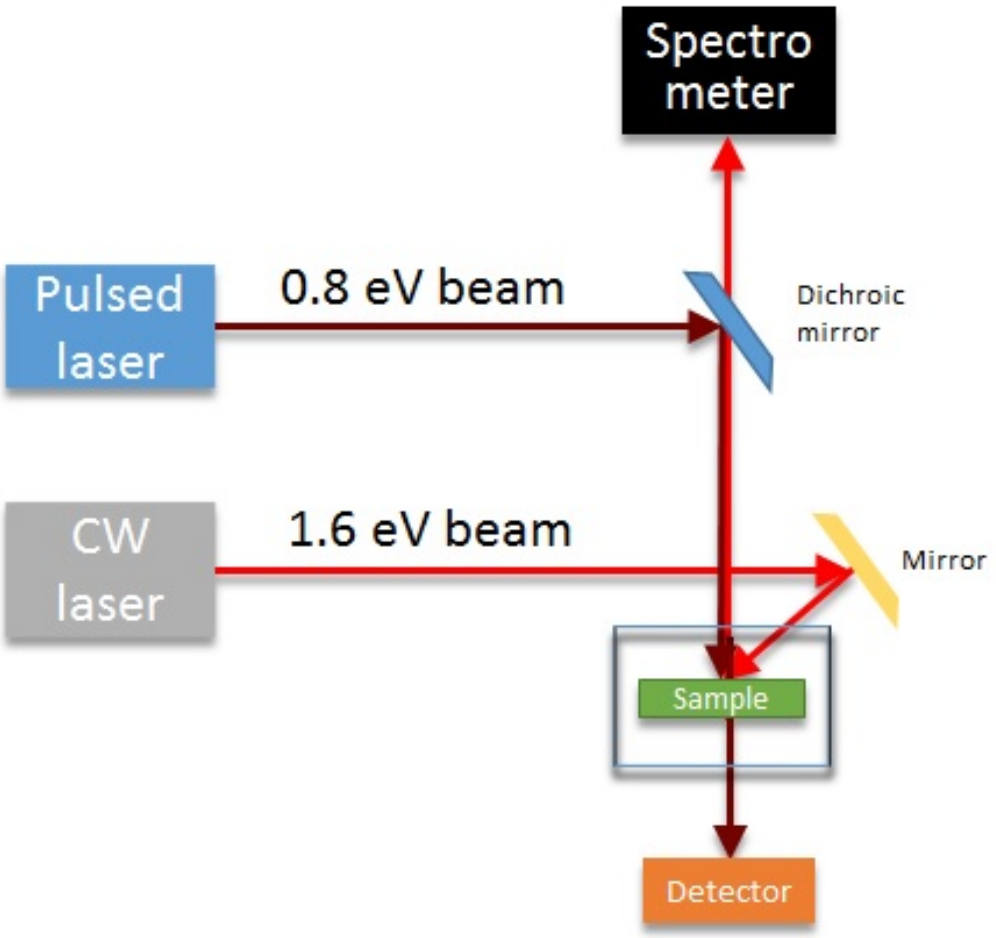

Figure 34: A representation of the experimental setup for stimulated absorption experiment where the condensate is created by non-resonant pumping. The condensate was created by a beam coming in at an angle while the two-photon beam was incident normally on the sample and was measured coming out through the back of the sample.

the sample reflect a portion of the beam back, while another portion will be absorbed by the GaAs substrate. In order to lessen the absorption by the substrate, a portion of it was removed by polishing. Also, since we only wanted the change in the pump beam in the presence and absence of the condensate, it was unnecessary to know the absolute beam strength in the absence of the condensate. The experimental setup was similar to the QDs (see Chapter 3, Section 3.1) but with a dichroic mirror, which helped us send the two-photon beam and the non-resonant beam simultaneously and co-linearly. The non-resonant excitation beam creates a large final-state occupation which enhances the absorption of the two-photon beam.

In order to measure the amount of two-photon beam passing through the sample, a specially prepared sample holder was used (Figure 25(d)). This holder had a hole in the center which allowed two-photon beam to pass through. The hole was $\sim$ 2 mm in diameter, which was sufficient to allow the pump beam to pass through. In fact, our focused beam was the order of a few tens of μm^2 at that position, which gave us the freedom to move along the cavity a little bit to study the polaritons at different detunings. Although, as discussed in Chapter 5, two-photon excitation is better while the pump beam is incident at a large angle, we had to send the beam in normal to the sample since we needed to collect the beam going through the back of the sample. However, the beam was expanded to a size of 1 inch and sent through a focusing lens which gave it a range of k-values.

The sample was placed in the bath cryostat, where the sample is receded from the front window of the cryostat by 7 cm. This meant that we could no longer use a microscope objective and had to use a longer focal length lens instead. By placing the sample at the center of the cryostat and the focusing lens against the front cryostat window, we were able to collect the beam coming through the sample by placing a collecting lens with similar focal length against the back window. The pump beam going through the sample was measured using a Germanium photodiode, a power meter or a avalanche photodiode (APD), while the luminescence leaking out through the front of the sample was viewed using the CCD and streak camera.

The non-resonant beam used to create the condensate (referred to here as the "single-photon" beam) was sent at an angle using a small side mirror. A schematic of this set up

is shown in Figure 34. The beam was sent at an angle for two reasons. One, our focusing lens for the two-photon beam was the same as the collection lens, we wished to not move the lens once we are done with alignment, but we needed to control the position spot where one of two beams hit the sample since we wanted the beams to overlap on the sample. Thus we needed to be able to control the position of the single-photon beam to get the two beams to overlap on the sample and needed a separate control of the single-photon beam. We also required separate focusing of the two beams since they were at different wavelengths and the focal length changes slightly with wavelength. Two, by sending the single-photon beam normal, we risked the beam going through the sample and overwhelming our photo-diode and power meter. Although we could have used multiple long pass filters, our average single-photon beam intensity was two orders of magnitude greater than the average two-photon beam intensity and enough of the beam could leak through and interfere with our photo-diode. It is worth mentioning that for the non-resonant beam, the in-plane momentum given by the large angle does not play a part since the momentum is dispersed to phonons by the time it cools down to the polariton energy.

Although two-photon absorption is a very weak process in polaritons, the rate of absorption can be controlled by the occupation number of the final state. Even if the process is weakly allowed, the large occupation number in polariton condensate should enhance the process. Change in absorption was measured in two ways: first the two-photon beam going through the sample was measured with and without the presence of a condensate and second, the luminescence from the sample was measured for changes due to the stimulated absorption.

7.4.1 Measurement of the beam going through the sample

A condensate was created at 5 K and the two-photon beam was sent through the condensate and measured coming out through the back of the sample. The two-photon beam going through the sample was measured with and without the condensate by blocking the beam creating the condensate with a blocker. The two-photon beam was measured with a Thorlabs power meter attached to a low-power head. If there is indeed a stimulated absorption of

Power with the condensate blocked (in W)	Power with the condensate (W)
190	185
116	110
51	48

Table 1: Power of the two-photon beam in the presence and absence of the condensate. The power was measured with a power meter. There seems to be a small decrease in the power of the two-photon beam due to the presence of the condensate.

the two-photon beam, we would expect a decrease in the beam intensity when there is a condensate present. The power was integrated over a 10 second time period to get rid of noise and fluctuations in the laser.

The measured results are shown in Table 1. In this table, the power of the beam creating the condensate was kept constant while power of the two-photon beam was varied. As seen from the table, there seems to be a small decrease of ∼5-6% in the power of the two-photon beam due to the presence of the condensate, which indicates that there may indeed be a modulation of the two-photon absorption by the presence of the condensate.

We also changed the intensity of the beam creating the condensate while keeping the intensity of the two-photon beam constant at 760 μW. Since the change in intensity of the beam creating the condensate should affect the number density of the condensate, we would expect to see a change in the amount of two-photon beam absorbed by the condensate as we change the density of the condensate. The results from this experiment are shown in Figure 35. While we see a slight increase in the amount of two photon absorbed, the change is not too high. The weak dependence indicates that the condensate is not strongly modulating the absorption since we would expect the absorption to be linear with the condensate density. Our reason for the sub-linear dependence could be because as we increase the intensity of the beam, the condensate flows out of the trapped region faster, and thus the number density of the ground state of the condensate might not increase linearly with increase in pump

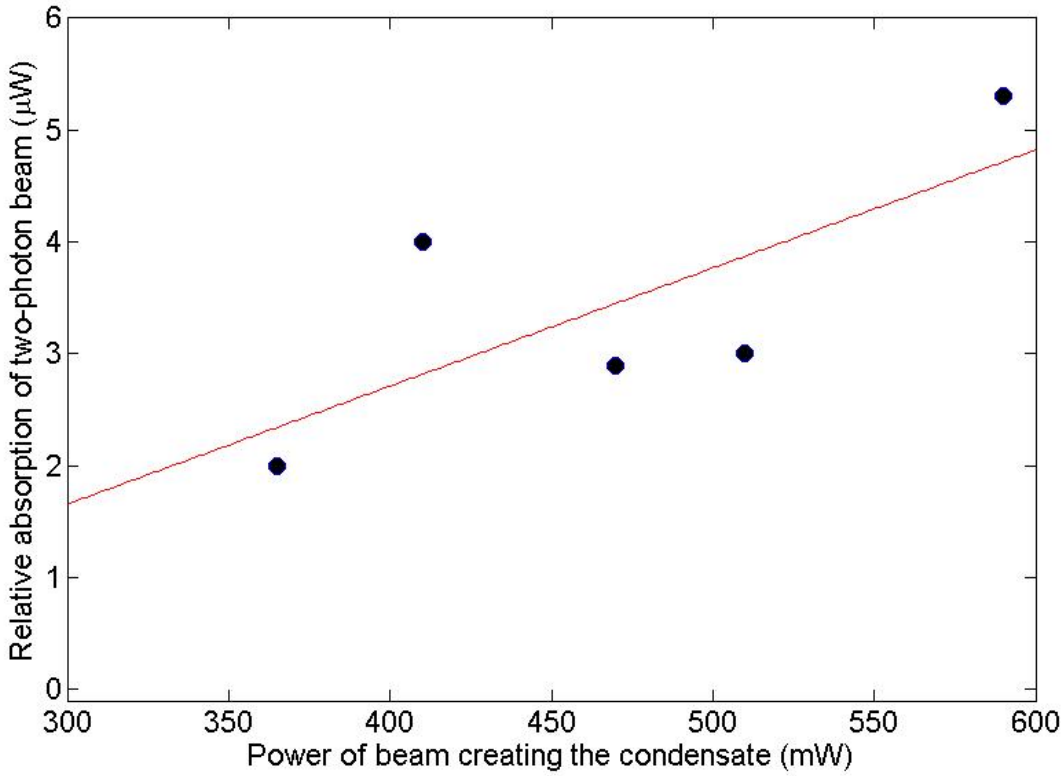

Figure 35: Change in two-photon beam intensity against change the intensity of the beam creating the condensate. The intensity of the two-photon beam was constant at 760 μW. There is a slight increase in the amount of two photon absorbed. The change is not too high since as we increase the intensity of the beam, we provide the condensate a certain amount of energy to escape the lower energy state. The threshold power required to create the condensate was 300 mW.

intensity.

Another point of consideration was the localized heating of the sample due to the presence of the condensate. The condensate was created with a high-power CW beam and the measurement was done with an integration of 10 seconds. The high-power beam could cause heating and expansion of the sample over this time period, which could cause a change in the absorption of the two-photon beam itself. Since the absorption seen in the beam was marginal, we were not entirely convinced that that the beam measured was due to the condensate itself and not due to heating effects of the condensate.

To reduce the effect of localized heating due to the high intensity beam, we used a chopper to chop the pump beam creating the condensate. The chopper is controlled by a controller which lets us set the frequency with which we chop the beam at 500 Hz. The two-photon beam is sent to an avalanche photo-diode (APD). The frequency of the chopper and the signal from the APD were sent to a lock-in amplifier. The lock-in amplifier only picks out the frequency of the signal which matches that of the chopper. This helps eliminate the laser beam coming through the sample and pick out the signal modulated by the presence of the condensate alone and we get a direct reading of the deterministic absorption of the two-photon beam. The experimental setup is shown in Figure 36. Even though there is still heating from the CW pump beam, the effect is uniform during the presence and absence of the condensate since the system doesn't have time to cool down again between the "on" and "off" period of the condensate.

We changed the point of incidence of the two-photon beam on the sample and scanned across the condensate. We looked for a maximum APD reading as we scanned across the sample - we expected a maximum as we cross the condensate. The results are shown in Figure 37. As seen, the a maximum corresponds to the location of excitonic cloud rather than the condensate itself, which is centered at $x = 0.025$. Also, we noticed that the decrease in the change in absorption on both sides of the condensates are different. This indicates that the polaritons are indeed playing a role, since heat diffusion should be symmetric. The polaritons cloud is not symmetric because to the left of the condensate, the polaritons hit the cavity barrier, while on the right, the polaritons continue to flow. The fact that there is some modulation on the downhill side indicates that heating is playing a role in addition to

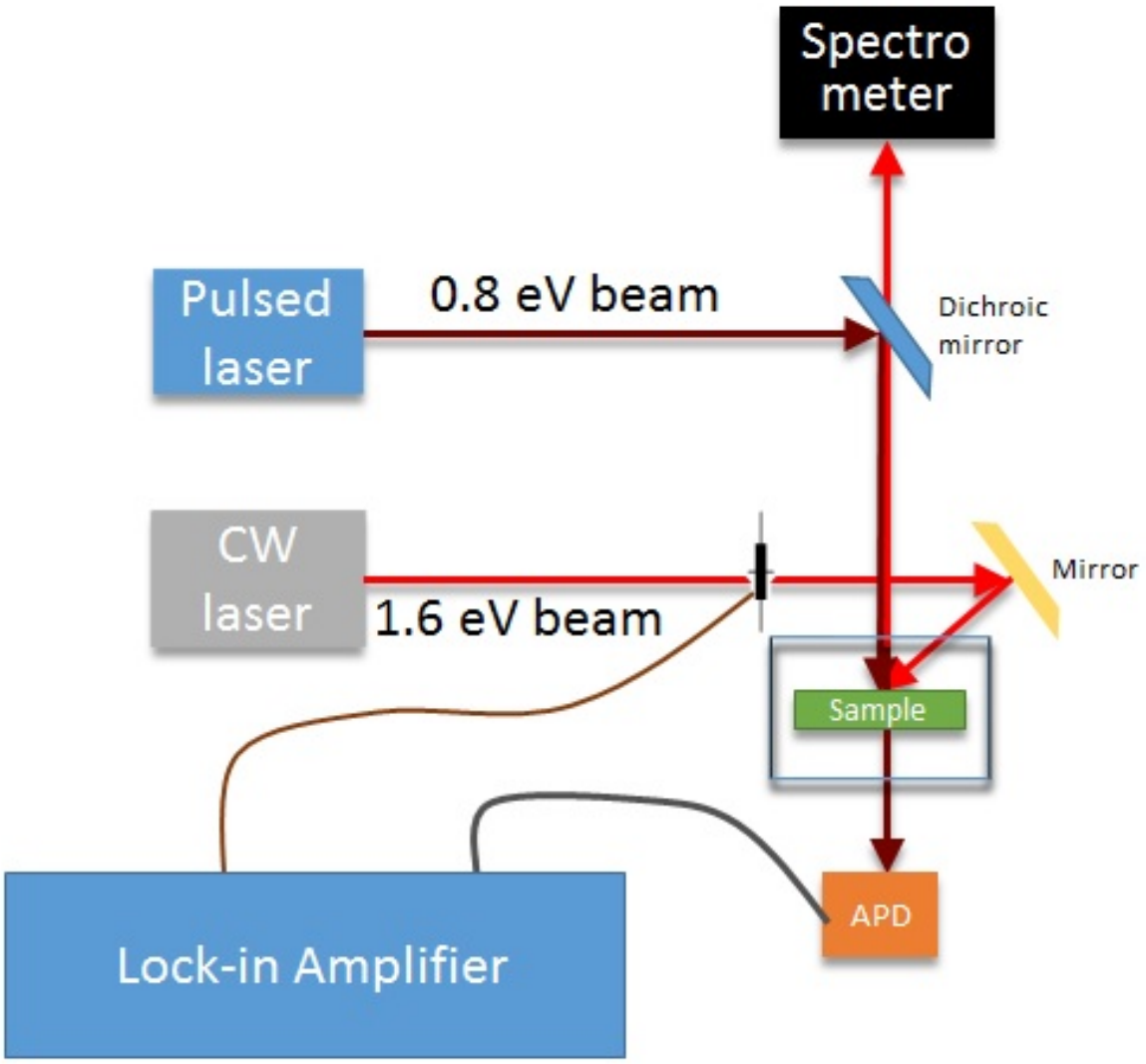

Figure 36: A representation of the experimental setup where we used a chopped to chop the beam creating the condensate. The frequency of the chopper and the signal from the APD were sent to a lock-in amplifier, which picks out the frequency of the signal which matches that of the chopper.

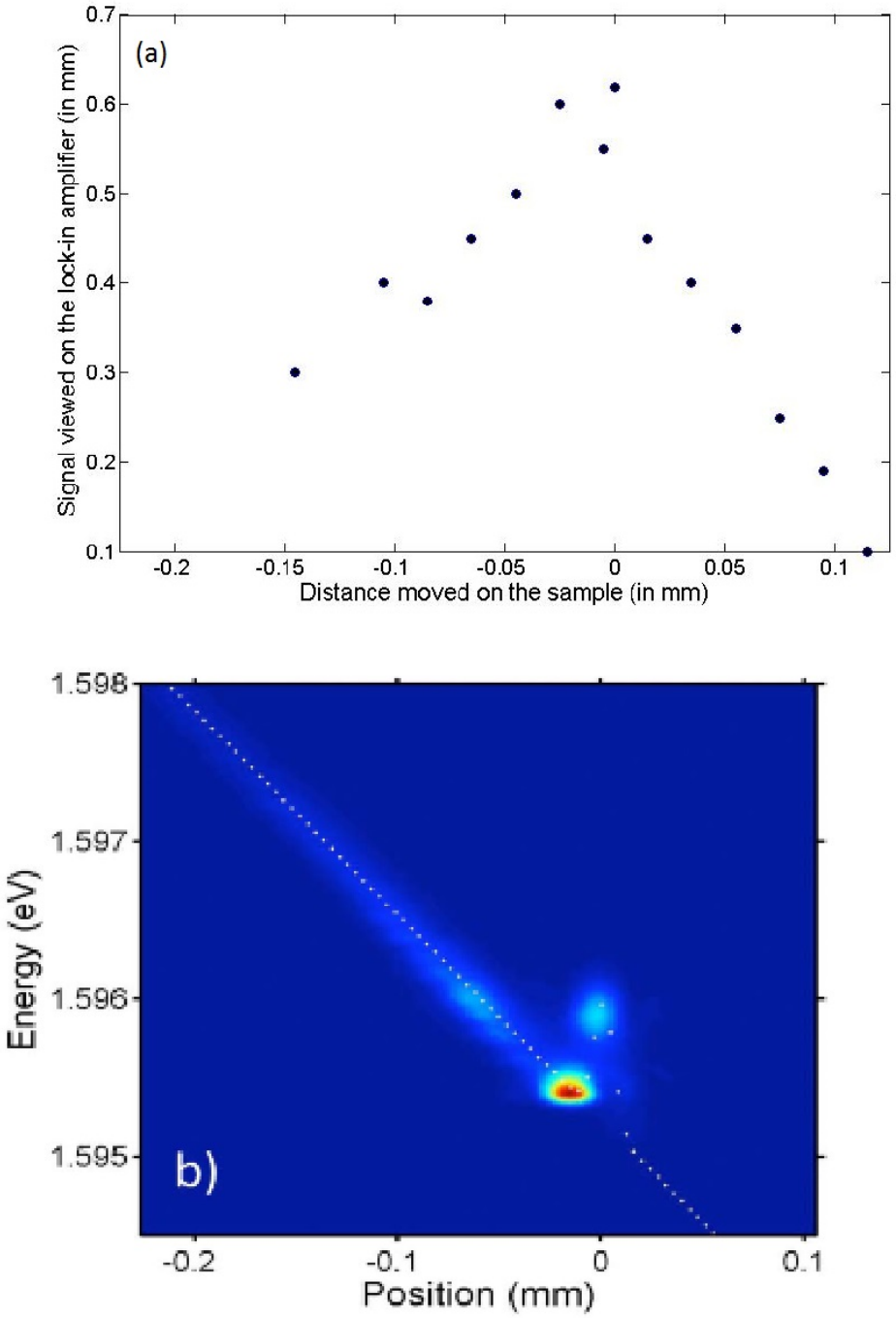

Figure 37: Change of the position at which the two-photon beam was incident on the sample vs change in signal power. (a) Change in power observed on the lock-in amplifier. (b) Real-space image with position at which we are observing marked out.

the polaritons.

We also performed a power series of the two-photon beam keeping the number density of the condensate constant. As we increase the pump intensity, we should see an increase in absorption followed by a decrease. This can be explained by considering the model shown in Figure 38(a). We consider a two-photon beam with intensity I_0 incident on the sample. It is absorbed both in the microcavity region of the sample as well as in the substrate. Since it undergoes two-photon absorption, we consider absorption until the second order and the change in intensity of the incident beam with distance is given as

$$\frac{dI}{dx} = aI + bI. \tag{7.2}$$

Integrating we get the intensity to be

$$I = \frac{I_0}{1 + bxI_0}. \tag{7.3}$$

Since the length of the sample remains constant, we assume the absorption coefficient in the microcavity to be $b_{1\text{off}}$ and $b_{1\text{on}}$ in the absence and presence of the condensate respectively, and the co-efficient of absorption in the substrate to be b_2. If I_{off} is the intensity of the two-photon beam coming out through the back of the sample in the absence of a condensate and I_{on} in the presence of the condensate, we obtain

$$\frac{I_{\text{off}} - I_{\text{on}}}{I_0} = \frac{1}{1 + b_{1\text{off}} b_2 I_0 + \frac{1}{I_0}} - \frac{1}{1 + b_{1\text{on}} b_2 I_0 + \frac{1}{I_0}} \tag{7.4}$$

As seen in Figure 38(b), as we increase the intensity of the two-photon beam incident on the sample, the change in intensity of the beam coming through the back of the sample in the presence and absence of the condensate increases until it reaches a maximum and then decreases. Our data is shown in Figure 39, where we can see that the change in intensity of the beam increases with increasing intensity of the two-photon beam and then decreases as expected. This is true for absorption due to both heating effects as well as stimulated absorption.

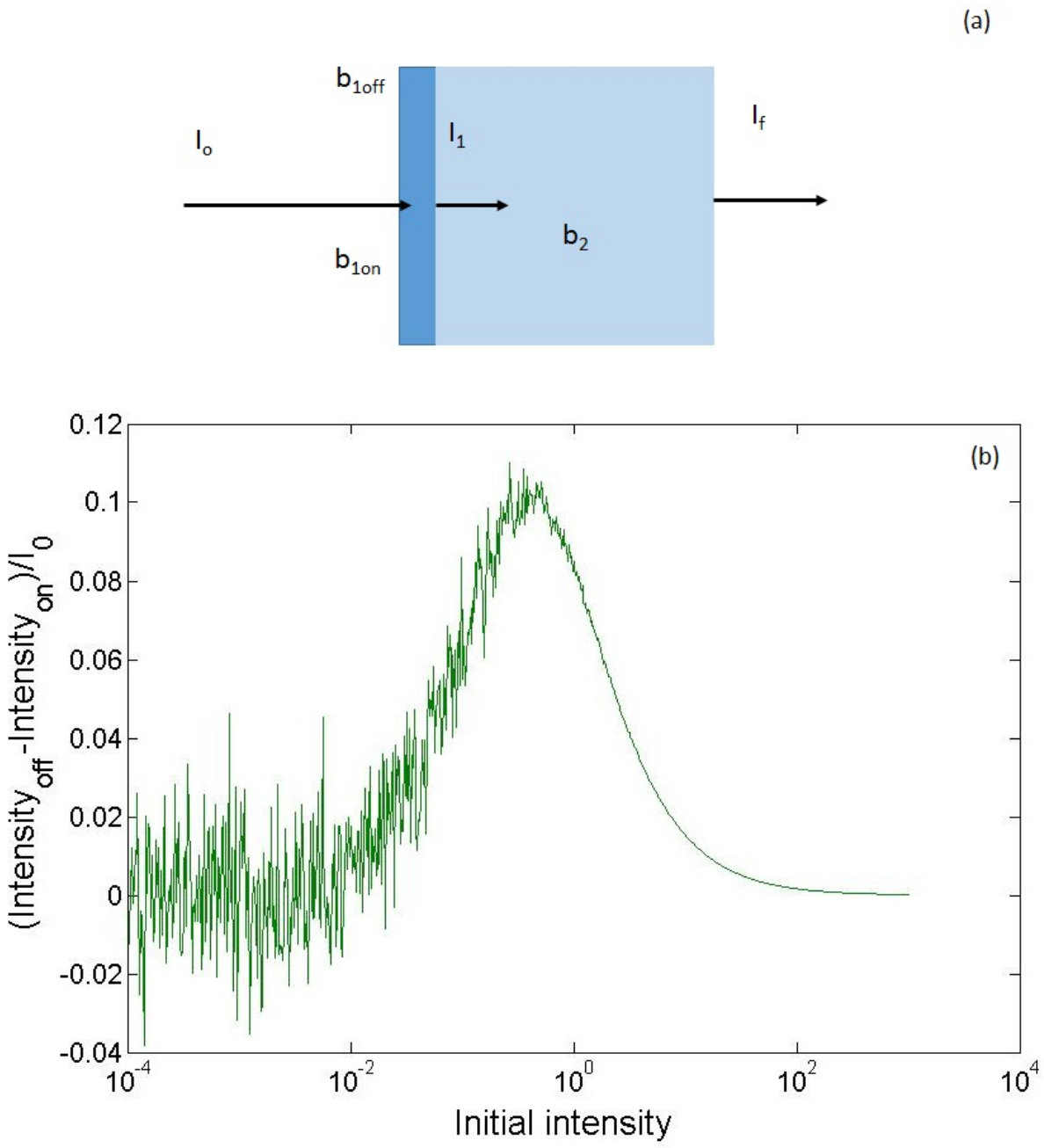

Figure 38: (a) Simplified model of the polariton sample assumed. (b) Simulation of the change in absorption with increasing intensity of the two-photon beam. Note: Noise was artificially added.

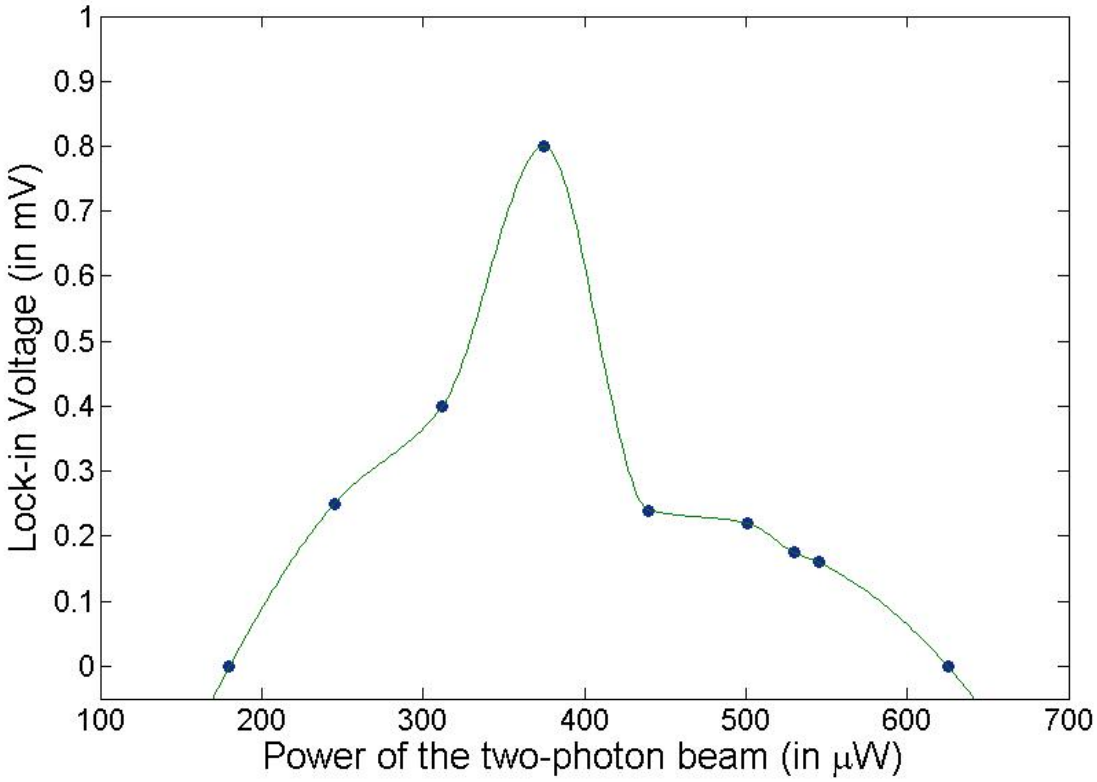

Figure 39: Our experimental data for change in absorption of two-photon beam due to change in intensity of the beam. As expected from the simulation, the intensity of the beam increases with increasing intensity of the two-photon beam and then decreases.

7.4.2 Measurement of the photoluminescence

We also measured the intensity of luminescence from the polariton sample coming out through the front of the sample, when a condensate alone is present, when there is a condensate and the sample is being pumped with a two-photon beam, and when only the two-photon beam is present. If the intensity due to the condensate and the two-photon beam together is greater than the intensity due to the condensate and two-photon beam incident separately, we can conclude that we see deterministic absorption of the two-photon beam.

Since the two-photon beam is a pulsed beam and the condensate is created by a CW beam, we used the streak camera to look at the difference. The streak camera was time-locked to the pulsed two-photon beam while a condensate was created with a CW laser. We looked for a change in the condensate intensity at the moment the two-photon beam hits the condensate. However, the luminescence from the condensate is $\sim 10^6$ stronger than the polariton created by the 2-photon beam and hence a change in intensity could not be detected by the streak camera.

The problem so far with non-resonant pumping was that a lot of power ($\sim$300 mW) is required to create the condensate which heats up the sample. When we block the high-power pump beam, we visibly see the temperature drop by a couple of degrees, which might affect the change in absorption of the two-photon beam. Although we have used a chopper to chop the beam, we might still have instantaneous heating effects. The other problem is since we have a very strong luminescence from the condensate, it masks the luminescence due to the two-photon beam and it is hard to estimate the change in luminescence due to the two-photon beam. To circumvent this problem, we created the condensate with resonant excitation.

7.5 STIMULATED ABSORPTION WITH RESONANT PUMPING

We created a condensate by pumping resonantly at an angle as detailed in Section 7.3.3. In non-resonant excitation, much of the power used to create the condensate is dissipated as

phonons. A large laser intensity is required to create the power trap. However in resonant pumping, we directly pump the polariton states. This minimizes the pump power required to create the condensate. Also, since there is no exciton cooling from the excited state to the ground state by the emission of phonons, we reduce the heating effects that we saw previously.

We pumped far away from our field of view using the method described in Section 6.2. Since the pump spot is not in our field of view, we see no interference from the pump beam. Since the incident beam had a large angle, we imparted a large in-plane momentum to the polaritons. However, they lost this momentum as they traveled "uphill" against the cavity gradient as discussed in Section 6.2. We looked at the polaritons as they came into our field of view and turned around since they are at $k_{||} = 0$ at that point. We used the microscope cryostat to pump the sample since we needed a wide field of view. The cryostat was maintained at a temperature of 4-5 K

Unlike the non-resnonant experiment, where the polarization of the laser beam is lost, from experiments in Section 6.4 we know that for resonant experiments, the polarization of the polaritons depends on the polarization of the pump beam. Hence, we made sure that the two beams - pump beam creating the condensate and the two-photon beam — are polarized in the same direction. We also made sure that the two-photon beam is TM polarized to ensure maximum absorption of the beam.

7.5.1 Condensate creation with a CW beam

We used a Ti:Sapphire MIRA laser in its CW mode to create the condensate. A CW beam was chosen since the condensate should be present when the pulsed two-photon is incident on the sample and since we were using two different lasers to create polaritons in the sample, having them be incident at the same time would be hard if they were both pulsed - one of our lasers has a repetition rate of 76 MHz, while the other has a repetition rate of 250 kHz. Since we needed a higher intensity to create polaritons with two-photon excitation, we used a pulsed two-photon beam and created the condensate using a CW beam. A pulsed femtosecond laser was used to send in the two-photon beam. This laser was tweaked to be

at exactly half the energy of the the CW laser, while the CW laser was tuned to the lower polariton energy.

We created a polariton away from our field of view and changed the power of both the laser creating the polariton condensate as well as the two-photon beam such that the intensity of the polariton luminescence due to both the beams was comparable. The experimental setup is given in Figure 40(a). We control the $k_{||}$ of the two-photon beam with a periscope and look for a change in intensity of the two photon signal with and without the single photon beam.

The images were viewed initially on the CCD camera where the luminescence was time-averaged for about 10 seconds. We measured the intensity of the polariton luminescence due to the CW beam alone, due to the two-photon beam alone, and due to both the two-photon beam and CW beam incident at the same time. If there is deterministic absorption of the two-photon beam, the difference between the intensity of polariton luminescence due to two-photon beam and the CW beam at the same time, and the two-photon beam and CW beam separately should be non-zero, i.e., intensity due to CW beam and two-photon beam - (intensity due to CW beam + intensity due to two-photon beam) should be greater than zero. However, we do have a bit of background noise due to various aspects such as changes in room light, etc. To make sure any luminescence we see is due to deterministic absorption, we changed the momentum of the two-photon beam incident on the sample by varying the position on the microscope objective using the periscope. If there is deterministic absorption, we should see a peak when the two-photon beam is incident on the exact spot as the condensate created by the CW beam. However, no real change in intensity was noticed as $k_{||}$ was varied to make sure there is an overlap.

The single-photon beam is CW, while the two-photon beam is pulsed and much more intense for a shorter period of time. However on the CCD camera, the intensity is time-averaged. In order to get better comparable intensities due to the two beams, we viewed it on the streak camera and increased the intensity of the CW beam to make the short time intensities comparable. We phase-locked the streak camera to the two-photon beam so that we observed the polariton luminescence due to the two-photon beam on the screen. Again, we varied $k_{||}$ using the periscope and saw no change in intensity due to the CW beam.

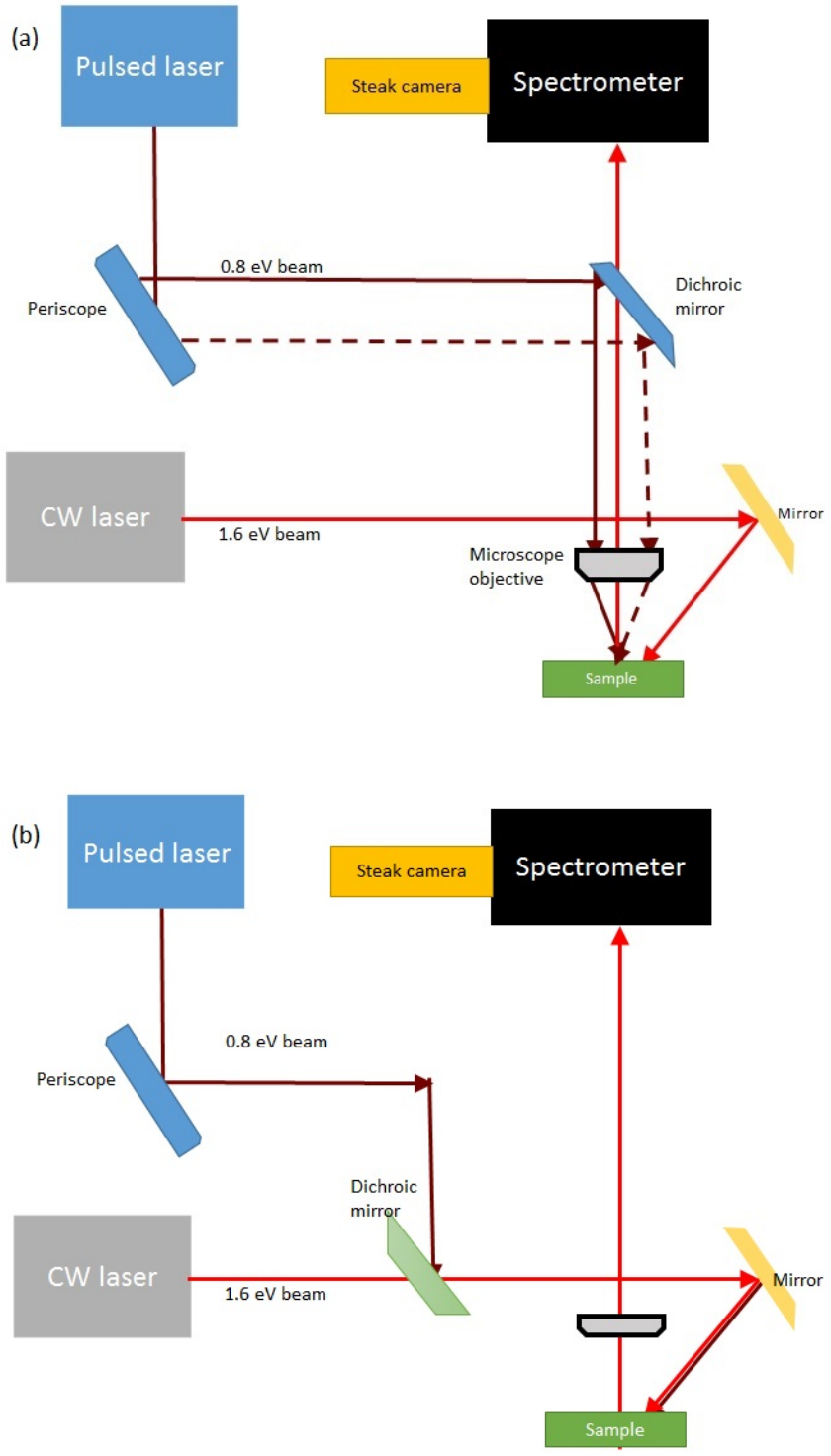

Figure 40: The experimental setup for deterministic absorption of pulsed two-photon beam by a condensate created by resonant excitation using a CW beam. (a) The two-photon beam was sent in normal to the sample through a microscope objective. The in-plane momentum was controlled using a periscope. (b) The two-photon beam was sent it co-linear with the CW beam.

Since we needed a high intensity two-photon beam, we used a microscope objective which required us to come in normal to the sample. This required the added step of k-matching since the two beams needed to have the same $k_{||}$ at the same spot. Though we tried to vary k of the two-photon beam to match that of the single-photon beam as it comes into our field of view, k-matching has to be exact. To get better k-matching, we made the two beam collinear and incident on the same spot as shown in Figure 40 since we should see an increased absorption even if the signal due to the two-photon beam isnt intense.

The luminescence was again viewed on both the streak camera and CCD Camera, but we did not see any change in the absorption of the two-photon beam. We calculated the occupation number of the condensate (discussed in detail in Appendix A) and found it to be less than 1. This told us that we needed to increase the occupation number of the polariton state quite steeply to see any deterministic absorption.

7.5.2 Condensate creation with a pulsed beam

The occupation number calculation told us that the occupation number of the polaritons created with the CW pump beam is off by a factor of 10 from the desired occupation number. However, this calculation is for the ideal case. In our experiment, we have defects on the sample, cryostat window, etc. which add to the loss in power making the desired intensity to achieve an occupation number ≥ 1 harder to achieve using the CW beam.

However, if we use a pulsed 200 femtosecond beam, with a repetition rate of 250 kHz, we will increase the intensity of the input beam for the same power by 10^7. In order to do this we split the pulsed beam from the OPA into two using a beam splitter. Half the beam is sent directly to the sample and was used as the two-photon beam, while the other half was sent to a frequency doubler (a BBO crystal) as shown in Figure 41, where the beam is doubled in energy. This beam is used to create the condensate. We will lose two-photon beam intensity but theoretically should still have enough power to see an increase in absorption compared to the condensate.

The two-photon beam was initially sent co-linear to the frequency doubled beam - and hence at a large angle. Since we were viewing the two beams on the CCD camera and the

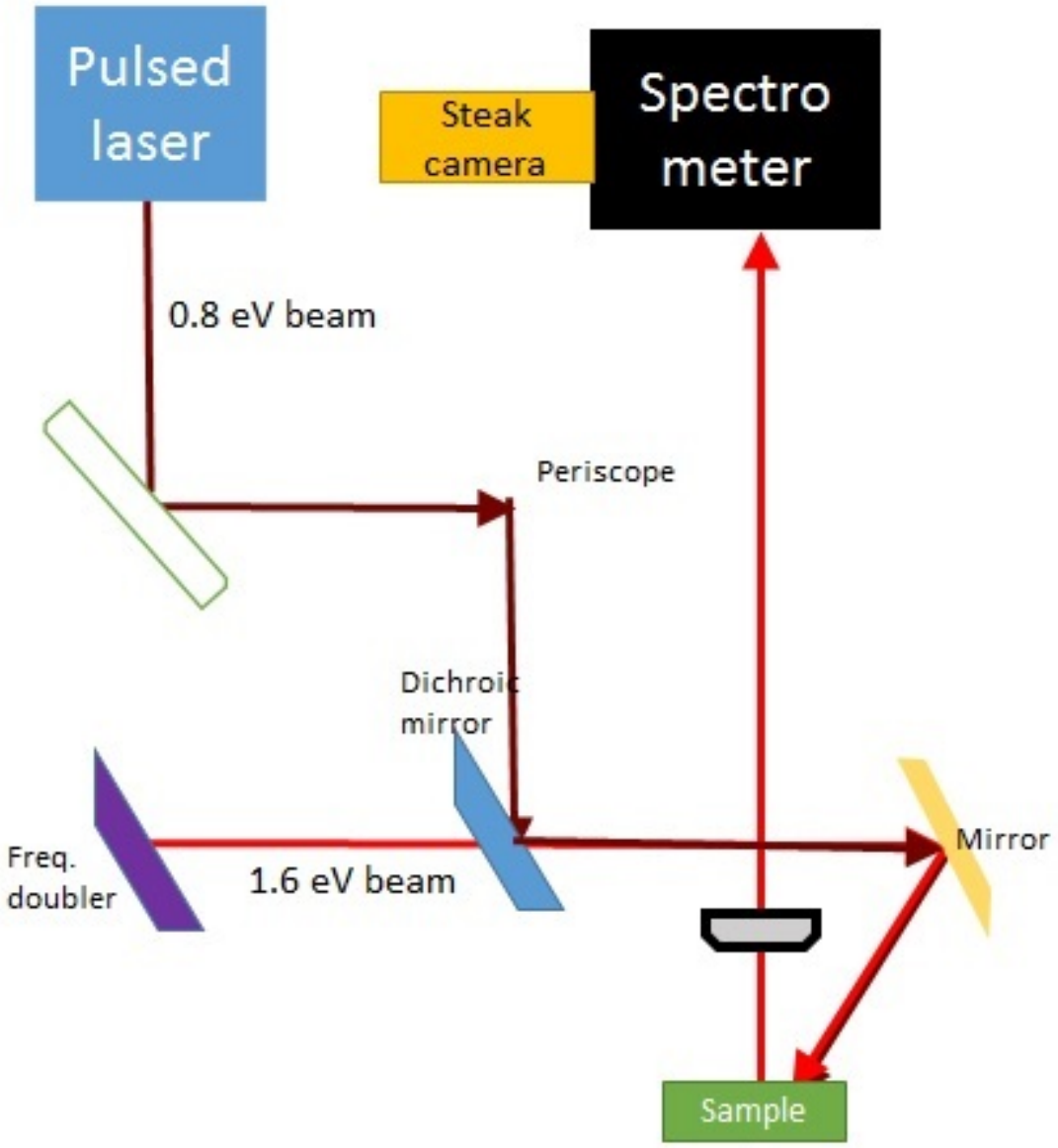

Figure 41: The experimental setup for deterministic absorption of pulsed two-photon beam by a condensate created by resonant excitation using a pulsed beam.

streak camera, we decreased the intensity of the frequency doubled beam so the luminescence from both were comparable within an order of magnitude. However, since we are coming in at a large angle, we couldn't use a microscope object and couldn't get a tight focus with the two-photon beam, so the intensity of the luminescence was really weak. When we reduced the pump intensity of the frequency doubled beam to match the luminescence from the two-photon beam, it wasn't enough to create a condensate.

Since the absorption of the two-photon beam should increase by the occupation number of the condensate state, we sent in the entire frequency doubled pulse. The power of the femto-second one-photon beam hitting the sample was $\sim$20 μW, which should give us an occupation number of $\sim$100. This should give an increased absorption of the two-photon beam by two orders of magnitude. However, the luminescence due to the two-photon beam was three orders of magnitude weaker than the condensate created by the single-photon beam and we were unable to see a change in the absorption.

Thus, while we do see absorption due to the presence of polaritons in the condensate created by laser-generated trap, we are unable to verify this by a condensate created by resonant excitation.

8.0 CONCLUSIONS AND FUTURE DIRECTIONS

8.1 CONCLUSION

Two-photon absorption, while having direct applications in many devices, can also be used to study aspects of quantum systems using methods that are not possible using single-photon excitation. For example, the energy of excitation is far from the energy of interest and thus we do not see any interference from the pump beam. More importantly, two-photon excitation gives us a means to probe dark states. In this thesis, I have looked at two-photon excitation of both quantum dots and microcavity polaritons. The motivation for these experiments were quite different.

Spin flip times of excitons in quantum dots are important for their possible applications in quantum information and quantum computing. In this thesis we have probed the spin flip times of excitons in self-assembled GaAS quantum dots by exciting the dark state and time-resolving the luminescence from the bright state. This told us that the spin flip time of these excitons is of the order of a few hundred picoseconds, while the "cool-down" time. i.e., the time taken by the quantum dots to emit phonons and go from a higher energy excited state to the lowest excited state is of the order of a few tens of picoseconds. This time is short compared to the dephasing time in other systems. Spin-flip requires emission of a particle carrying angular momentum while cool-down occurs through emission of a particle carrying away energy. Since phonons could do both, we believe that both transitions occur through phonon emission.

We used time-resolved spectroscopy to study the microcavity polariton system and showed that direct two-photon excitation of lower polaritons is possible under certain circumstances. Although other studies of two-photon excitation of exciton-polaritons have

considered the possibility of an allowed absorption process into the 2p state of the excitons or through second harmonic generation[66, 70], we have conclusively shown — both experimentally as well as theoretically — that we have dark/bright state mixing when the polaritons are created with a non-zero in-plane momentum. This mechanism does not involve higher-lying $J = 2$ or $2p$ exciton states and instead is seen when the pump beam is tuned to be resonant to the lower polariton. We have also shown that direct two-photon excitation is proportional to $k_{||}^4$ and happens only when the beam is TM polarized. Direct two-photon excitation of polaritons leads us to expect nonlinear effects such as interaction of macroscopically occupied polariton states and light waves at half their frequency. When we time-resolve the luminscence while resonantly pumping the higher energy states, we do see those states being excited. However, the luminescence from excitation of these states has a long rise time since they must cool down to the lower polariton energy.

We also created polaritons away from our field of view and watched them travel into our field of view exchanging kinectic energy for potential energy, turn around once they reached zero-momentum and leave. This conclusively told us that we were indeed are seeing direct two-photon absorption. We were also able to use this to measure the lifetime of the lower polariton in our microcavity sample and found the lifetime to be similar to the lifetime measured with single-photon excitation.

Fermi's rule states that absorption into the final state goes as the occupation of that state. We used a laser beam to create a condensate and control the two-photon absorption of a second beam which was at half the energy. Deterministic absorption of the two-photon beam could be used to build optical gates. We used different methods to create the condensate. While creating the condensate non-resonantly we saw a slight modulation of the two-photon beam but were not sure if the modulation was due to the condensate or heating effects from the condensate since there is evidence for both. In order to minimize the heating effects, we created the condensate using resonant excitation. In this case we looked at the luminescence from the sample in the presence and absence of the condensate. However, we were unable to achieve an occupation number greater than one when we tried to match the the luminescence from the two-photon beam with the luminescence from the resonant beam and since the luminescence due to the two-photon beam was too weak. When we created

the condensate with a more intense signal, the change in the the luminescence due to the one-photon beam washed away a possible change in the luminescence due to the two-photon signal.

8.2 FUTURE DIRECTIONS

Achieving deterministic absorption of the two-photon beam could have tremendous applications. If we are able to control the absorption of the two-photon beam by the presence of the condensate, we could use it as an optical gate. Further, the two-photon of the polaritons we study are right in the communication wavelength. Since the two beams can be propagated using a optical fiber, deterministic absorption can happen far away from the laser system.

One of the biggest challenges in deterministic absorption of the two-photon beam has been creating a condensate with resonant excitation and viewing deterministic absorption of the two-photon beam at the same time. While creating the condensate resonantly we have been unable to achieve an occupation number greater than one in the experiment where we tried to match the the luminescence from the two-photon beam with the luminescence from the resonant beam and the luminescence since two-photon beam was too weak. In the experiment where we created the condensate and viewed the change in two-photon beam, the luminescence from the condensate over-powered any possible change in the luminescence due to the two-photon signal. However, if we are able to measure the two-photon beam going through the sample, it would not be necessary to reduce the intensity of the beam creating the condensate.

The other challenge is matching the position and momentum of the two-photon beam with the beam creating the condensate. This is done by scanning over a wide range of momentum. However, if we are able to confine the polaritons to move along channels etched in the microcavity sample, we could overlap the two beams quite easily.

APPENDIX A

CONDENSATE CALCULATION

For a resonantly-injected polariton gas, elastic scattering will cause the polaritons to quickly scatter to all directions of k within the range of energy of the optical injection. Thermalization to other magnitudes of k will happen much slower. Therefore we can estimate the number of photons needed to give amplification as the number of polariton states within the energy range of the injection. Injecting this number of photons will give an average occupation number of unity, which can be taken as the threshold for onset of amplification.

For a 2-D system, the density of states per unit area is given by:

$$\frac{D(E)}{A}\Delta E = \frac{m}{2\pi\hbar^2}\Delta E \tag{A.1}$$

where m is the mass of the polariton and ΔE is the line width. In our system

$$m = 10^{-4} m_e \tag{A.2}$$

where m_e is the mass of an electron. The energy relevant for our optical resonant injection experiment is the cavity line width which is, approximately,

$$\Delta E = 0.05 \text{ meV}, \tag{A.3}$$

which gives us

$$\frac{D(E)}{A}\Delta E = 10^6 \text{cm}^{-2} \tag{A.4}$$

In the resonant experiments the power of our laser hitting the sample was ∼1 mW. Since the spot size of the beam on the sample is $\sim 10\ \mu m^2$, our intensity is

$$I = \frac{P}{A} = 10^{-3}\ \mathrm{W/cm^2} \tag{A.5}$$

The energy of a single photon hitting the sample is ~ 1.5 eV. Thus the number of photons hitting the sample front of the sample per second is

$$\frac{1}{A}\frac{dN}{dt} = \frac{I}{E_{ph}} \simeq 10^{21}\ \mathrm{cm^{-2}s^{-1}}. \tag{A.6}$$

and the number of photons hitting the sample for the lifetime of the polaritons ($\tau \sim 200$ ps) is

$$\frac{N}{A} = \frac{1}{A}\frac{dN}{dt}\tau \simeq 10^{11}\ \mathrm{cm^{-2}}. \tag{A.7}$$

However the transmission of the front mirrors is $T = 10^{-6}$. This gives us the total number of photons inside the microcavity in the lifetime of the polaritons to be

$$\frac{N}{A} = 10^{5}\ \mathrm{cm^{-2}}. \tag{A.8}$$

Thus we are not sending through enough photons to cause simulated absorption. However, if we use a femto-second pulsed laser with a repetition rate of 250 kHz and a pulse width of 100 fs, we increase the peak intensity by an order of magnitude of 10^4 for the same intensity.

APPENDIX B

GROUP THEORY CALCULATIONS

Bulk GaAs has cubic symmetry and is generally represented by the T_d group. However we interested in studying the creation of polaritons in quantum wells. Quantum Wells can be represented by the D_{2d} group.

The valence band of the QW is two-fold degenerate at $k = 0$. They are represented by Γ_6 which represents the light hole and Γ_7 which represents the heavy hole. If you had add in the spin state represented by Γ_6, you get

$$\begin{aligned} \Gamma_6 \otimes \Gamma_6 &= \Gamma_1 \oplus \Gamma_2 \oplus \Gamma_5 \\ \Gamma_6 \otimes \Gamma_7 &= \Gamma_3 \oplus \Gamma_4 \oplus \Gamma_5 \end{aligned} \tag{B.1}$$

as representations of the light hole exciton and the heavy hole exciton respectively. In our samples, the light hole exciton is higher in energy than the heavy hole and hence we excite the heavy hole.

The lowest conduction band in D_{2d} is represented by Γ_1. We are interested in excitation to the conduction band with the dipole operator, given by $\overrightarrow{p}$, which is represented by $\Gamma_4 \oplus \Gamma_5$. Here Γ_4 represents the components of the electric field perpendicular to the plane of the sample, and Γ_5 represents the components of the electric field parallel to the sample. We are interested in finding out $\langle f|\overrightarrow{p}|i\rangle$, where f is the final exciton state and i is the initial ground state of the semiconductor.

While performing single-photon excitation with $k = 0$ we come in normal to the sample and only have the electric field components represented by Γ_5. We have a single dipole

operator acting on the heavy hole state. We look up the operator multiplication in the D_{2d} multiplication table to see if it's possible to excite to the final state and obtain

$$\begin{aligned} \langle \Gamma_1 | \Gamma_5 | \Gamma_3 \rangle &= 0 \\ \langle \Gamma_1 | \Gamma_5 | \Gamma_4 \rangle &= 0 \\ \langle \Gamma_1 | \Gamma_5 | \Gamma_5 \rangle &\neq 0 \end{aligned} \tag{B.2}$$

The first two states Γ_3 and Γ_4 cannot be excited directly. They are called the dark states, and the third state, Γ_5 which can be excited directly, is called the bright state.

For two-photon excitation with $k = 0$ we have two dipole operators $\overrightarrow{p} \times \overrightarrow{p}$ acting on the initial state. Again, since we are coming in normal to the sample we only consider the Γ_5 representation of the photon. Looking it up on the multiplication table our operator is

$$\Gamma_5 \otimes \Gamma_5 = \Gamma_1 \oplus \Gamma_2 \oplus \Gamma_3 \oplus \Gamma_4. \tag{B.3}$$

This gives us

$$\begin{aligned} \langle \Gamma_1 | \Gamma_1 \oplus \Gamma_2 \oplus \Gamma_3 \oplus \Gamma_4 | \Gamma_3 \rangle &\neq 0 \\ \langle \Gamma_1 | \Gamma_1 \oplus \Gamma_2 \oplus \Gamma_3 \oplus \Gamma_4 | \Gamma_4 \rangle &\neq 0 \\ \langle \Gamma_1 | \Gamma_1 \oplus \Gamma_2 \oplus \Gamma_3 \oplus \Gamma_4 | \Gamma_5 \rangle &= 0 \end{aligned} \tag{B.4}$$

As expected only the transition to the dark states is allowed for two-photon excitation, while transition into the bright state is forbidden, which indicates that there should be no direct creation of polaritons at normal incidence since only the bright states would interact with the cavity photon.

However, we have only considered normal incidence so far. For incidence at an angle we consider the $\overrightarrow{k} \cdot \overrightarrow{p}$ theory, which tells us that transition to a forbidden state could be allowed at non-zero $\overrightarrow{k}$, if there is an intermediate state to which transition from both the initial and final state is allowed. However, the probability of transition depends on how far away in energy the intermediate state is from both the initial and final states.

In general the initial and final states can be written as[28]

$$|u_{nk}\rangle = |u_{n0}\rangle + \frac{\hbar}{m} \sum_m \overrightarrow{k} \cdot \frac{\langle u_{mo} | \overrightarrow{p} \otimes \overrightarrow{p} | u_{nk} \rangle}{E_n - E_m} |u_{mo}\rangle \tag{B.5}$$

For non-zero k instead of only calculating $\langle u_{f0}|\overrightarrow{p}\otimes\overrightarrow{p}|u_{io}\rangle$ to first order we can write

$$\begin{aligned}\langle u_{f\,\overrightarrow{k}}|\overrightarrow{p}\otimes\overrightarrow{p}|u_{i\,\overrightarrow{k}}\rangle = &\frac{h}{m}\sum_m \frac{\big(\overrightarrow{k}\cdot\langle u_{f0}|\overrightarrow{p}\times\overrightarrow{p}|u_{m0}\rangle\big)\langle u_{m0}|\overrightarrow{p}\times\overrightarrow{p}|u_{i0}\rangle}{E_{f0}-E_{m0}}\\ &+\frac{h}{m}\sum_m \frac{\big(\overrightarrow{k}\cdot\langle u_{m0}|\overrightarrow{p}\times\overrightarrow{p}|u_{i0}\rangle\big)\langle u_{f0}|\overrightarrow{p}\times\overrightarrow{p}|u_{m0}\rangle}{E_{i0}-E_{m0}}\end{aligned} \tag{B.6}$$

If we come in with a beam that is transverse electric(TE) polarized, we only have components of the electric field parallel to the surface. However if we come in with a beam that is transverse magnetic(TM) polarized we would have a increasing component of electric field with increasing k. It is apparent that the possibility of the transition occurring only depends on $\langle u_{f0}|\overrightarrow{p}\times\overrightarrow{p}|u_{m0}\rangle\langle u_{m0}|\overrightarrow{p}\times\overrightarrow{p}|u_{i0}\rangle$ and $\langle u_{m0}|\overrightarrow{p}\times\overrightarrow{p}|u_{i0}\rangle\langle u_{f0}|\overrightarrow{p}\times\overrightarrow{p}|u_{m0}\rangle$ Thus we check if this matrix could be non-zero for both the TE and TM cases below.

For TE polarized beam we only use $\Gamma_5\otimes\Gamma_5$ for $\overrightarrow{p}\times\overrightarrow{p}$ and consider transitions from the bright state Γ_5 into Γ_1. We obtain

$$\begin{aligned}\langle\Gamma_1|\Gamma_5\otimes\Gamma_5|m\rangle\langle m|\Gamma_5\times\Gamma_5|\Gamma_5\rangle = 0\\ \langle m|\Gamma_5\times\Gamma_5|\Gamma_5\rangle\langle\Gamma_1|\Gamma_5\times\Gamma_5|m\rangle = 0\end{aligned} \tag{B.7}$$

for all values of m. Thus it is not possible to perform two-photon excitation with a TE polarized light even at a large k.

In a TM polarized beam, we have Γ_4 components as well. Thus for the dipole operators $\overrightarrow{p}\times\overrightarrow{p}$, we'll have to consider $\Gamma_5\otimes\Gamma_5$, $\Gamma_4\otimes\Gamma_4$ as well as $\Gamma_4\otimes\Gamma_5$. Since there are two matrix elements, we will have twenty-four different possibilities out of which sixteen are unique and listed below.

If both the operators are the same, i.e., we have either $\Gamma_5 \otimes \Gamma_5$, $\Gamma_4 \otimes \Gamma_5$ or $\Gamma_4 \otimes \Gamma_4$ for the operators, we get

$$\begin{aligned}
\langle \Gamma_1 | \Gamma_5 \otimes \Gamma_5 | m \rangle \langle m | \Gamma_5 \times \Gamma_5 | \Gamma_5 \rangle &= 0 \\
\langle m | \Gamma_5 \times \Gamma_5 | \Gamma_5 \rangle \langle \Gamma_1 | \Gamma_5 \times \Gamma_5 | m \rangle &= 0 \\
\langle \Gamma_1 | \Gamma_4 \otimes \Gamma_5 | m \rangle \langle m | \Gamma_4 \times \Gamma_5 | \Gamma_5 \rangle &= 0 \\
\langle m | \Gamma_4 \times \Gamma_5 | \Gamma_5 \rangle \langle \Gamma_1 | \Gamma_4 \times \Gamma_5 | m \rangle &= 0 \\
\langle \Gamma_1 | \Gamma_4 \otimes \Gamma_4 | m \rangle \langle m | \Gamma_4 \times \Gamma_4 | \Gamma_5 \rangle &= 0 \\
\langle m | \Gamma_4 \times \Gamma_4 | \Gamma_5 \rangle \langle \Gamma_1 | \Gamma_4 \times \Gamma_4 | m \rangle &= 0
\end{aligned} \tag{B.8}$$

for all values of m. For operators that are different, we get

$$\begin{aligned}
\langle \Gamma_1 | \Gamma_4 \otimes \Gamma_4 | m \rangle \langle m | \Gamma_5 \times \Gamma_5 | \Gamma_5 \rangle &= 0 \\
\langle m | \Gamma_5 \times \Gamma_5 | \Gamma_5 \rangle \langle \Gamma_1 | \Gamma_4 \times \Gamma_4 | m \rangle &= 0
\end{aligned} \tag{B.9}$$

for all values of m.

However, we obtain

$$\begin{aligned}
\langle \Gamma_1 | \Gamma_4 \otimes \Gamma_5 | m \rangle \langle m | \Gamma_5 \times \Gamma_5 | \Gamma_5 \rangle &\neq 0 \\
\langle m | \Gamma_5 \times \Gamma_5 | \Gamma_5 \rangle \langle \Gamma_1 | \Gamma_4 \times \Gamma_5 | m \rangle &\neq 0
\end{aligned} \tag{B.10}$$

for a state, m, represented by Γ_5 and

$$\begin{aligned}
\langle \Gamma_1 | \Gamma_4 \otimes \Gamma_4 | m \rangle \langle m | \Gamma_4 \times \Gamma_5 | \Gamma_5 \rangle &\neq 0 \\
\langle m | \Gamma_4 \times \Gamma_5 | \Gamma_5 \rangle \langle \Gamma_1 | \Gamma_4 \times \Gamma_4 | m \rangle &\neq 0
\end{aligned} \tag{B.11}$$

from a state, m, represented by Γ_1.

Thus we observe a non-zero matrix element when exciting with a TM polarized beam which tells us that it is possible to excite directly into the bright state using two-photon excitation provided we excite with a TM polarized beam through intermediate states of the light hole. It is worth noting that the further away these states are in energy from the initial and final states, the less likely it would be to excite through them.

From Equation (B.6), we see that the matrix element will have a factor of k as well. Since we square the matrix element, we have a k^2 dependence for the transition. However, as explained in Chapter 5 in our experiments, the Γ_4 component increases as k^2.

Thus

$$\langle u_{f\vec{k}}|\,\vec{p}\otimes\vec{p}\,|u_{i\vec{k}}\rangle \propto k^4. \tag{B.12}$$

This was shown to be true experimentally in Chapters 5 and 6.

APPENDIX C

EXPERIMENTAL DETAILS

In this section I'll go over the details of the experimental setup used in both the quantum dots experiment as well as the polariton experiments. The pump beam used for all the experiments was the tunable output beam from the OPA (described in Section 3.1.1). In order to be consistent with the definitions used previously, we have defined x-axis and y-axis to be the plane of the sample and the z-axis to be perpendicular to the sample.

C.1 QUANTUM DOT EXPERIMENTS

The details of the experimental set-up is shown in Figure 42. The pump beam (output from the OPA) was sent through two longpass filters, a telescope - which expanded the beam, and a dichroic mirror (DMSP1000 from Thorlabs), which reflected the mid-IR two-photon beam while transmitting the near-IR signal from the sample. The beam was sent through a periscope which gave us control over the beam along the x and y axis (the plane of the sample) and allowed us to chose the point on the sample we'd like to pump. Finally, the beam was sent through a microscope objective placed on a z-axis stage which allowed us to control the focus on the sample.

We placed our sample in an Oxford instruments microscope cryostat. The sample was placed right up against the window of the microscope cryostat. The experiment was performed at $\sim$4 K. The signal from the sample was sent through an imagining lens which

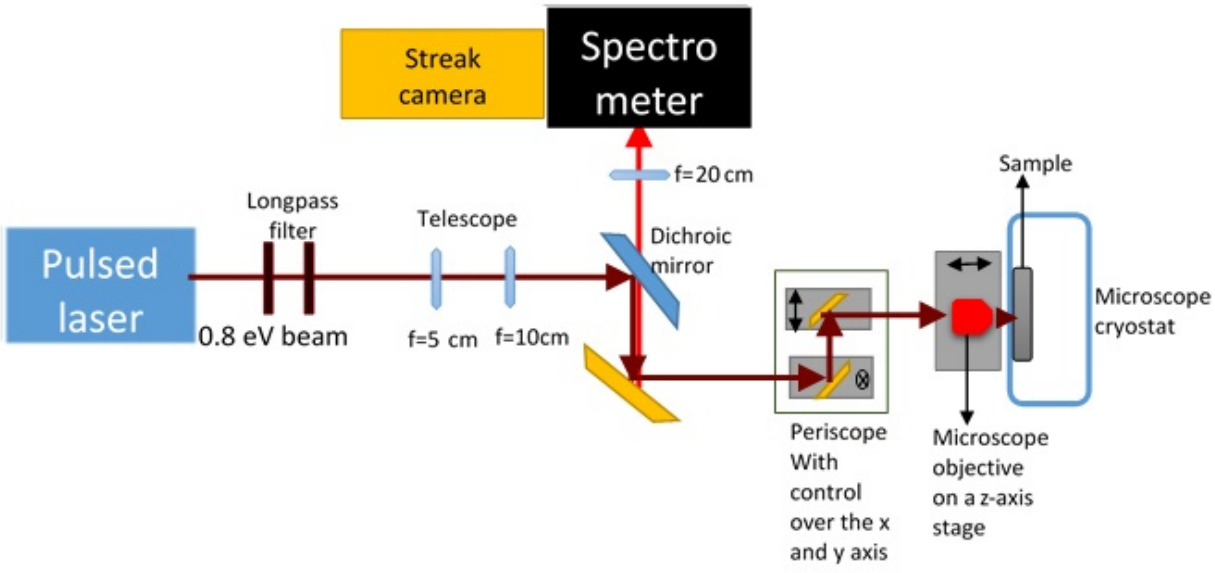

Figure 42: A detailed representation of the experimental setup for the quantum dots experiment reported in Chapter 5.

focused it to our spectrometer slit. The signal was spectrally resolved using a Princeton instruments Acton SP2500 spectrometer and time-resolved using a Hamamatsu streak camera. While the time-resolved image was directly viewed on the streak camera, the signal not sent to the streak camera was viewed on a Photometrics Cascade CCD camera.

C.2 POLARITON EXPERIMENT

The experimental setup for the data reported in Sections 5.4, 5.5, and 5.6 is shown in Figure 43. The initial beam path and the imaging system was similar to the one in Section C.1. However, the sample was placed in a Janis bath cryostat, which allowed us to control the temperature of the sample.

Two irises were used to steer the pump beam into the cryostat. Since the sample was placed at the center of the bath cryostat, we could not use a microscope objective to send

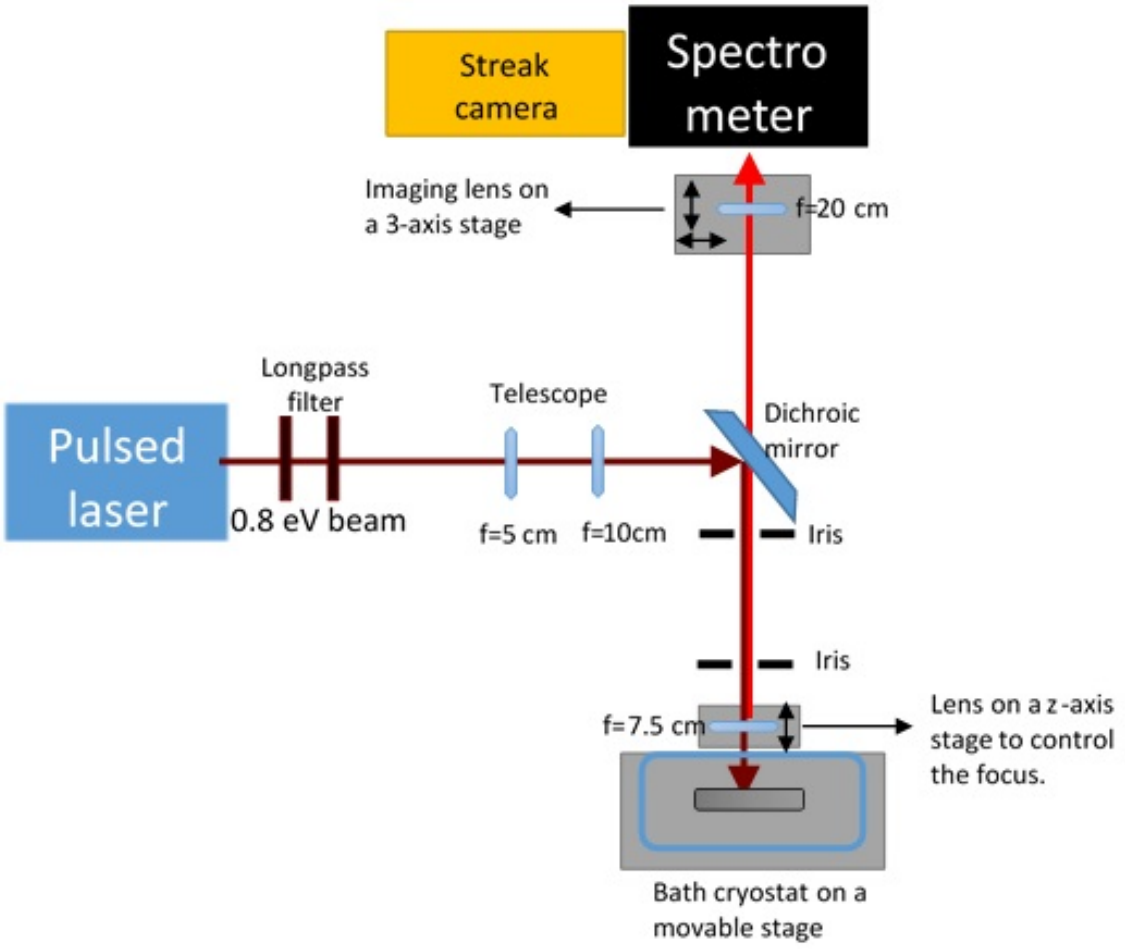

Figure 43: A detailed representation of the experimental setup for the initial polariton experimental setup reported in Chapter 5.

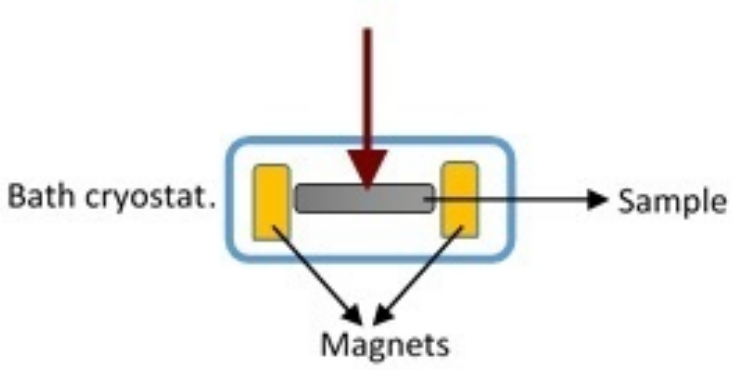

Figure 44: Two magnets were placed on either side of our polariton sample inside the bath cryostat.

the beam to our sample and used a short focal length lens instead. The lens was placed right up against the cryostat window. The imaging lens was placed on a three-axis stage which allowed us to correct for changes in the beam path. The bath cryostat was placed on a movable stage.

For the experiments reported in Section 6.1, the pumping and imaging setup shown in Figure 43 was used. However, inside the cryostat, the sample was placed between two solenoids as shown in Figure 44. A superconducting wire (a copper-clad Niobium-titanium wire with a clad-diameter of 0.114 mm and an insulated diameter of 0.14 mm) was used to construct the solenoid[120]. Two rolls of the super conducting wire was prepared and the sample was placed between them. A current of up to 6 A was sent through the superconducting wires at a temperature of 1.9 K. When the current was 6 A, the magnetic field produced by each coil at the center of the sample was calculated to be 1 T, which gave us a total of 2 T at the point of interest.

For the experiments reported in Sections 5.8, 6.3, and 6.4, the setup shown in Figure 45 was used. In this setup, we used a telescope to shrink the pump beam in order to have greater control over the in-plane momentum as explained in Section 6.3. We used a periscope to control the point of incidence on the microscope objective, and two quarter waveplates to

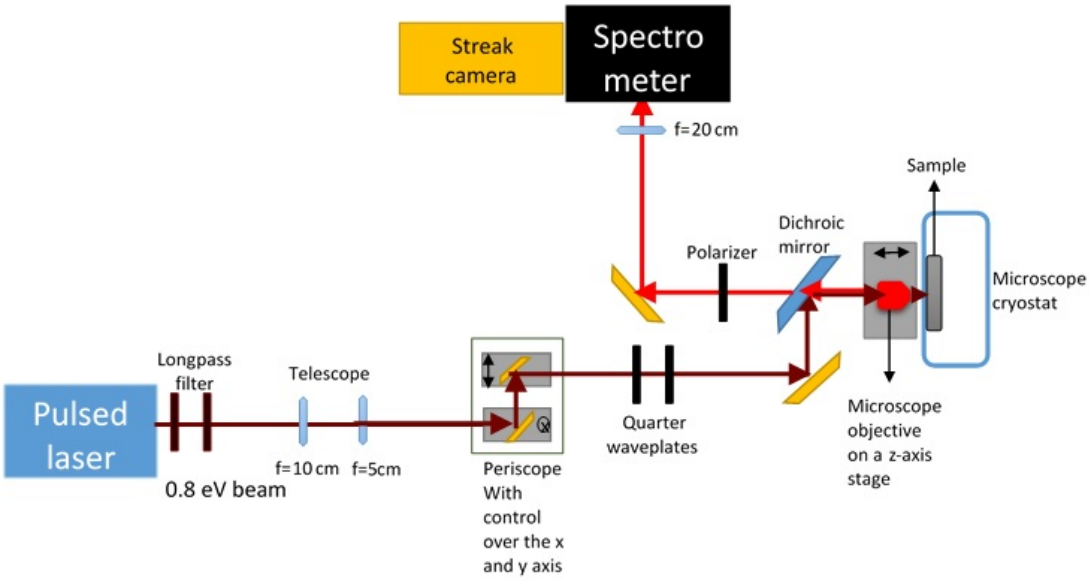

Figure 45: Detailed schematic of the experimental setup used to measure k-dependence.

rotate the polarization of the incident beam. This allowed us to look at the intensity of the signal for both TE as well as the TM polarized pump beam as reported in Section 6.3. We used a polarizer on the path of the output beam to study the polarization of the polariton state as reported in Section 6.4.

For the experiments reported in Section 28, we used the setup shown in Figure 46. We sent the beam at a large angle in order to obtain a large in-plane momentum. The sample was pumped far away from our field of view. We used a long focal length lens to focus the beam and the signal was collected using a microscope objective as before.

C.3 DETERMINISTIC ABSORPTION EXPERIMENTS

The experiments reported in Section 7.4 were performed using the setup shown in Figure 47. A CW laser was used to create a condensate. The beam from this laser was expanded using a telescope and sent through a chopper which chopped the beam. The frequency of the

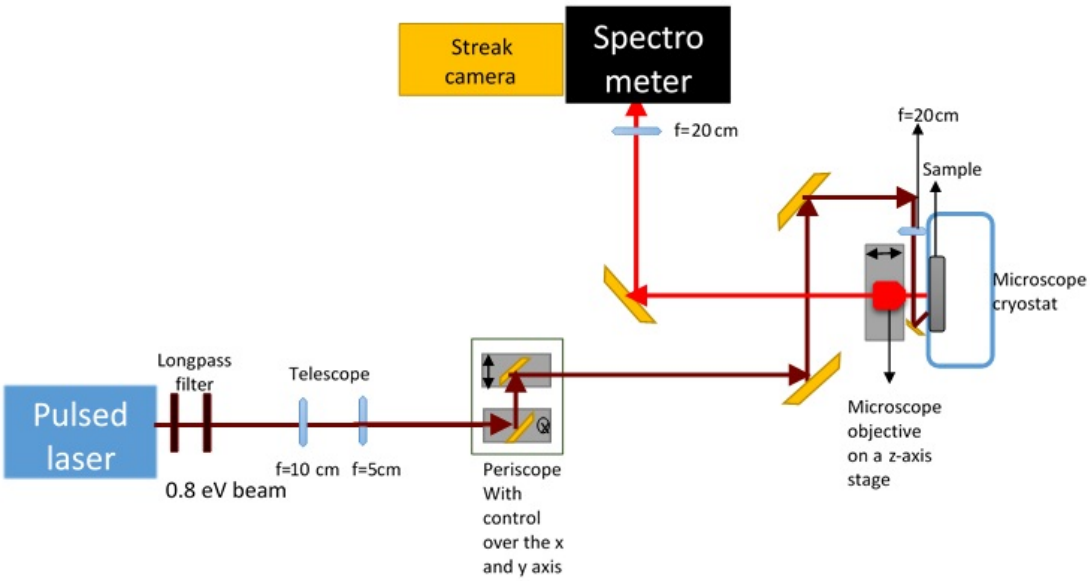

Figure 46: Detailed schematic of the experimental setup used to measure the polariton lifetime.

chopper was fed into a lock-in amplifier. The beam was sent through a lens mounted on a three-axis stage and was incident on the sample at an angle.

The two-photon beam incident on the sample had the same setup as that shown in Figure 43. The remnant two-photon beam going through the sample was collected by an avalanche photodiode(APD). The output from the APD was fed into a lock-in amplifier.

In the experiments reported in Section 7.5, the condensate was created using a resonant excitation. The sample was placed in a microscope cryostat. The path of the two-photon beam was similar to the one shown in Figure 45, while the single-photon beam followed the path of the two-photon beam shown in Figure 46. The complete setup is shown in Figure 48. The two beams were sent through separate periscopes to obtain control over where they hit the sample and to achieve k-matching. In a separate experiment, the two-photon beam was sent along the same path as the single-photon beam. This was done with the help of a dichroic mirror placed in the path of the single-photon beam.

To obtain greater occupation of the polariton state, we used a pulsed single-photon

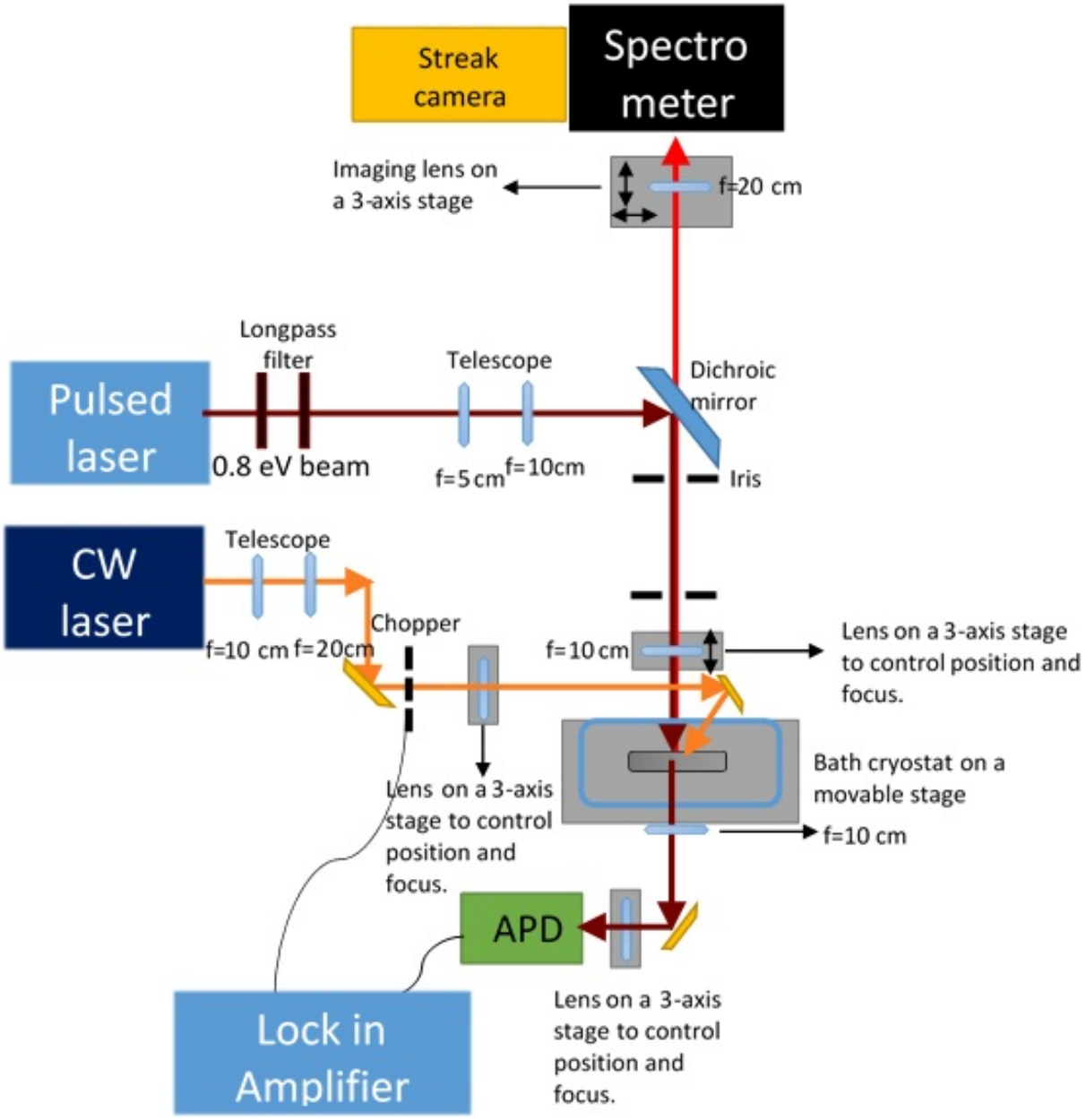

Figure 47: Detailed schematic of the experimental setup for deterministic absorption of a two-photon beam by a condensate created by by non-resonant pumping using a CW beam.

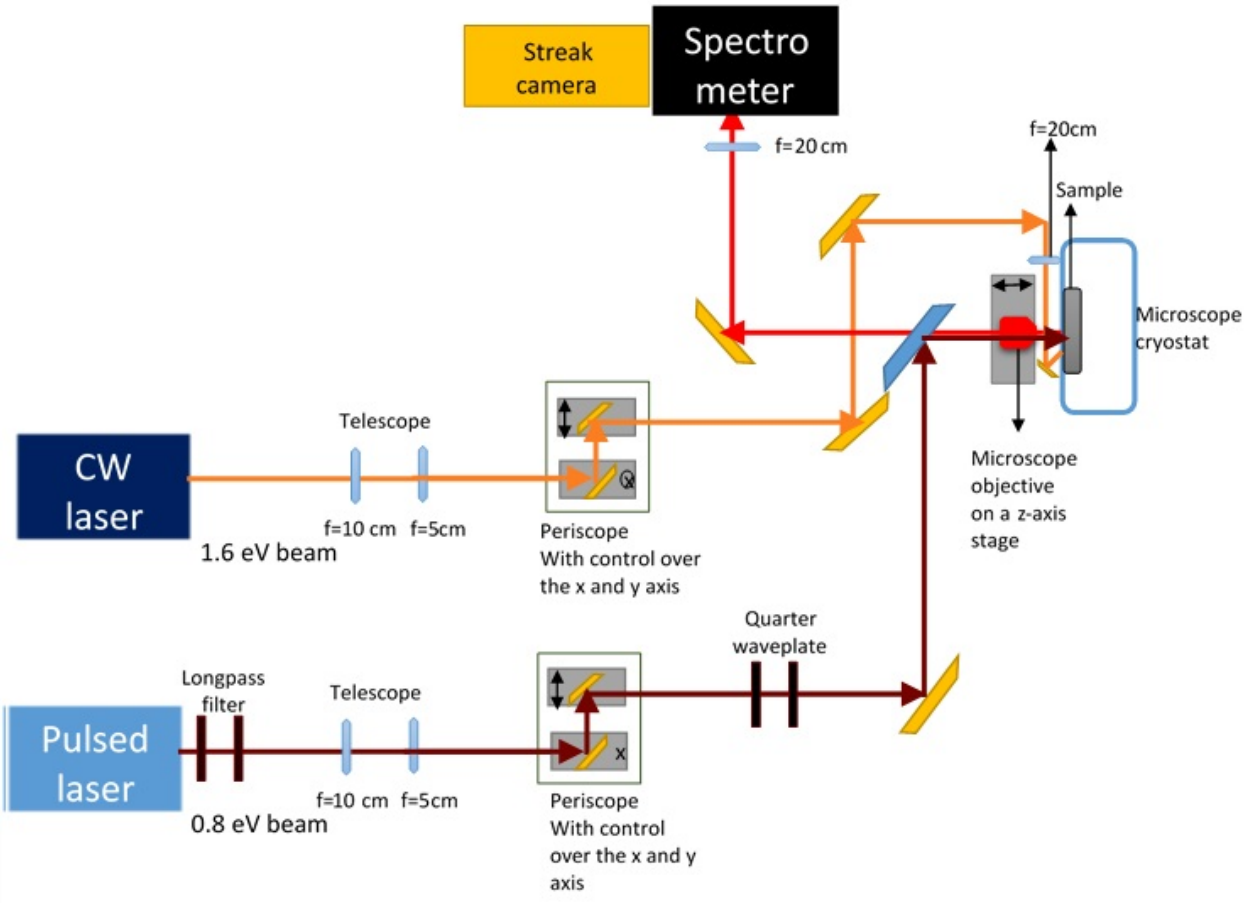

Figure 48: Detailed schematic of the experimental setup for deterministic absorption of a two-photon beam by a condensate created by by resonant pumping using a CW beam.

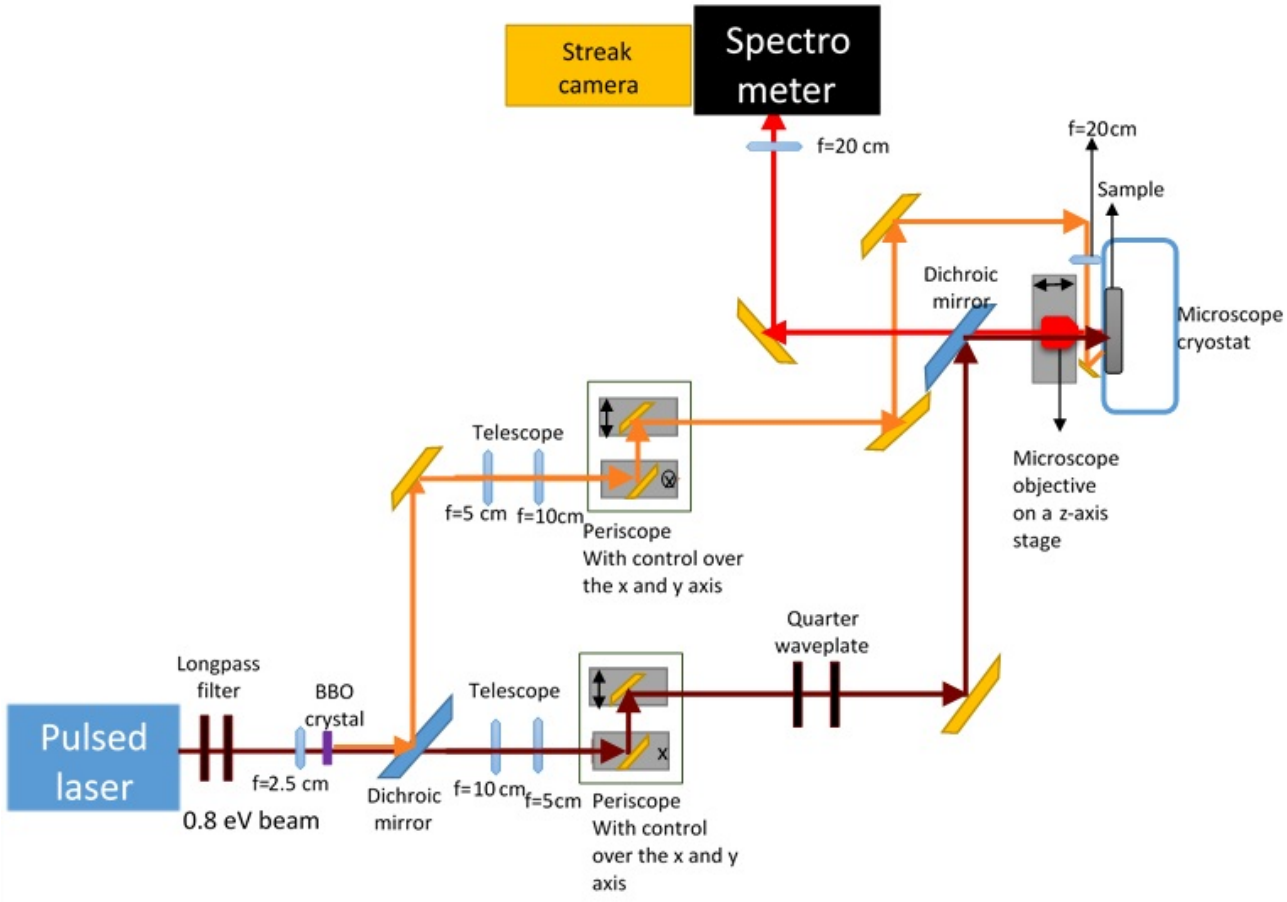

Figure 49: Detailed schematic of the experimental setup for deterministic absorption of a two-photon beam by a condensate created by by resonant pumping using a pulsed beam. The pulsed beam was created by frequency doubling the output from the OPA.

beam to create the condensate. The pulsed beam was obtained by frequency doubling the two-photon beam. The output from the OPA was focused on a BBO crystal using a short focal length lens. The frequency doubled beam coming out of the OPA was picked out and reflected using a dichroic mirror (Thorlabs DMLP1180) and sent through a separate telescope which expands the beam. The detailed schematic of this setup is shown in Figure 49. As before, the two-photon beam was sent through the microscope objective, and collinear with the frequency doubled beam in separate experiments. The signal was viewed on the CCD camera and the streak camera.

BIBLIOGRAPHY

[1] M. Göppert-Mayer, "Uber elementarakte mit zwei quantensprngen," *Annals of Physics*, vol. 9, pp. 273 – 294, 1931.

[2] T. H. Maiman, "Stimulated optical radiation in ruby," *Nature*, vol. 187, no. 4736, pp. 493–494, 1960.

[3] J. P. Gordon, H. J. Zeiger, and C. H. Townes, "The masernew type of microwave amplifier, frequency standard, and spectrometer," *Physical Review*, vol. 99, no. 4, p. 1264, 1955.

[4] J. P. Gordon, H. J. Zeiger, and C. H. Townes, "Molecular microwave oscillator and new hyperfine structure in the microwave spectrum of NH_3," *Physical Review*, vol. 95, no. 1, p. 282, 1954.

[5] W. Kaiser and C. G. B. Garrett, "Two-photon excitation in CaF_2:Eu^{2+}," *Phys. Rev. Lett.*, vol. 7, pp. 229–231, Sep 1961.

[6] S. J. H. Denk, W. and W. W. Webb, "Two-photon laser scanning fluorescence microscopy," *Science*, vol. 248, p. 7376, 1990.

[7] J. H. Strickler and W. W. Webb, "Three-dimensional optical data storage in refractive media bytwo-photon point excitation," *Opt. Lett.*, vol. 16, pp. 1780–1782, Nov 1991.

[8] W. Swainson and S. Kramer, "Method and media for accessing data in three dimensions," Sept. 11 1984. US Patent 4,471,470.

[9] M. Farsari and B. N. Chichkov, "Materials processing: two-photon fabrication," *Nature photonics*, vol. 3, no. 8, pp. 450–452, 2009.

[10] H.-B. Sun and S. Kawata, "Two-photon photopolymerization and 3D lithographic microfabrication," in *NMR 3D Analysis Photopolymerization*, vol. 170 of *Apvances in Polymer Science*, pp. 169–273, Springer Berlin Heidelberg, 2004.

[11] S. Juodkazis, V. Mizeikis, K. K. Seet, M. Miwa, and H. Misawa, "Two-photon lithography of nanorods in SU-8 photoresist," *Nanotechnology*, vol. 16, no. 6, p. 846, 2005.

[12] T. Liang, L. Nunes, M. Tsuchiya, K. Abedin, T. Miyazaki, D. V. Thourhout, W. Bogaerts, P. Dumon, R. Baets, and H. Tsang, "High speed logic gate using two-photon absorption in silicon waveguides," *Optics Communications*, vol. 265, no. 1, pp. 171 – 174, 2006.

[13] Y. Takagi, S. Imamura, T. Kobayashi, and K. Yoshihara, "Multiple- and single-shot autocorrelator based on two-photon conductivity in semiconductors," *Opt. Lett.*, vol. 17, pp. 658–660, May 1992.

[14] Z. Wei, J. Bai, J. Xu, C. Wang, Y. Yao, N. Hu, Y. Liang, K. Wang, and G. Yang, "Focused laser lithographic system with sub-wavelength resolution based on vortex laser induced opacity of photochromic material," *Opt. Lett.*, vol. 39, pp. 6707–6710, Dec 2014.

[15] Q. Zheng, G. S. He, and P. N. Prasad, "A novel near-IR two-photon absorbing chromophore: Optical limiting and stabilization performances at an optical communication wavelength," *Chemical Physics Letters*, vol. 475, no. 46, pp. 250 – 255, 2009.

[16] K. P. Chan, H. Inaba, M. Yamada, and B. Devaraj, "Optical imaging through highly scattering media by use of heterodyne detection in the 1.3-μm wavelength region," *Opt. Lett.*, vol. 20, pp. 492–494, Mar 1995.

[17] G. Burkard, D. Loss, and D. P. DiVincenzo, "Coupled quantum dots as quantum gates," *Phys. Rev. B*, vol. 59, pp. 2070–2078, Jan 1999.

[18] S. Fafard, K. Hinzer, S. Raymond, M. Dion, J. McCaffrey, Y. Feng, and S. Charbonneau, "Red-emitting semiconductor quantum dot lasers," *Science*, vol. 274, pp. 1350–1353, 1996.

[19] V. Zwiller, T. Aichele, F. Hatami, W. T. Masselink, and O. Benson, "Growth of single quantum dots on preprocessed structures: Single photon emitters on a tip," *Applied Physics Letters*, vol. 86, no. 9, pp. –, 2005.

[20] T. Fujisawa, D. G. Austing, Y. Tokura, Y. Hirayama, and S. Tarucha, "Nonequilibrium transport through a vertical quantum dot in the absence of spin-flip energy relaxation," *Phys. Rev. Lett.*, vol. 88, p. 236802, May 2002.

[21] M. Paillard, X. Marie, P. Renucci, T. Amand, A. Jbeli, and J. M. Gérard, "Spin relaxation quenching in semiconductor quantum dots," *Phys. Rev. Lett.*, vol. 86, pp. 1634–1637, Feb 2001.

[22] H. Deng, H. Haug, and Y. Yamamoto, "Exciton-polariton Bose-Einstein condensation," *Rev. Mod. Phys.*, vol. 82, pp. 1489–1537, May 2010.

[23] R. Balili, V. Hartwell, D. Snoke, L. Pfeiffer, and K. West, "Bose-Einstein condensation of microcavity polaritons in a trap," *Science*, vol. 316, no. 5827, pp. 1007–1010, 2007.

[24] J. D. Plumhof, T. Stöferle, L. Mai, U. Scherf, and R. F. Mahrt, "Room-temperature Bose–Einstein condensation of cavity exciton–polaritons in a polymer," *Nature materials*, vol. 13, no. 3, pp. 247–252, 2014.

[25] A. Das, P. Bhattacharya, J. Heo, A. Banerjee, and W. Guo, "Polariton Bose–Einstein condensate at room temperature in an Al(Ga)N nanowire–dielectric microcavity with a spatial potential trap," *Proceedings of the National Academy of Sciences*, vol. 110, no. 8, pp. 2735–2740, 2013.

[26] J. Kasprzak, M. Richard, S. Kundermann, A. Baas, P. Jeambrun, J. Keeling, F. Marchetti, M. Szymańska, R. Andre, J. Staehli, *et al.*, "Bose–Einstein condensation of exciton polaritons," *Nature*, vol. 443, no. 7110, pp. 409–414, 2006.

[27] H. Deng, G. Weihs, C. Santori, J. Bloch, and Y. Yamamoto, "Condensation of semiconductor microcavity exciton polaritons," *Science*, vol. 298, no. 5591, pp. 199–202, 2002.

[28] D. Snoke, *Solid State Physics: Essential Concepts*. Addison-Wesley, 2009.

[29] S. Adachi, "GaAs, AlAs, and $Al_xGa_{1x}As$: Material parameters for use in research and device applications," *Journal of Applied Physics*, vol. 58, no. 3, 1985.

[30] G. A. Samara, "Temperature and pressure dependences of the dielectric constants of semiconductors," *Physical Review B*, vol. 27, no. 6, p. 3494, 1983.

[31] B. Van Zeghbroeck, "Principles of semiconductor devices," *Colarado University*, 2004.

[32] P. Guyot-Sionnest, "Colloidal quantum dots," *Comptes Rendus Physique*, vol. 9, no. 8, pp. 777 – 787, 2008. Recent advances in quantum dot physics / Nouveaux dveloppements dans la physique des botes quantiques.

[33] P. Michler, *Single semiconductor quantum dots*. Springer, 2009.

[34] A. Yoffe, "Semiconductor quantum dots and related systems: Electronic, optical, luminescence and related properties of low dimensional systems," *Advances in Physics*, vol. 50, no. 1, pp. 1–208, 2001.

[35] M. Nirmal, , and L. Brus, "Luminescence photophysics in semiconductor nanocrystals," *Accounts of Chemical Research*, vol. 32, no. 5, pp. 407–414, 1999.

[36] G. H. Carey, A. L. Abdelhady, Z. Ning, S. M. Thon, O. M. Bakr, and E. H. Sargent, "Colloidal quantum dot solar cells," *Chemical reviews*, 2015.

[37] A. Imamoglu, D. D. Awschalom, G. Burkard, D. P. DiVincenzo, D. Loss, M. Sherwin, and A. Small, "Quantum information processing using quantum dot spins and cavity qed," *Phys. Rev. Lett.*, vol. 83, pp. 4204–4207, Nov 1999.

[38] F. Troiani, U. Hohenester, and E. Molinari, "Exploiting exciton-exciton interactions in semiconductor quantum dots for quantum-information processing," *Phys. Rev. B*, vol. 62, pp. R2263–R2266, Jul 2000.

[39] D. Loss and D. P. DiVincenzo, "Quantum computation with quantum dots," *Phys. Rev. A*, vol. 57, pp. 120–126, Jan 1998.

[40] M. Kroutvar, Y. Ducommun, D. Heiss, M. Bichler, D. Schuh, G. Abstreiter, and J. J. Finley, "Optically programmable electron spin memory using semiconductor quantum dots," *Nature*, vol. 432, no. 7013, pp. 81–84, 2004.

[41] B. E. Kane, "A silicon-based nuclear spin quantum computer," *nature*, vol. 393, no. 6681, pp. 133–137, 1998.

[42] D. V. Bulaev and D. Loss, "Spin relaxation and anticrossing in quantum dots: Rashba versus dresselhaus spin-orbit coupling," *Phys. Rev. B*, vol. 71, p. 205324, May 2005.

[43] R. Hanson, L. P. Kouwenhoven, J. R. Petta, S. Tarucha, and L. M. K. Vandersypen, "Spins in few-electron quantum dots," *Rev. Mod. Phys.*, vol. 79, pp. 1217–1265, Oct 2007.

[44] J. Danon, "Spin-flip phonon-mediated charge relaxation in double quantum dots," *Phys. Rev. B*, vol. 88, p. 075306, Aug 2013.

[45] A. J. Ramsay, "A review of the coherent optical control of the exciton and spin states of semiconductor quantum dots," *Semiconductor Science and Technology*, vol. 25, no. 10, p. 103001, 2010.

[46] J. Elzerman, R. Hanson, L. W. Van Beveren, B. Witkamp, L. Vandersypen, and L. P. Kouwenhoven, "Single-shot read-out of an individual electron spin in a quantum dot," *nature*, vol. 430, no. 6998, pp. 431–435, 2004.

[47] F. Koppens, C. Buizert, K.-J. Tielrooij, I. Vink, K. Nowack, T. Meunier, L. Kouwenhoven, and L. Vandersypen, "Driven coherent oscillations of a single electron spin in a quantum dot," *Nature*, vol. 442, no. 7104, pp. 766–771, 2006.

[48] B. Nelsen, R. Balili, D. W. Snoke, L. Pfeiffer, and K. West, "Lasing and polariton condensation: Two distinct transitions in GaAs microcavities with stress traps," *Journal of Applied Physics*, vol. 105, p. 122414, June 2009.

[49] K. G. Lagoudakis, M. Wouters, M. Richard, A. Baas, I. Carusotto, R. André, L. S. Dang, and B. Deveaud-Plédran, "Quantized vortices in an exciton–polariton condensate," *Nature Physics*, vol. 4, no. 9, pp. 706–710, 2008.

[50] M. Richard, J. Kasprzak, A. Baas, S. Kundermann, K. Lagoudakis, M. Wouters, I. Carusotto, R. Andre, B. Deveaud-Pledran, and L. Dang, "Exciton-polariton Bose-Einstein condensation: advances and issues," *International journal of nanotechnology*, vol. 7, no. 4-8, pp. 668–685, 2010.

[51] G. Liu, D. W. Snoke, A. Daley, L. N. Pfeiffer, and K. West, "A new type of half-quantum circulation in a macroscopic polariton spinor ring condensate," *Proceedings of the National Academy of Sciences*, vol. 112, no. 9, pp. 2676–2681, 2015.

[52] A. Amo, J. Lefrère, S. Pigeon, C. Adrados, C. Ciuti, I. Carusotto, R. Houdré, E. Giacobino, and A. Bramati, "Superfluidity of polaritons in semiconductor microcavities," *Nature Physics*, vol. 5, no. 11, pp. 805–810, 2009.

[53] A. Amo, S. Pigeon, D. Sanvitto, V. G. Sala, R. Hivet, I. Carusotto, F. Pisanello, G. Lemnager, R. Houdr, E. Giacobino, C. Ciuti, and A. Bramati, "Polariton superfluids reveal quantum hydrodynamic solitons," *Science*, vol. 332, no. 6034, pp. 1167–1170, 2011.

[54] H. Flayac, D. D. Solnyshkov, and G. Malpuech, "Oblique half-solitons and their generation in exciton-polariton condensates," *Phys. Rev. B*, vol. 83, p. 193305, May 2011.

[55] K. Lagoudakis, B. Pietka, M. Wouters, R. André, and B. Deveaud-Plédran, "Coherent oscillations in an exciton-polariton Josephson junction," *Physical review letters*, vol. 105, no. 12, p. 120403, 2010.

[56] M. Abbarchi, A. Amo, V. Sala, D. Solnyshkov, H. Flayac, L. Ferrier, I. Sagnes, E. Galopin, A. Lemaître, G. Malpuech, *et al.*, "Macroscopic quantum self-trapping and Josephson oscillations of exciton polaritons," *Nature Physics*, vol. 9, no. 5, pp. 275–279, 2013.

[57] H. Deng, G. Weihs, C. Santori, J. Bloch, and Y. Yamamoto, "Condensation of semiconductor microcavity exciton polaritons," *Science*, vol. 298, no. 5591, pp. 199–202, 2002.

[58] J. Jeans, "On the partition of energy between matter and ether," *Philosophical Magazine Series 6*, vol. 10, no. 55, pp. 91–98, 1905.

[59] J. J. Hopfield, "Theory of the contribution of excitons to the complex dielectric constant of crystals," *Phys. Rev.*, vol. 112, pp. 1555–1567, Dec 1958.

[60] C. Weisbuch, M. Nishioka, A. Ishikawa, and Y. Arakawa, "Observation of the coupled exciton-photon mode splitting in a semiconductor quantum microcavity," *Phys. Rev. Lett.*, vol. 69, pp. 3314–3317, Dec 1992.

[61] G. Malpuech, A. Di Carlo, A. Kavokin, J. J. Baumberg, M. Zamfirescu, and P. Lugli, "Room-temperature polariton lasers based on GaN microcavities," *Applied physics letters*, vol. 81, no. 3, pp. 412–414, 2002.

[62] B. Nelsen, Polariton Condensates in a trap and photon lasing in two-dimensional semiconductor microcavities 2012. PhD thesis, University of Pittsburgh.

[63] O. Penrose and L. Onsager, "Bose-Einstein condensation and liquid helium," *Phys. Rev.*, vol. 104, pp. 576–584, Nov 1956.

[64] A. Legett, *Quantum Liquids*. Oxford University Press, 2006.

[65] R. Pathria and P. Beale, *Statistical Mechanics*. Elsevier Science, 1996.

[66] A. V. Kavokin, I. A. Shelykh, T. Taylor, and M. M. Glazov, "Vertical cavity surface emitting terahertz laser," *Phys. Rev. Lett.*, vol. 108, p. 197401, May 2012.

[67] P. C. Hohenberg, "Existence of long-range order in one and two dimensions," *Phys. Rev.*, vol. 158, pp. 383–386, Jun 1967.

[68] J. M. Kosterlitz and D. J. Thouless, "Ordering, metastability and phase transitions in two-dimensional systems," *Journal of Physics C: Solid State Physics*, vol. 6, no. 7, p. 1181, 1973.

[69] J. Schmutzler, M. Aßmann, T. Czerniuk, M. Kamp, C. Schneider, S. Höfling, and M. Bayer, "Nonlinear spectroscopy of exciton-polaritons in a GaAs-based microcavity," *Phys. Rev. B*, vol. 90, p. 075103, Aug 2014.

[70] G. Leménager, F. Pisanello, J. Bloch, A. Kavokin, A. Amo, A. Lemaitre, E. Galopin, I. Sagnes, M. De Vittorio, E. Giacobino, *et al.*, "Two-photon injection of polaritons in semiconductor microstructures," *Optics letters*, vol. 39, no. 2, pp. 307–310, 2014.

[71] P. Bhattacharya, B. Xiao, A. Das, S. Bhowmick, and J. Heo, "Solid state electrically injected exciton-polariton laser," *Phys. Rev. Lett.*, vol. 110, p. 206403, May 2013.

[72] C. Schneider, A. Rahimi-Iman, N. Y. Kim, J. Fischer, I. G. Savenko, M. Amthor, M. Lermer, A. Wolf, L. Worschech, V. D. Kulakovskii, *et al.*, "An electrically pumped polariton laser," *Nature*, vol. 497, no. 7449, pp. 348–352, 2013.

[73] R. W. Boyd, *Nonlinear optics*. Academic press, 2003.

[74] B. B. Laud, "Lasers and nonlinear optics," 1986.

[75] R. J. Elliott, "Theory of the effect of spin-orbit coupling on magnetic resonance in some semiconductors," *Phys. Rev.*, vol. 96, pp. 266–279, Oct 1954.

[76] Y. Yafet, *Solid State Physics, Vol. 14*. Academic Press, New York, 1963.

[77] M. D. Mower, G. Vignale, and I. V. Tokatly, "Dyakonov-Perel spin relaxation for degenerate electrons in the electron-hole liquid," *Phys. Rev. B*, vol. 83, p. 155205, Apr 2011.

[78] M. Z. Maialle, E. A. de Andrada e Silva, and L. J. Sham, "Exciton spin dynamics in quantum wells," *Phys. Rev. B*, vol. 47, pp. 15776–15788, Jun 1993.

[79] Y. Yafet, "Conduction electron spin relaxation in the superconducting state," *Physics Letters A*, vol. 98, no. 56, pp. 287 – 290, 1983.

[80] F. Simon, B. Dóra, F. Murányi, A. Jánossy, S. Garaj, L. Forró, S. Bud'ko, C. Petrovic, and P. C. Canfield, "Generalized Elliott-Yafet theory of electron spin relaxation in metals: Origin of the anomalous electron spin lifetime in MgB_2," *Phys. Rev. Lett.*, vol. 101, p. 177003, Oct 2008.

[81] P. Boross, B. Dóra, A. Kiss, and F. Simon, "A unified theory of spin-relaxation due to spin-orbit coupling in metals and semiconductors," *Scientific Reports*, vol. 3, p. 3233, Nov. 2013.

[82] M. D'yakonov and V. Perel, "Spin orientation of electrons associated with the interband absorption of light in semiconductors," *Soviet Journal of Experimental and Theoretical Physics*, vol. 33, p. 1053, 1971.

[83] A. Rastelli, S. Stufler, A. Schliwa, R. Songmuang, C. Manzano, G. Costantini, K. Kern, A. Zrenner, D. Bimberg, and O. G. Schmidt, "Hierarchical self-assembly of GaAs/AlGaAs quantum dots," *Phys. Rev. Lett.*, vol. 92, p. 166104, Apr 2004.

[84] H. Htoon, T. Takagahara, D. Kulik, O. Baklenov, A. L. Holmes, and C. K. Shih, "Interplay of Rabi oscillations and quantum interference in semiconductor quantum dots," *Phys. Rev. Lett.*, vol. 88, p. 087401, Feb 2002.

[85] R. Songmuang, S. Kiravittaya, and O. G. Schmidt, "Formation of lateral quantum dot molecules around self-assembled nanoholes," *Applied physics letters*, vol. 82, no. 17, pp. 2892–2894, 2003.

[86] H. Schuler, N. Jin-Phillipp, F. Phillipp, and K. Eberl, "Size modification of self-assembled InAs quantum dots by *in-situ* etching," *Semiconductor science and technology*, vol. 13, no. 11, p. 1341, 1998.

[87] B. Nelsen, G. Liu, M. Steger, D. W. Snoke, R. Balili, K. West, and L. Pfeiffer, "Dissipationless flow and sharp threshold of a polariton condensate with long lifetime," *Phys. Rev. X*, vol. 3, p. 041015, Nov 2013.

[88] M. Steger, C. Gautham, D. W. Snoke, L. Pfeiffer, and K. West, "Slow reflection and two-photon generation of microcavity exciton–polaritons," *Optica*, vol. 2, pp. 1–5, Jan 2015.

[89] C. Gautham, D. Snoke, A. Rastelli, and O. Schmidt, "Time-resolved two-photon excitation of dark states in quantum dots," *Applied Physics Letters*, vol. 104, no. 14, p. 143114, 2014.

[90] A. L. Efros, M. Rosen, M. Kuno, M. Nirmal, D. J. Norris, and M. Bawendi, "Band-edge exciton in quantum dots of semiconductors with a degenerate valence band: Dark and bright exciton states," *Phys. Rev. B*, vol. 54, pp. 4843–4856, Aug 1996.

[91] M. Bayer, G. Ortner, O. Stern, A. Kuther, A. A. Gorbunov, A. Forchel, P. Hawrylak, S. Fafard, K. Hinzer, T. L. Reinecke, S. N. Walck, J. P. Reithmaier, F. Klopf,

and F. Schäfer, "Fine structure of neutral and charged excitons in self-assembled In(Ga)As/(Al)GaAs quantum dots," *Phys. Rev. B*, vol. 65, p. 195315, May 2002.

[92] Y. Huo, B. Witek, S. Kumar, J. Cardenas, J. Zhang, N. Akopian, R. Singh, E. Zallo, R. Grifone, D. Kriegner, *et al.*, "A light-hole exciton in a quantum dot," *Nature Physics*, vol. 10, no. 1, pp. 46–51, 2014.

[93] K. De Greve, P. L. McMahon, D. Press, T. D. Ladd, D. Bisping, C. Schneider, M. Kamp, L. Worschech, S. Höfling, A. Forchel, *et al.*, "Ultrafast coherent control and suppressed nuclear feedback of a single quantum dot hole qubit," *Nature Physics*, vol. 7, no. 11, pp. 872–878, 2011.

[94] S. Laurent, B. Eble, O. Krebs, A. Lemaître, B. Urbaszek, X. Marie, T. Amand, and P. Voisin, "Electrical control of hole spin relaxation in charge tunable InAs/GaAs quantum dots," *Phys. Rev. Lett.*, vol. 94, p. 147401, Apr 2005.

[95] Y. Sidor, B. Partoens, F. M. Peeters, N. Schildermans, M. Hayne, V. V. Moshchalkov, A. Rastelli, and O. G. Schmidt, "High-field magnetoexcitons in unstrained GaAs/$Al_xGa_{1-x}As$ quantum dots," *Phys. Rev. B*, vol. 73, p. 155334, Apr 2006.

[96] J. Y. Marzin, J. M. Gérard, A. Izraël, D. Barrier, and G. Bastard, "Photoluminescence of single InAs quantum dots obtained by self-organized growth on GaAs," *Phys. Rev. Lett.*, vol. 73, pp. 716–719, Aug 1994.

[97] M. Paillard, X. Marie, P. Renucci, T. Amand, A. Jbeli, and J. M. Gérard, "Spin relaxation quenching in semiconductor quantum dots," *Phys. Rev. Lett.*, vol. 86, pp. 1634–1637, Feb 2001.

[98] M. Syperek, D. R. Yakovlev, I. A. Yugova, J. Misiewicz, I. V. Sedova, S. V. Sorokin, A. A. Toropov, S. V. Ivanov, and M. Bayer, "Long-lived electron spin coherence in CdSe/Zn(S,Se) self-assembled quantum dots," *Phys. Rev. B*, vol. 84, p. 085304, Aug 2011.

[99] D. W. Snoke, J. Hübner, W. W. Rühle, and M. Zundel, "Spin flip from dark to bright states in InP quantum dots," *Phys. Rev. B*, vol. 70, p. 115329, Sep 2004.

[100] B. Zhang, D. W. Snoke, and A. P. Heberle, "Trion formation in GaAs/AlGaAs quantum dots by tunneling," *Solid State Communications*, vol. 152, no. 4, pp. 296 – 299, 2012.

[101] A. S. Bhatti, M. Grassi Alessi, M. Capizzi, P. Frigeri, and S. Franchi, "Optical spectroscopy of quasimonolayer InAs at the onset of quantum-dot nucleation," *Phys. Rev. B*, vol. 60, pp. 2592–2598, Jul 1999.

[102] H. Benisty, C. M. Sotomayor-Torrès, and C. Weisbuch, "Intrinsic mechanism for the poor luminescence properties of quantum-box systems," *Phys. Rev. B*, vol. 44, pp. 10945–10948, Nov 1991.

[103] A. Tackeuchi, R. Ohtsubo, K. Yamaguchi, M. Murayama, T. Kitamura, T. Kuroda, and T. Takagahara, "Spin relaxation dynamics in highly uniform inas quantum dots," *Applied Physics Letters*, vol. 84, no. 18, 2004.

[104] S. Denev and D. W. Snoke, "Stress dependence of exciton relaxation processes in Cu_2O," *Phys. Rev. B*, vol. 65, p. 085211, Feb 2002.

[105] I. Carusotto and C. Ciuti, "Quantum fluids of light," *Rev. Mod. Phys.*, vol. 85, pp. 299–366, Feb 2013.

[106] A. Kavokin, J. J. Baumberg, G. Malpuech, and F. P. Laussy, *Microcavities*. Oxford University Press, 2007.

[107] A. Legett, *Exciton Polaritons in Microcavities: New Frontiers*. Springer Series in Solid-State Sciences, 2012.

[108] T. Byrnes, N. Y. Kim, and Y. Yamamoto, "Exciton-polariton condensates," *Nature Physics*, vol. 10, no. 11, pp. 803–813, 2014.

[109] P. Cristofolini, A. Dreismann, G. Christmann, G. Franchetti, N. G. Berloff, P. Tsotsis, Z. Hatzopoulos, P. G. Savvidis, and J. J. Baumberg, "Optical superfluid phase transitions and trapping of polariton condensates," *Phys. Rev. Lett.*, vol. 110, p. 186403, May 2013.

[110] A. Amo, D. Sanvitto, F. Laussy, D. Ballarini, E. Del Valle, M. Martin, A. Lemaitre, J. Bloch, D. Krizhanovskii, M. Skolnick, *et al.*, "Collective fluid dynamics of a polariton condensate in a semiconductor microcavity," *Nature*, vol. 457, no. 7227, pp. 291–295, 2009.

[111] K. Lagoudakis, T. Ostatnickỳ, A. Kavokin, Y. G. Rubo, R. André, and B. Deveaud-Plédran, "Observation of half-quantum vortices in an exciton-polariton condensate," *Science*, vol. 326, no. 5955, pp. 974–976, 2009.

[112] D. Sanvitto, F. Marchetti, M. Szymańska, G. Tosi, M. Baudisch, F. Laussy, D. Krizhanovskii, M. Skolnick, L. Marrucci, A. Lemaitre, *et al.*, "Persistent currents and quantized vortices in a polariton superfluid," *Nature Physics*, vol. 6, no. 7, pp. 527–533, 2010.

[113] R. Hivet, E. Cancellieri, T. Boulier, D. Ballarini, D. Sanvitto, F. M. Marchetti, M. H. Szymanska, C. Ciuti, E. Giacobino, and A. Bramati, "Interaction-shaped vortex-antivortex lattices in polariton fluids," *Phys. Rev. B*, vol. 89, p. 134501, Apr 2014.

[114] F. Manni, T. C. H. Liew, K. G. Lagoudakis, C. Ouellet-Plamondon, R. André, V. Savona, and B. Deveaud, "Spontaneous self-ordered states of vortex-antivortex pairs in a polariton condensate," *Phys. Rev. B*, vol. 88, p. 201303, Nov 2013.

[115] C. Gautham and D. Snoke, "Modulation of two-photon excitation by a polariton condensate," August 2013. Preliminary results from this work were reported in August 2013.

[116] S. Chuang, *Physics of Photonic Devices*. Wiley Series in Pure and Applied Optics, Wiley, 2012.

[117] J. K. Wuenschell, N. W. Sinclair, Z. Vörös, D. W. Snoke, L. N. Pfeiffer, and K. W. West, "Darkening of interwell excitons in coupled quantum wells due to a stress-induced direct-to-indirect transition," *Phys. Rev. B*, vol. 92, p. 235415, Dec 2015.

[118] J. Puls, M. Rabe, H.-J. Wünsche, and F. Henneberger, "Magneto-optical study of the exciton fine structure in self-assembled CdSe quantum dots," *Phys. Rev. B*, vol. 60, pp. R16303–R16306, Dec 1999.

[119] M. Bayer, G. Ortner, O. Stern, A. Kuther, A. Gorbunov, A. Forchel, P. Hawrylak, S. Fafard, K. Hinzer, T. Reinecke, *et al.*, "Fine structure of neutral and charged excitons in self-assembled In(Ga)As/(Al)GaAs quantum dots," *Physical Review B*, vol. 65, no. 19, p. 195315, 2002.

[120] N. Sinclair, Luminescence darkening of strain-trapped excitons in coupled quantum wells 2014. PhD thesis, University of Pittsburgh.

[121] R. Y. Chiao, T. H. Hansson, J. M. Leinaas, and S. Viefers, "Two-dimensional 'photon fluid': effective photonphoton interaction and physical realizations," *Journal of Physics B: Atomic, Molecular and Optical Physics*, vol. 37, no. 7, p. S81, 2004.

[122] H. F. Hofmann and H. Nishitani, "Pulse-shape effects on photon-photon interactions in nonlinear optical quantum gates," *Phys. Rev. A*, vol. 80, p. 013822, Jul 2009.

[123] O. El Daïf, A. Baas, T. Guillet, J.-P. Brantut, R. I. Kaitouni, J.-L. Staehli, F. Morier-Genoud, and B. Deveaud, "Polariton quantum boxes in semiconductor microcavities," *Applied Physics Letters*, vol. 88, no. 6, p. 061105, 2006.

[124] M. Cardona and Y. Y. Peter, *Fundamentals of semiconductors*. Springer, 2005.

[125] D. Snoke, "Predicting the ionization threshold for carriers in excited semiconductors," *Solid State Communications*, vol. 146, no. 1, pp. 73–77, 2008.

[126] D. Semkat, F. Richter, D. Kremp, G. Manzke, W.-D. Kraeft, and K. Henneberger, "Ionization equilibrium in an excited semiconductor: Mott transition versus Bose-Einstein condensation," *Physical Review B*, vol. 80, no. 15, p. 155201, 2009.